Experimental and Computational Study of Interphase Properties and Mechanics in Titanium Metal Matrix Composites at Elevated Temperatures

Final Report
March 2005

By

D. Osborne and H. Ghonem

Mechanics of Materials Laboratory
Department of Mechanical Engineering
University of Rhode Island
Kingston, RI 02881

prepared for

USAF Office of Scientific Research
Bolling Air Force Base, DC 20332

20051024 090

REPORT DOCUMENTATION PAGE

AFRL-SR-AR-TR-05-

0456

Public reporting burden for this collection of information is estimated to average 1 hour per response, including the time for reviewing data needed, and completing and reviewing this collection of information. Send comments regarding this burden estimate or any oth this burden to Department of Defense, Washington Headquarters Services, Directorate for Information Operations and Reports (0704 4302. Respondents should be aware that notwithstanding any other provision of law, no person shall be subject to any penalty for failing to comply, ... ly valid OMB control number. PLEASE DO NOT RETURN YOUR FORM TO THE ABOVE ADDRESS.

1. REPORT DATE *(02-03-2005)*	2. REPORT TYPE	3. DATES COVERED *(From - To)*1999-2002

4. TITLE AND SUBTITLE	5a. CONTRACT NUMBER
Experimental and Computational Study of Interphase Properties and Mechanics in Titanium Metal Matrix Composites at Elevated Temperatures	5b. GRANT NUMBER F49620-99-1-0275
	5c. PROGRAM ELEMENT NUMBER

6. AUTHOR(S)	5d. PROJECT NUMBER
D. Osborne and H. Ghonem NA	5e. TASK NUMBER
	5f. WORK UNIT NUMBER

7. PERFORMING ORGANIZATION NAME(S) AND ADDRESS(ES) University of Rhode Island, Department of Mechanical Engineering, Kingston RI 02881	8. PERFORMING ORGANIZATION REPORT NUMBER MML-05-2

9. SPONSORING / MONITORING AGENCY NAME(S) AND ADDRESS(ES)	10. SPONSOR/MONITOR'S ACRONYM(S)
	11. SPONSOR/MONITOR'S REPORT NUMBER(S)

12. DISTRIBUTION / AVAILABILITY STATEMENT

Approved for public release, distribution unlimited

13. SUPPLEMENTARY NOTES

14. ABSTRACT An elevated temperature fiber pushout apparatus has been built and used to test the interfacial shear strenght and frictional shear stress at various temperatures in Ti matrix composites. The pushout apparatus, coupled with thermal aging studies, was used to investigate the influence of temperature and thermal exposure on tangential interfacial shear strength and frictional shear stress. Additionally, the effect of variation of processing conditions, including variation of fiber volume fraction and of the time-temperature-pressure profile during consolidation, has been examined using concentric cylinder numerical mode, and compared to experimental test results. Using interface properties, composite failure maps have been established for this material that describe the dominant failure mode as a function of the temperature and stress intensity factor during loading. Furthermore, iInterface debonding behavior, in terms of the cohesive zone model parameters of maximum traction, maximum separation and cohesive energy, in both the normal and tangential direction, has been established for the MMC composite system SCS-6/Timetal-21S, for temperatures from 23 to 650 °C

15. SUBJECT TERMS
Titanium Metal Matricx Composites, Elevated Temperature, Interface, Decohesion, Fracture, Crack Growth, Processing

16. SECURITY CLASSIFICATION OF:			17. LIMITATION OF ABSTRACT	18. NUMBER OF PAGES	19a. NAME OF RESPONSIBLE PERSON H. Ghonem
a. REPORT	b. ABSTRACT	c. THIS PAGE			19b. TELEPHONE NUMBER *(include area code* (401) 874-2909)

Standard Form 298 (Rev. 8-98)
Prescribed by ANSI Std. Z39.18

ABSTRACT

The high temperature interfacial properties, in the tangential and normal direction, of a continuous SiC fiber reinforced Ti matrix composites, primarily SCS-6/Timetal-21S, have been examined in this experimental/numerical study. An elevated temperature fiber pushout apparatus has been built and used to test the interfacial shear strenght and frictional shear stress at various temperatures. It was found that as temperature increases, both interface properties decrease, but the debonding behavior changes for test temperatures above 400 $^{\circ}$C. Additionally, transverse loading tests have shown a similar decrease in normal separation stress with increasing temperature. The pushout apparatus, coupled with thermal aging studies, was used to investigate the influence of temperature and thermal exposure on tangential interfacial shear strength and frictional shear stress. It was found that thermal exposure under vacuum for temperatures up to 650 $^{\circ}$C conditions results in no noticeable increase in the interphase size, composition, or interphase strength properties. Aging in air causes a degradation of the interphase, resulting in deterioration of interphase properties, particularly at higher temperatures. The effect of variation of processing conditions, including variation of fiber volume fraction and of the time-temperature-pressure profile during consolidation, has been examined using concentric cylinder numerical mode, and compared to experimental test results. It was found that the processing conditions required for full consolidation of the material allow little variation in the composite stress state. An increase in the fiber volume fraction increases the interfacial shear stress at all temperatures, with the most noticeable difference at room temperature, as well as a change in the characteristics of fiber pushout curves. Using interface properties, composite failure maps have been established for this material that describe the dominant failure mode as a function of the temperature and stress intensity factor during loading. For reasonable use temperatures, the boundary between fiber bridging and interface debonding occurs at decreasing K_{max} with increasing temperature.. Interface debonding behavior, in terms of the cohesive zone model parameters of maximum traction, maximum separation and cohesive energy, in both the normal and tangential direction, has been established for the MMC composite system SCS-6/Timetal-21S, for temperatures from 23 to 650 $^{\circ}$C. The numerical model yields good agreement with experimental results. For both normal and tangential decohesion, the maximum traction, T_{max}, decreases with increasing temperature.

PREFACE

This report consists of five chapters which are written as independent studies. Each chapter contains its own abstract and introduction, and ends with a summary and results. Chapter 1 is an introduction to the study, which includes a review of Ti-MMCs and damage mechanisms occurring in this type of material, as well as a review of interphase studies and debonding theories. The experimental work discussed in chapter 2 focuses on the interphase of this material and its response to elevated temperature, including thermal aging in air and vacuum. This response is investigated in two ways. Observations of interphase size were made visually using scanning electron microscopy and verified using Auger Electron Spectroscopy. Interphase properties were obtained experimentally, using fiber pushout testing to measure interphase shear strength and frictional shear stress , and transverse loading tests to measure normal separation stress. Also included in this section is a complete description of the elevated temperature fiber pushout apparatus built for this study. The work in Chapter 3 uses both experimental and numerical techniques to study the effect of processing-related parameters on interface properties. Included are the effects of post-processing heat treatment and fiber volume fraction. This chapter includes a complete description of the numerical model used in this study for the generation of residual stresses. Chapter 4 focuses on establishing high temperature damage map for this composite, based on interfacial shear properties established in previous chapters. In Chapter 5, normal and tangential decohesion properties are established for this composite, by relating experimental debonding curves with results from numerical model using a cohesive zone approach to describe the interface separation behavior.

LIST OF CONTENTS

LIST OF TABLES

LIST OF FIGURES

CHAPTER 1: INTRODUCTION

1.1   Review of Ti-MMCs

New materials are constantly in demand, as advances in technology raise the operating temperature and applied loads typical to aerospace applications. These applications require a stable material, both chemically and structurally, during monotonic and cyclic loading and temperature conditions. Many of the monolithic materials currently used in these applications are not able to meet these increasing demands. Additionally, light weight and corrosion resistance can be critical for aerospace applications. The development of composites, in which materials having very different mechanical and physical properties are combined to provide a material having superior properties to both constituents, is meeting these needs[1], sincethe addition of a reinforcing phase offers the ability to tailor the material for a particular application.

Various types of composites have been developed, which can be classified by the type of reinforcement used to modify the matrix material properties. The two basic types are discontinuously and continuously reinforced composites. Discontinuous reinforcement has a small length to diameter ratio, and includes particles, chopped fibers, and whiskers. The main benefit of this type of reinforcement is an increase in stiffness. Continuous reinforcement consists of fibers, either unidirectional or crossed. In this type of composite, the direction of the fibers dictates the composite properties. The composite is stronger in the longitudinal direction and weaker in the transverse directions. The benefits of these types of composites include higher stiffness, greater strength and an increase in the

1

modulus. An important factor in continuous fiber reinforced composites is the ability to tailor the material properties in a particular direction.

Continuous fiber reinforced composites, both metal- and ceramic-matrix, have been proposed as candidate materials for structural and machine applications because they possess unique combinations of several attractive properties such as high specific stiffness, high specific strength, excellent corrosion resistance and good thermal stability. Ceramic fiber reinforced titanium alloys are of specific interest for aerospace applications because they offer significant improvements in specific strength and stiffness over their monolithic counterparts. They combine the toughness and ductility of metal with the strength and stiffness of a ceramic, in order to create a material having properties that can be tailored for particular applications.

A common family of continuous fiber reinforced composites is titanium-based metal matrix composites, MMCs, reinforced with SiC fibers. This type of material was designed for operating temperatures of 650 °C, with high environmental resistance. The addition of the SiC fibers creates a material with an ultimate tensile strength that is 60% higher than un-reinforced titanium [2]. It is promising for the aerospace industry since it has a density that is 50% of that of Ni based superalloys, its main competitor for high temperature usage [2]. Additionally, the strong silicon carbide fibers, linked with a weak fiber/matrix interface which is typical in this type of composite, provides the potential to control the damage mechanisms in this material.

Titanium-based metal matrix composites, MMCs, reinforced with SiC fibers are fabricated at high temperature in excess of 900 °C [3,4]. During cooldown from a stress-free temperature to room temperature, due to the significantly different coefficients of thermal expansion between the SiC fiber (5×10^{-6} / °C) and Ti alloy matrix material (

$11 \times 10^{-6} / \, ^{\circ}C$) phases [5], residual stresses are built up in both materials. The intensity of these stresses is dependent on the actual consolidation temperature and the cooling rate.[6]. The axial component of the residual stress superimposes directly on the applied stress and directly affects the debonding and fiber bridging processes [5,7, 8, 9, 10]. The compressive radial residual stress is generated in the matrix along the interface and acts as a clamping force, holding the fiber in the matrix and aiding in the transfer of load from the matrix to the fiber during loading of the composite. In some composite systems having weak chemical bonding at the interface, such as SCS-6/Ti-15V-3Al-3Cr-3Sn, the frictional force provided by this compressive stress is a key factor in achieving the load transfer.

The residual stresses can also have a detrimental effect on the composite system. For example, matrix yielding has been observed during cooling 500 $^{\circ}C$ in a SCS-6/Ti-24Al-11Nb (at.%) composite [11]. The cooldown process can result in the generation of radial cracks along the fiber-matrix interface, as observed in SCS-6/Ti-15V-3Al-3Cr-3Sn and SCS-6/Ti-24Al-11Nb [12] composite systems. Similarly, multiple circumferential cracks caused by the thermal expansion mismatch were observed in the matrix near the interface in SCS-6/Ti-24Al-10Nb-3Cr-1Mo due to cool down from 927 $^{\circ}C$ [4]. In order to avoid these problems, the fiber-matrix interface should be able to accommodate the strain mismatch between the fiber and matrix and act as a crack blunting layer to minimize crack propagation [13].

After consolidation, at least three distinct phases are present in a fiber in a unidirectional MMC. The fiber reinforcement is designed as the load-carrying member while the matrix phase serves to hold the fiber and transfer the load from the matrix to the fiber. An interphase region, which develops along the fiber-matrix interface, acts as a bond between the fiber and matrix and enables load transfer. The properties of this region

depend directly upon the chemical, mechanical and thermodynamic nature of the bonding process between the matrix and the fiber materials. The interfacial characteristics, such as the frictional shear stress, τ_s, and debond strength, τ_d, are influenced by elevated temperatures and durations of thermal exposure [14].

The metallurgical processes employed to fabricate continuous fiber-reinforced MMC include casting, plasma spray bonding and diffusion bonding. The casting process involves passing continuous reinforcing fibers through a pot of molten metal or introducing the molten metal into, around and through bundles of fibers by vacuum, gravity pouring or pressure casting . In plasma spray bonding, a layer of fibers is laid on a rotating mandrel and the matrix is deposited on the fibers by plasma spraying. A second layer of fibers is the applied and the operation is repeated until the desired number of layers is completed. Consolidation, by diffusion bonding, of the final layup of alternating layers of metal foils and the reinforcing fibers is achieved by the simultaneous application of heat and pressure in hot isostatic pressing or vacuum hot pressing. The foil-fiber-foil layup method is used for for β-titanium alloys that can be rolled into thin foils without texture effects. Sheets of SiC fibers are created by either weaving the fibers with molybdenum wire, or holding them in place with an organic binder. Layers of Ti foils are alternated with layers of fibers, and then consolidated using a vacuum hot pressing technique.

The extreme reactivity of titanium matrices with the ceramic reinforcing fibers during this fabrication at elevated temperature causes degradation of mechanical properties of the composite material. This problem has been minimized thorough the use of fibers with coating layers, such as BORSIC, SIGMA and SCS, which limit the rate of reaction between the fiber and the titanium matrix. The various processing methods to fabricate MMCs also leads to the formation of micro-defects such as voids and cracks which are

4

likely to propagate under cyclic loading. The degradation of thermally cycled MMCs has been primarily attributed to the formation of reaction products at the fiber/matrix interface leading to stress-strain amplification at the interface [15]. As a result, the fiber/matrix interphase region is the weakest and most highly stressed region in a MMC, becoming a prime source of fatigue cracking.

This introduction presents an overview of the fiber-matrix interface in titanium metal matrix composites reinforced with silicon carbide fibers and the parameters that affect its behavior. The following section discusses damage mechanisms in TiMMCs and the role of the interface on those damage processes, particularly the fiber bridging process. The next section identifies the parameters that define the interface response and their influence on the mechanical properties of the composite. This is followed by a section reviewing the published studies on the fiber-matrix interface region. The last section of the chapter focuses on the various interface debonding theories that have been or are currently being used.

1.2   Damage mechanisms and the role of the interface in TiMMCs

Fiber reinforced Ti-matrix composites are used for elevated temperature applications that subject the composite to cyclic loading. Under cyclic loading conditions, for a single crack propagating perpendicular to the fiber direction (Mode I loading), several distinct damage modes can occur, as shown in Figures 1-1 and 1-2. These modes are governed by the fiber-matrix properties. A weak interface is required for fatigue crack growth resistance, but in the case of an extremely weak interface, full delamination can occur, with the fiber/matrix interface debonding completely as the Mode I crack passes the fiber,

resulting in little work required for fiber pullout, and little effect on the crack growth rate.(Fig. 1-1(a)) A strong interface is desirable for high transverse strength, but a very strong interface will cause the fibers to break simultaneously with the matrix, with no pullout, offering very little improvement over a monolithic material. (Fig. 1-1(b))

(a) full delamination   (b) fiber failure
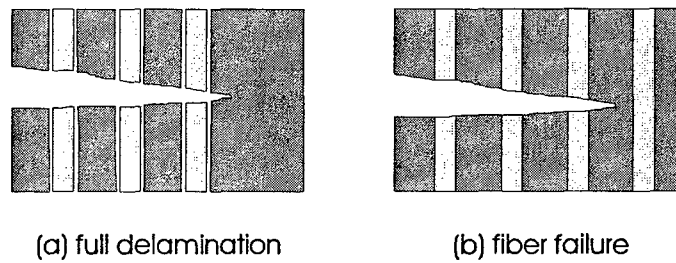
Figure 1-1   Damage modes in TiMMCs, (a) full delamination (very weak interface) (b) fiber failure without delamination (very strong interface)

The full benefit of fiber reinforcement is obtained with strong fibers and a fairly weak interface [5, 16-19]. As the Mode I matrix crack approaches the reinforcing fibers the stress state becomes complicated, due to the mixed mode conditions at the crack tip at this location.[20-22] A large interfacial shear stress is induced by the crack opening displacement, Δu, resulting in the initiation of a debond crack along the interface. [20, 23, 24]. Under certain conditions, the Mode I crack will pass the reinforcing fibers, leaving intact fibers in its wake, as shown in Fig. 1-2. As the matrix crack length increases, the number of these fibers bridging the crack increases. This fiber bridging will lead to an increase in the toughness of the composite due to the reduction of the crack tip intensity

factor as the intact fibers carry some of the load, thus reducing the crack growth rate [17,20].
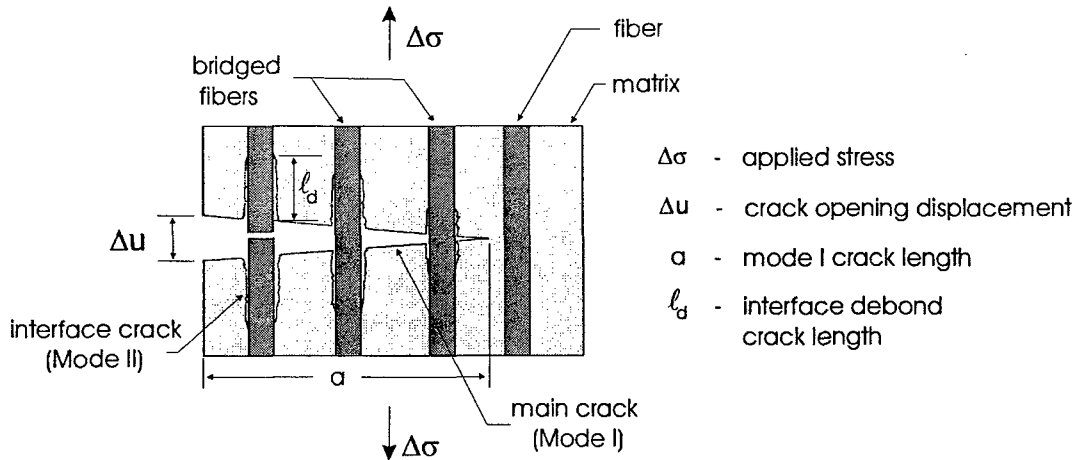
Figure 1-2   Schematic of crack bridging in TiMMC

Fiber bridging is accompanied by sliding of the matrix along the debonded length of the fiber. [20]. The compressive residual stresses at the interface due to the consolidation process causes the two debonded surfaces to contact one another, resulting in the introduction of friction along the interface. Studies have shown that this frictional sliding results in the wear of asperities and deterioration of the interface [25, 26], and that fracture of a bridging fiber is likely to occur in the region where extensive frictional wear of the fiber has occurred. [5, 27, 28].

This process of interface debonding and sliding continues to a steady state condition produced by a balance between the creation of more bridging fibers as the crack length increases and the fracture of those fibers as more stress is transferred from the matrix to the

fibers. This balance controls the next mechanism, either crack arrest or crack acceleration, which is associated with the fracture of one or more bridging fibers, particularly those farthest away from the crack tip, where the fiber stress is highest. Figure 1-3 shows a schematic of a crack growth curve with fiber bridging followed by crack acceleration. The initial portion of the curve, where the crack growth rate decreases with increasing ΔK, is an indication of fiber bridging. This is followed by a transition to crack acceleration, where the crack growth rate increases with increasing ΔK.
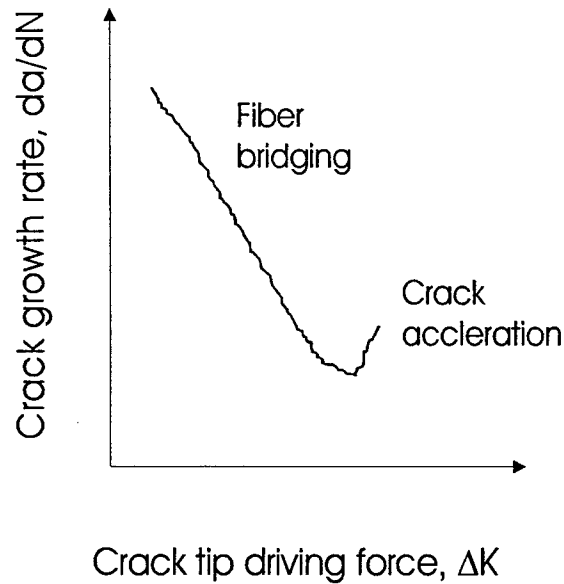
Figure 1-3   Crack growth curve during fiber bridging and transition to crack acceleration

During the fiber bridging process, the applied crack tip driving force, ΔK_{app}, for the Mode I crack can be expressed in terms of the Mode I crack tip driving force of the matrix crack, and a shielding term. The shielding term is a function of the crack length, a, and the closure pressure, Δp. The fiber traction, ΔS, which is related to the closure pressure

through the fiber volume fraction, can be expressed as a function of the elastic stress component resulting from elongation of the bridged fiber due to the crack opening displacement, Δu, and a frictional component corresponding to the frictional forces acting along the debonded length, ℓ_d. The parameters involved in crack tip shielding are shown schematically in Figure 1-4.
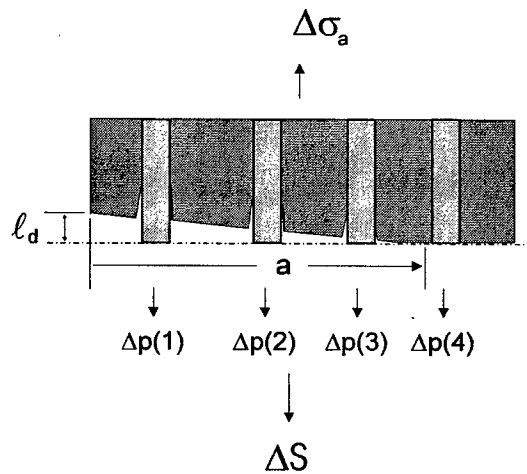
Figure 1-4   Schematic of fiber bridging showing parameters for crack tip shielding

In a monolithic material, for the same applied stress range, the crack growth rate, da/dN, increases as the ΔK, or crack length, increases, as shown in Figure 1-5(a). For a composite in the crack bridging stage, however, the crack growth rate is reduced by the shielding influence of the bridged fibers. This shielding term increases faster than the Mode I matrix crack tip driving force increases, due the increase in the number of bridging fibers as the crack propagates. The effective crack tip driving force is reduced, therefore the crack growth rate decreases with increasing crack length, as illustrated in Figure 1-5(b)

$$\Delta K = Y\Delta\sigma\sqrt{\pi a}$$

$$\Delta K_{eff} = Y\Delta\sigma\sqrt{\pi a} - 2Y\sqrt{\frac{a}{\pi}}\int_{a_o}^{a}\frac{\Delta p(x)}{\sqrt{a^2 - x^2}}dx$$
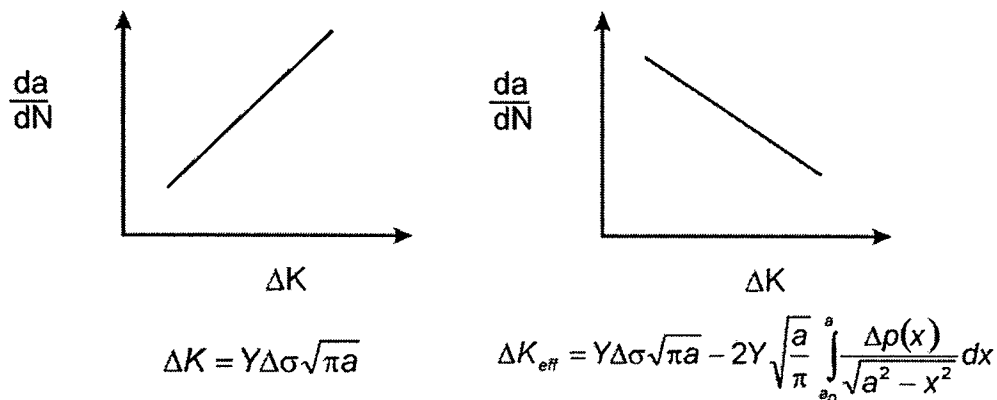
Figure 1-5   Crack growth rate curves for (a) monolithic material, (b) TiMMC during fiber bridging

Studies on several unidirectional fiber-reinforced MMCs, including SCS-6/Ti-6Al-4V, SCS-6/Ti-15V-3Al-3Cr-3Sn (Ti-15-3), SCS-6/Ti-24Al-11Nb (Ti-24-11), SCS-6/Ti-25Al-10Nb-3Cr-1Mo, and SM1240/Timetal®21S have shown that fiber bridging is an operative mechanism under loading conditions of practical interest [5, 12, 29-34]. The extent of the fiber bridging during the crack growth process depends, in addition to the applied stress range, stress ratio, and the fiber strength, on the properties of the fiber/matrix interface. This was shown in the work of Gayda, et al. [35] on SCS-6/Ti15-3 composites at elevated temperature and in the work of McMeeking and Evans [36] on SCS-6/Ti-Al composites.

Additionally, the degradation of thermally cycled MMCs has been primarily attributed to the mismatch of coefficients of thermal expansion between fiber and matrix phase and to the formation of reaction products at the fiber/matrix interface, which lead to a stress-strain amplification at the interface [15].

1.3 Parameters defining interphase response and influence on mechanical properties

The previous section described the damage mechanisms of TiMMCs and the importance of interface debonding, particularly on the fiber bridging process. The factors that influence the fiber/matrix debonding in these materials can be inferred from fatigue crack growth experiments performed on TiMMCs under various test conditions.

The influence of test temperature can be seen in the fatigue crack growth tests performed on several TiMMCs. In a comparison of three point bending tests of single edge notched (SEN) SCS-6/Ti-15-3 specimens at 25 and 500 °C, Cotterill and Bowen found that, for similar loading conditions, crack growth rates were higher at higher temperatures [37]. The fatigue response of a SEN specimen of SiC/Ti-6Al-4V composite exhibits a similar trend of higher crack growth rates at 550 °C than at room temperature [33]. Opposite results were found in fatigue testing carried out on SM1240/Timetal® 21S using center notched specimens by Zheng and Ghonem [38]. Figure 1-6 shows the results of these tests, where the initial crack bridging stage, indicated by the portion of the curve where the crack growth rate, da/dN, is decreasing, is followed by repeated events of crack growth acceleration and retardation. These tests, performed at room temperature, 500 and 650 °C for loading frequencies of 10, 0.1, and 0.02 Hz, show that for the same loading frequency, during the initial crack bridging stage, the crack growth rate decreases with increasing temperature. This behavior is an indication of an increase in the crack tip shielding,

11

suggesting a longer debond length. Additionally, the slope of the crack growth rate curve is lowest in the room temperature case, and highest at 650 °C, suggesting that the crack tip shielding force increases with increasing temperature. These conflicting observations of the effect of elevated temperature on the bridging crack growth rate in different composites could be attributed to the variations in chemical composition at the interface which results in different interphase characteristics, including interphase shear strength, surface roughness of the debonded interface and debonding length.
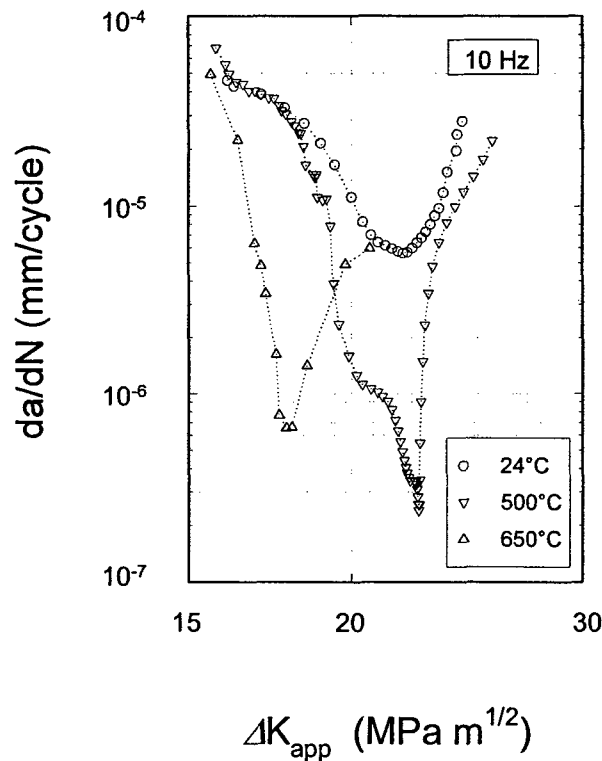
Figure 1-6   Fatigue crack growth of SM1240/Timetal®21S at 23, 500 and 650 °C
for loading frequencies of 10 Hz using center notched specimens [38]

In addition to test temperature, the effect of prior thermal exposure has been shown to affect the fatigue crack growth behavior of metal matrix composites. In a study of

12

SM1240/Timetal®21S [38], the crack growth rates for both as received specimens and those aged for 42 hours at 650 °C were measured at room temperature (see Figure 1-7). Although both samples display identical crack growth rates, the duration of crack bridging is prolonged for the aged sample. This result indicates a delay in the fracture of bridging fibers, which triggers the transition from deceleration to acceleration crack growth rate. This delay is explained as follows. In addition to the expected changes in microstructural properties of the matrix or degradation of the interphase due to thermal exposure, thermal aging of a metal matrix composite, particularly at a temperature as high as 650 °C, could result in decreasing the residual stress acting in the fiber. A separate study on SCS-6/Timetal®21S [39] showed that the decrease in the mean stress for a particular applied stress range, although not influencing the growth rate in the crack bridging stage, causes a delay in reaching a condition of crack growth rate acceleration. This argument is also supported by the results of an investigation of the effect of aging on a B_4C-B/Ti-6Al-4V composite using a single edge-notched (SEN) specimen [20].In the as-received specimen, Mode I cracking was observed. However, in a specimen that was thermally exposed for 7 days at 500 °C, crack growth occurred both across the fiber and along the fiber/matrix interfaces. Thermal exposure was found to increase the amount of crack growth along the interface. Interface debonding occurred while the main crack was relatively far from the interface (typically 80 to 100 μm at ΔK=32 MPa/√m). In the as-received specimen, on the other hand, a crack much closer to the interface (as close as 20 μm at ΔK=22 MPa/√m) did not cause debonding. This reflects the higher interface strength in the latter case. Chan [40] also proposed that the lowering of the interphase shear strength value due to thermal exposure would favor intensive interface cracking and crack bridging mechanisms over fracture of fibers, provided that thermal exposure does not degrade the fiber strength.
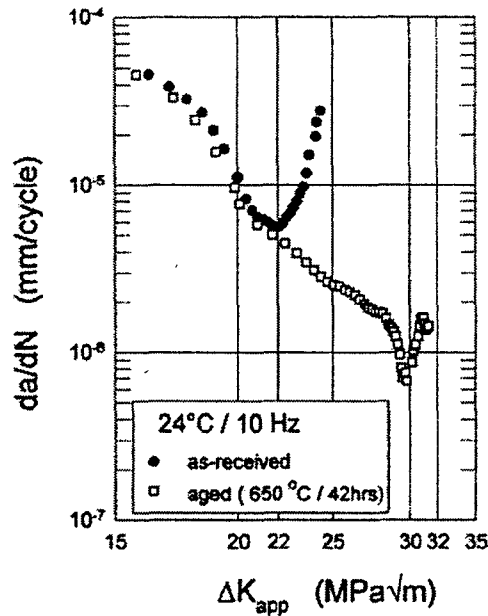
Figure 1-7   Fatigue crack growth of SM1240/Timetal-21S in as-received condition

and thermally aged for 42 hours at 650 °C at room temperature

Environmental exposure also has been shown to affect the fatigue crack growth rate in

TiMMCs. In testing done at 650 °C on SM1240/Timetal-21S [38] , shown in Figure 1-8,

the crack growth rate during the fiber bridging stage for the specimen tested in air was

lower than that for the specimen tested in vacuum. This indictes that, at elevated

temperature, exposure to the environment leads to a higher crack tip shielding, again

suggesting a longer debond length, or a weaker fiber/matrix interfce strength.

14
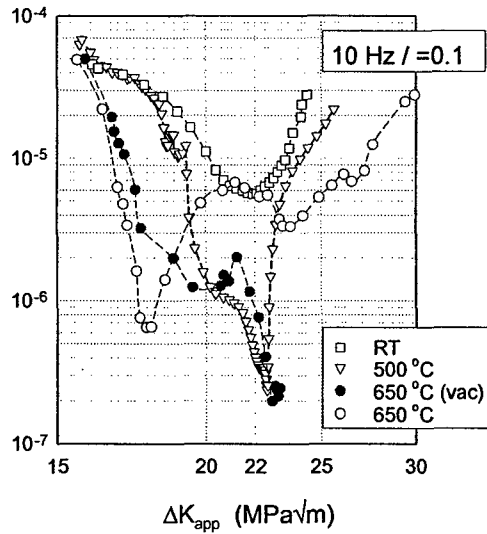
Figure 1-8   Fatigue crack growth of SM1240/Timetal-21S in vacuum and air

These studies indicate that the fiber/matrix debonding behavior of TiMMCs is affected by several parameters, including test temperature, thermal aging, and environmental exposure. These parameters, in addition to changing the actual properties of the composite constituents, affect the residual stress state in the composite. The usage temperature plays a factor in the behavior of the interface, as the residual stresses in the composite will decrease with increasing temperature. This phenomenon was observed by Eldridge and Ebihara [14] who tested an unaged SCS-6/Ti-24-11 intermetallic composite and found a decrease in fiber pushout load with increasing test temperature. Numerical results in finite element analysis of fiber pushout tests by Ananth and Chandra [41] also showed a decrease in peak pushout load with increasing temperature.

Additionally, the residual stress state is a function of the consolidation parameters of temperature, pressure and cooling rate. During cooldown from the consolidation

15

temperature, the residual stresses in the composite are established. The radial compressive stresses, which build up in the matrix, provide a "clamping force" which holds the fiber in the matrix and aid in the transfer of load from the matrix to the fiber during composite loading. Since little chemical bonding occurs between the fiber and/or fiber coatings and the matrix, the interface strength is predominantly a function of these compressive stresses at the fiber/matrix interphase. Changes in the consolidation temperature or cooling rate could change the residual stresses, as it would allow more or less time for these stresses to build up.

1.4   Review of Interphase Studies

Researchers have predominantly looked at the problem of understanding fiber/matrix interface behavior in metal matrix composites from an experimental viewpoint. Typically, studies focus on either the kinetics of the interphase itself, including the effect of temperature and environment on the size and composition of the interphase, or on the parameters governing the debonding of the fiber/matrix interface. This section will review both of these types of studies.

. In order to understand the interfacial behavior of fiber-reinforced composites, much attention has been focused on the interphase, the brittle reaction zone formed during the prolonged time and temperature of consolidation due to the chemical reactions between the constituents of the fiber, coating and matrix. Many studies have been performed involving interfacial kinetics at various aging times and temperature in order to try to characterize this behavior, which varies for different composite systems. Using transmission electron microscopy (TEM), Lerch [42], et al showed an interphase thickness of 0.10-0.35 μm for

unaged Ti-15-3 reinforced with SCS-6 fibers. Through chemical analysis, they found that the main constituents on the fiber side of the reaction zone were Ti and C, probably TiC, while the matrix side of the interphase consisted of Ti and Si, assumed to be titanium silicides. Rhodes, et al [43], in a study of fiber/matrix reactions in two types of SCS-6/Ti composites, noted that carbon diffuses much more quickly in beta titanium that in alpha titanium. They observed a reaction zone size of approximately 1 μm in SCS-6/Ti-1100 and of 1.5 μm in SCS-6/β21S. For both composite systems, they report the interphase to be a mixture of titanium carbides (TiC) and titanium silicides (Ti_5Si_3). Reeves et al. [44] found similar interphase chemical composition particulate-reinforced composites produced from Ti and SiC powders.

Additional temperature exposure after consolidation has been found to increase in the size of the interphase [22-24]. Yang and Jeng [45], in a study of the titanium aluminides Ti-24-11 and Ti-25-10, and a metastable beta titanium Ti-15-3, all reinforced with SCS-6 fibers, observed an increase in the reaction zone size with exposure time for the composites heat treated at 700 to 1000 °C. They report that the thickness of the reaction zone increases linearly with the square root of time at a given temperature, suggesting that the reaction is controlled mainly by diffusion. The reaction rates increase slowly at temperatures below 900 °C, but dramatically at higher temperatures. For temperatures from 800–950 °C, the reaction obeys an Arrhenius law: $k = k_o e^{-Q/RT}$, where the activation energy, Q, can be obtained as the slope of: $ln(k) = f(T^{-1})$. Morel [46] studied the reaction kinetics of SCS-6/Ti-15-3-3 in vacuum at temperatures from 600 to 950 °C for times ranging from 4 to 96 hours. As with Yang and Jeng, he found that for a given temperature, the reaction zone thickness increased linearly as a function of the square root of time, observing reaction

17

zone thickness as large as 18 mm at 950°C after approximately 100 hours thermal exposure. Gundel and Wawner [47] studied the effects of vacuum thermal exposure from 700 to 1100 °C in SCS-6 reinforced Ti-1100, β21S, Ti-6-4, Ti-15-3 and Ti-14Al-21Nb. They found a similar relationship between thickness and exposure time, reporting reaction zone thickness ranging from 0.7 mm for Ti-1100 to 2.1 mm for Ti-6-4 after 1000 hours at 700 °C. Thermal exposure of pure titanium reinforced with SCS-6 fibers, at temperatures above and below the beta transus temperature of 882 °C, showed that although the beta and alpha phase react differently with the fiber coatings at different temperatures, the effect of alloying elements has a greater effect on the on the reactivity at the interface than the Ti phase present.

Changes in interface reaction zone size due to prolonged thermal exposure, such as those described above, could potentially lead to changes in the stress state and subsequently in the interfacial properties of the composite. An example of such changes are seen in studies done by Watson and Clyne [48], who observed an increase in the frictional sliding resistance during pushout testing with increased aging time. Additionally, in fatigue testing on SCS-6/Timetal®21S composites, Zhang and Ghonem [49] observed that crack growth rates during the initial crack bridging stage decreased with increased aging time, suggesting that the aging changed the interface properties. Conversely, elevated temperature during testing and applications of this material leads to a relaxation of the residual stresses due to time dependent flow of the matrix material, which in turn influences the interphase mechanical response [27].

In addition to studies of the kinetics of the interphase, attention has also focused on the debonding mechanisms of the fiber/matrix interface. Three categories of experimental techniques are commonly used, which yield global values for the interphase properties,

18

including shear strength and frictional shear stress along a debonded interface. These include fiber pullout, fiber indention, and "thin slice" fiber pushout. Each method has unique advantages, disadvantages, limitations and problems with data interpretation.

Fiber pullout   Fiber Indention   Fiber Pushout
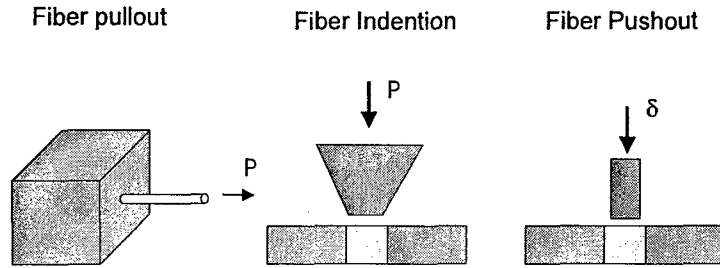
Figure 1-9   Schematic of experimental techniques for determining
               interface properties

Single fiber pullout [50-53], shown in Figure 1-6(a), most closely represents the actual conditions in a fiber and the surrounding matrix during crack bridging, but special fabrication of the material may not reproduce the residual stress state in an actual composite. In this method, a single fiber is embedded along the length of a block of matrix material, with one end protruding. The matrix material is then clamped, and a uniaxial tensile load is applied to the free end of the fiber until debonding takes place. An alternate approach is to etch away the matrix material from an existing composite, then cut away all but one fiber for testing.[54] Some drawback to this technique are that reproduction of results is difficult due to difficulties in alignment of the applied load with the direction of the fiber and that testing is limited to one fiber per specimen. The latter problem is a major concern, not only because of the time required to prepare additional specimens, but because, due to the variation in local stresses in a composite, an average of several tests within one specimen is necessary in order to get an accurate property measurement.

19

Fiber indention methods, illustrated in Figure 1-6(b), which were first introduced by Marshall [55], allow the use of already fabricated composite samples. Sample preparation involves cutting, and polishing a "slice" of composite material. This specimen is then clamped in such a way that a single fiber can be loaded. Increments of increasing load are applied with an indentor, usually either a microhardness indentor or nano indentor until fiber debonding is observed. The load is then removed and the penetration of the tip into the matrix is measured and subtracted from the total tip movement to yield displacement of the fiber. Yang, et al [56] used this technique to measure the interfacial debond strength in Ti-25-10, Ti-15-3, and Ti-6-4, all reinforced with SCS-6 fibers, and Ti-6-4 reinforced with SM1240 fibers. They reported debond shear strengths varying from 85 to 153 MPa, depending on the fiber/matrix combination and aging condition, and noted that the fiber surface chemistry dominates the interfacial properties of the composite. An advantage of this technique is that many sets of data can be obtained from a single specimen. The main disadvantage is that, due to static loading, no information is available for the frictional sliding portion of the debonding process.

"Thin slice" single fiber pushout methods [17, 26, 48, 57], shown in Figure 1-6(c), are a variation of the indention method, using specimens prepared in a manner similar to those used in fiber indention tests, although generally thinner. This technique involves the application of a continuous load to the fiber, while recording the applied force vs. punch displacement. Loading originally was done with an Instron type machine, but recently a desktop fiber pushout device was designed to allow testing at elevated temperatures in vacuum environment [14]. Since the load is continuous and the punch is smaller than the diameter of the fiber, "thin slice" fiber pushout tests allow the constant monitoring of load vs. displacement as the fiber pushout progresses from the debonding through the frictional

sliding stage, thereby yielding a more complete picture of the fiber debonding process. This technique also allows collection of a large data set from a single specimen.

Testing has shown that fiber pullout and fiber pushout methods do not produce similar results, even under the same conditions. For the same embedded fiber length, the stress required for fiber pushout has been shown to be greater than that for pullout, due to the difference in the Poisson effect for each type of loading [18]. During pushout, the Poisson effect causes an expansion of the fiber, which increases the clamping stress on the fiber, especially noticeable during frictional sliding. Conversely, during fiber pullout, the Poisson effect causes a reduction in the fiber diameter, thereby reducing the clamping force and decreasing the effect of friction during sliding. It has been shown that pushout and pullout tests will yield similar results if the Poisson effect is not considered [50]. Analytical methods have been developed for the interpretation of data obtained from fiber pushout or pullout testing. [8,51]

Several researchers have used and analyzed the fiber pushout technique as a means to study the interface behavior of fiber reinforced composites. Watson and Clyne [48] used the fiber pushout method to determine the load needed to push a fiber out of the matrix as a function of its aspect ratio, in Ti-6-4 reinforced with SM1240 fibers. They found that the onset of resistance to frictional sliding determined the pushout load. Hsueh [35] analytically studied the mechanical properties of the fiber/matrix interface using an SCS-6/Al_2O_3 composite and found that the interfacial shear stress increases as the coefficient of friction, radial clamping stress and Poisson's ratio of the fiber increase. Ananth and Chandra [41], through numerical simulations, found that specimen thickness, as well as frictional conditions at the interface, affect the debonding behavior of a composite during fiber pushout testing. Mackin, et al [57] modeled the effect of asperities at the fiber/matrix

during fiber pushout testing, explaining the initial increase in sliding stress after debonding that has been seen experimentally.

Although it has been established that test temperature plays a factor in the behavior of the interface, there has been little experimental work done to investigate the interfacial behavior in fiber reinforced composites at high temperatures. Recently Eldridge [14] used a high temperature pushout technique to study the temperature dependence of fiber debonding and sliding in intermetallic and metallic matrix composites. These studies revealed a decrease in fiber pushout load with increasing temperature only at temperatures above 400 °C. A possible change in location of the initiation of the debonding crack along the interface, or a change in the location of the maximum total shear stress at higher temperatures, was proposed as a possible explanation for this behavior. In another study, Eldridge and Ebihara [14] tested an unaged SCS-6/Ti-24-11 intermetallic composite and found a decrease in fiber pushout load with increasing test temperature. Numerical results in finite element analysis of fiber pushout tests by Ananth and Chandra [41] also showed a decrease in peak pushout load with increasing temperature. More studies need to be done to explain the effect of temperature on the debonding behavior of these materials.

Additionally, Eldridge has shown that for some composites, the testing environment has an effect on the debonding behavior of the interphase. In fiber pushout studies of several composites in room air, dry air, nitrogen, and vacuum, he showed that the effect of environment, although small, was still significant. Also, it was shown that it is not air, but actually moisture in the air, that is the main cause of this environmental effect. The addition of heat to this environmental effect has not yet been studied.

1.5 Interface Debonding Theories

When a crack propagating through a monolithic material reaches an interface between two dissimilar materials, such as the fiber matrix interface, in order for propagation to continue, either the crack must deflect along the interface, or it will continue through the interface and penetrate the fiber. Which of these behaviors the crack exhibits depends on the properties of each of the two materials as well as those of the interface. Many researchers have tried to find a simple solution to predict the behavior of a crack in this bimaterial interface region. Debonding theories fall into two main categories, depending on the type of criteria that is used. Fracture based theories use a value of interface toughness, calculated from material properties of fiber, matrix and interface, to predict the single point where the interface failure will occur. On the other hand, energy based theories consider interface decohesion to occur over a range displacement values.

In terms of fracture parameters, the problem of fracture at a bimaterial interface has been studied for many years. In 1959, Williams [58] discovered that the stresses near the crack tip along a bimaterial interface exhibit an oscillatory behavior that is a function of the distance from the crack tip and the material constants. Sih and Rice [59] saw similar behavior in a crack subjected to bending loads. This oscillatory motion leads to interpenetration of crack faces behind the crack tip [22, 60], which is physically unrealistic. Rice and Sih [22] used an open tip interface crack configuration to get a closed form solution for the analysis of an infinite plate with a crack and gave stress intensity factors for this situation. Hutchinson, et al [61] dealt with the problem by considering that the oscillations and interpenetration occurred very close to the crack tip, within the plastic zone. They derived equations for cracks propagating near and parallel to a bimaterial interface in terms of a complex stress intensity vector. Chan and Davison [21], also using

23

an open-tip interface crack configuration, proposed the use of an equivalent stress intensity range, and correlated it to fatigue crack growth data for fiber reinforced composites.

These studies illustrate a problem which exists when using stress intensity factors as the controlling parameters in fracture analysis of the bimaterial interface. Due to the modulus mismatch between the fiber and matrix, a combination of Mode I and Mode II loading occurs at the interface, even if the xternal loading is tension or pure shear. For uniaxial loading, the mode mixity at the interface crack tip is a combination of the local stress intensity factors, $\Psi = \tan^{-1}(K_2/K_1)$, while in a homogeneous material, only one parameter, K_{Ic}, would be necessary to describe the interface fracture mechanics.[62]

This difficulty can be resolved through the use of the interface toughness, or crack tip driving force, G, as the controlling parameter to predict to interface fracture. A study done by Hutchinson showed that when an interface crack is introduced along a thin layer of material within a block of a second material, the local crack tip driving force, G, for the interface crack, is the same as that for a crack propagating through a block of the second material. In this case, the local stress intensity factors are different, but the local crack tip driving force, which is a function of the mode mixity, Ψ, is the same. He and Hutchinson [63] did extensive work comparing the energy release rates of a deflected crack with that of a penetrating crack. They supplied a range of interface toughness values relative to material toughness that would ensure the crack was deflected into the interface. Building on this work, Chan [24] established failure diagrams for uniaxial composites, establishing the failure mode based on composite properties at room temperature.

The main drawback to this type of fracture based approach to interface debonding is that it was created for use on ceramic matrix composites, where the properties are purely elastic. The interface failure is sudden, at a single applied stress level. While this may be a

24

good estimate of the debonding process in fiber-reinforced metal matrix composites, the effect of the plastic behavior of the matrix material is ignored. Additionally, while these analytical studies provided an understanding of the behavior of a crack near a bimaterial interface, a need existed for a simple means of modeling this behavior on a micromechanical scale. Linear elastic fracture mechanics is not adequate for analysis of this behavior, since it cannot deal with the problem of crack tip singularity. Analysis by this theory shows that the stresses at the crack tip are infinite and the material will fail at an infinitesimally small load. This is obviously not an accurate description of the physical phenomena.

For this reason, the cohesive zone model, an energy-based approach, was developed. This model deals with the area of the crack tip as a zone where the separation of the interface crack surfaces are related to the traction along the interface in a non-linear fashion. The cohesive zone model expresses the dependence of the normal or tangential tractions on the interface as a function of the normal or tangential displacements across the interface. In tis type of model, the normal and shear decohesion occur independently. As separation of the interface progresses, the traction across the interface first increases then decreases until complete separation is achieved. Although this traction-displacement relationship can be of any form, typically exponential and bilinear relationships are chosen. A separate relationship is used for decohesion in the normal and tangential direction. The fracture energy, which is equal to the area under this traction-displacement curve, is a measure of the interface toughness, G, in the specified direction.

The cohesive zone concept was used by Needleman [64] to describe the process of void nucleation from initial debonding through complete separation.. Due to dimensional considerations, a characteristic length was introduced, which corresponds to the

displacement at complete interface separation. Tvergaard [65, 66] applied this concept to whisker reinforced metal matrix composites in various fiber configurations. In these models, the debonding was described by decohesion in both the normal and tangential direction, and friction along the debonded portion of the interface was also considered.

1.6 Research Objectives

Prediction of damage in fiber reinforced composite materials requires knowledge, not only of the strain energy release rate at the crack tip as it propagates through the matrix, but also the characteristics of interphase debonding which occur along the length of the bridging fiber in the crack wake. Models exist that describe the global behavior of a composite during the crack growth process based on global characteristics of the fiber and matrix [18,40,43,44]. However, the contribution of the interface behavior to this process is not adequately described, leading to an incomplete understanding of the fiber bridging process and the influence of the interface on off-axis loading. Additionally, most of the experimental data that is available is based on the room temperature debonding behavior of the interphase, while the typical operating temperature of this material is in the 500-650 °C range[35].

The objective of this study is to investigate the interphase properties and mechanics of Ti-MMCs, in both the longitudinal and transverse direction under typical service conditions. These conditions will be selected in a manner that will establish the evolution pattern of the critical properties during the consolidation/cooldown path. The effect on these properties of processing conditions, including standard heat treatment as well as thermal and room temperature aging in air and vacuum are investigated. Temperature dependency of the interphase debond shear strength and frictional shear stress has been

investigated through a series of room and elevated temperature fiber pushout tests for both vacuum aged and unaged conditions. These properties are used to predict the controlling failure mode in the MMC systems under consideration. Finally, by coupling the experimental data with an analytical and numerical approach, the interface fracture energy will be established in the longitudinal and transverse directions, as functions of temperature, thermal exosure and environment.

The results of this study, provided in the following chapters, will provide the basic parameters required in modeling the interface debonding behavior of the interface for a range of practical temperatures and loading conditions. In doing so, this research will contribute to the fundamental understanding of the role of various loading factors on the damage response of fiber reinforced composite systems.

The following chapter, Chapter 2, examines the effect of temperature on the interphase behavior of the Ti-MMC system. Several parameters and the influence on these of temperature are investigated in relation to their effect on the debonding of the interface. These parameters include elevated temperature properties in both the longitudinal and transverse direction. The effect of aging in air and vacuum on the interface size and its subsequent influence on the tangential properties is investigated. Additionally, the effect of varying fiber volume fraction on the debonding behavior of the fiber/matrix interface is also examined.

Chapter 3 investigates the relationship between the processing parameters and the debonding behavior of the Ti-MMC. These parameters include the processing temperature and pressure. A numerical concentric cylinder model is used to investigate the residual stress built up in the composite during processing. The effect on these residual stresses of

considering the material to be purely elastic, elastic-plastic, and viscoplastic is also investigated.

Chapter 4 details the effect of high temperature interphase properties on damage mechanisms in the Ti-MMC composite. A temperature dependent damage map is constructed which divides damage mechanisms into regions based on material properties and knowledge of the relationship between interfacial properties. The regions considered are bridging, limited debonding followed by fiber fracture, and matrix yielding followed by fiber fracture.

Chapter 5 focuses on the extraction of debonding parameters, particularly the interface fracture toughness, from a numerical simulation of the debonding process. Comparison of the experimentally obtained and numerically generated data allows the quantification of the parameters necessary to accurately simulate the debonding of an interface under various loading and temperature conditions. A discussion of the numerical model, including the application of the decohesion properties and friction, is included.

1.7   References

[1]   Smith, P. R., and Fores, F. H., Developments in Titanium MMC, *Journal of Metals*, March, 1984

[2]   [Mall98].

[3]   Yang, J.M., Jeng, S.M., Yang, C.J., "Failure Mechanisms of Fiber Reinforced Titanium Alloy Matrix Composites, Part I: Interfacial Behavior," *Materials Science and Engineering*, Vol. A138, pp. 155-167, 1991

[4]   Sohi, M., Adams, J., Mahapatra, R., "Transverse Constitutive Response of Titanium-Aluminum Metal Matrix Composites," Constitutive Laws for Engineering Materials, C.D. Desai, ed., ASME Press, New York, NY, pp. 617-626, 1991

[5]   Davidson, D.L., "The Micromechanics of fatigue Crack Growth at 25 °C in Ti-6Al-4V Reinforced with SCS-6 Fibers," *Metallurgical Transactions*, Vol. 23A, pp. 865-879, 1992

[6]   Mirdamadi, M., Johnson, W.S., Bahei-El-Din, Y.A., and Castelli, M.G., "Analysis of the Thermomechanical Fatigue of Unidirectional Titanium Metal Matrix Composites," *Fatigue and Fracture, ASTM Spec Publ*, No. 1156, pp. 591-607, 1993

[7]   Hsueh, C. H., "Evaluation of Interfacial Shear Strength, Residual Clamping Stress and Coefficient of Friction for Fiber-Reinforced Ceramic Composites," *Acta Met. et Mat.*, Vol. 38, 1990, pp.403-409

[8]   Kerans, R. J., and Parthasarathy, T.A., "Theoretical Analysis of the Fiber Pullout and Pushout Tests," *Journal of the American Ceramic Society*, Vol. 74, pp.1585-1596, 1991

[9]   Marshall, D.B., Cox, B.N., and Evans, A.G., "The Mechanics of Matrix Cracking in Brittle-Matrix Fiber Composites," *Acta Metallurigica*, Vol. 33, No. 11, 1985, pp. 2013, 2021

[10]   Sensmeier, M.D., Wright, P.K., "The Effect of Fiber Bridging on Fatigue Crack Growth in Titanium Matrix Composites," in Fundamental Relati9onships Betweeen Microstructure & Mechanical Properties of Metal-Matrix Composites, P.K. Liaw and M.N. Gungor, eds. The Minerals, Metals, and Materials Society, pp. 441-457, 1990

[11]   Saigal, A., Kupperman, D.S., Majumdar, "Residual Strain in Titanium Matris High-Temperature Composites,", *Materials Science and Engineering*, 16, pp. 59-66, 1992

[12].   Brindley, P.K., Draper, S.L., Eldridge, J.I., Nathal, M.V. and Arnold, S.M., "The Effect of Temperature on the Deformation and Fracture of SiC/Ti-24Al-11Nb," *Metallurgical Transaction*, Vol.23A, pp.2527-2540, 1992

[13]   Agarwal, B.D., Broutman, L.J., Analysis and Performance of Fiber Composites, John Wiley & Sons, Inc., New York, NY, 1990

[14]   Eldridge, J.I., Ebihara, B.T., "Fiber Pushout Testing Apparatus for Elevated Temperatures," *Journal of Materials Research*, Vol. 9, No. 4, pp. 1035-1042, 1994

[15]   Kyno, T., Kuroda, E., Kitamuru, A., Mori, T., and Taya, M., "Effects of Thermal Cycling on Properteis of Carbon Fiber/Aluminum Composites," *Journal of Engineering Materials and Technology*, Vol. 110, pp. 89-95, 1989

[16]   Campbell, M.D., Cherry, B.W., "Fatigue Crack Propagation in Fibre Reinforced Composite Materials," Fracture Mechanics and Technology proceedings

[17]   Cox, B.N., Marshall, D.B., "Overview No. 111: Concepts for Bridged Cracks in Fracture and Fatigue," *Acta. metall. mater.*, Vol. 42, No. 2, pp. 341-363, 1994

[18]   Walls, D., Bao, G., Zok, F., "Fatigue Crack Growth in a Ti/SiC Composite," *Fatigue of Advanced Materials*, pp. 343-356, January 1991

[19]   Tamin, M.N. and Ghonem, H., "Evolution of Bridging Fiber Stress in Titanium Metal Composites at Elevated Temperature," *Advances in Fatigue Lifetime Predictive Technique, 3rd Volume, ASTM STP 1292*, M.R. Mitchell and R.W. Landgraf, eds., American Society for Testing and Materials, pp. 24-38, 1996

[20]   Chan, K.S., and Davidson, D.L., "Effects of Interfacial Strength on Fatigue Crack Growth in a Fiber-Reinforced Ti-Alloy Composite," *Metallurgical Transactions A*, Vol. 21A, pp. 1603-1612, June 1990

[21]   Chan, K.S. and Davidson, D.L., "Driving Force for Composite Interface Fatigue Cracks," *Engineering Fracture Mechnaics*, Vol 33, No 3, pp. 451-466, 1989

[22]   Rice, J.R., Sih, G.C., "Plane Problems of Cracks in Dissimilar Media", *Journal of Applied Mechanics*, pp.418-423, June 1965

[23]   Warrier, S.G., Majumdar, B.S., and Miracle, D.B., "Interface Effects on Crack Deflection and Bridging During Fatigue Crack Growth of Titanium Matrix Composites," *Acta Metallurgica*, Vol. 45, No. 12, pp.4969-4980, 1997

[24]   Chan, K.S., "Failure Diagrams for Unidirectional Fiber Metal-Matrix Composites," *Metallurgical Transactions A*, Vol. 24A, pp. 1531-1542, July 1993

[25]   Kantzos, P., Ghosn, L. and Telesman, J., "The Effect of Degradation of the Interface and Fiber Properties on Crack Bridging," *HITEMP Review*, Vol. 2, Cleveland, OH, pp. 32-1 -32-14, 1992

[26]   Warren, P.D., Mackin, T.J., Evans, A.G., "Design , Analysis and Application of an Improved Push-Through Test for the Measurement of Interface Properties in Composites," *Acta. metall. mater.*, Vol. 40, No. 6, pp. 1243-1249, 1992

[27]   Thouless, M.D., Sbaizero, O, Sigl, L.,Evan, A.G., Effect of Interface Mechanical Properties on Pullout in a SiC-fiber-reinfirced Lithium Aluminum Silicate Glass-Ceramic," J. Amer. Ceram. 36, pp 517, 1989

[28]   Jeng, S.M, Nguyen, T-H., Dana, O., Yang, J-M., "Fatigue cracking of fiber-reinforced titanium matrix composites," *Journal of Composites Technology & Research*, v 15, n 3, p 217-224, 1993

[29]   Telesman, J., Ghosn, L.J. and Kantzos, P., "Methodology for Prediction of Fiber Bridging Effects in Composites," *Journal of Composites Technology and Research*, Vol. 15, No. 3, pp. 234-241, 1993

30

[30] Bakuckas, J.G. and Johnson, W.S., "Application of Fiber Bridging Model in Fatigue Crack Growth in Unidirectional Titanium Matrix Composites," *Journal of Composites Technology and Research*, Vol. 15, No. 3, pp.242-255, 1993

[31] Jeng, S.M., Allassoeur, P and Yang, J.-M., "Fracture Mechanisms of Fiber Reinforced Titanium Alloy Matrix Composites. V. Fatigue Crack Propagation," *Material Science and Engineering*, A154, pp.11-19, 1992

[32] Bowen, P., Ibbotson, A.R. and Beevers, C.J., "Characterization of Crack Growth in Continuous Fibre Reinforced Titanium Based Composites under Cyclic Loading," in *Fatigue of Advanced Materials*, R.O. Ritchie, R.H. Dauskardt and B.N. Cox, eds., MCE, Birmingham, AL, pp. 379-394, 1991

[33] Ibbotson, A.R., Bowen, P. and Beevers, C.J., "Cyclic Fatigue Resistance of Fiber Reinforced Titanium Metal Matrix Composites at Ambient and Elevated Temperature," *Proceedings of the 7th Titanium Conference*, San Diego, CA, July, 1992

[34] Zheng, D., Ghonem, H., "High temperature/High Frequency Fatigue Crack Growth Damage Mechanisms in Titanium Metal Matrix Composites," in *Life Prediction Methodology for Titanium Matrix Composites, ASTM STP 1253*, W.S. Johnson, J.M. Larson and B.N. Cox, eds., American Society for Testing and Materials, Philadelphia, PA, 1995

[35] Gayda, J., Gabb, T.P. and Freed, A.D., "The isothermal Fatigue Behavior of a Unidirectional SiC/Ti Composite and the Ti Alloy Matrix" in *Fundamental Relationships Between Microstructure and Properties of Metal Matrix Composites*, P.K.Liaw and M.N. Gungor, eds., The Mineral, Metal and Materials Society, Warrendale, PA, pp. 497-513, 1990

[36] McMeeking, R.M. and Evans, A.G., "Matrix Fatigue Cracking in Fiber Composites," Mechanics of Materials, Vol. 9, pp.217-227, 1990

[37] Cotterill, P.J. and Bowen, P., "Fatigue Crack Growth in a Fibre-Reinforced Titanium MMC at Ambient and Elevated temperature," *Composites*, Vol.24, No.3, pp. 214-221, 1993

[38] Zheng, D. and Ghonem, H. "Fatigue Crack Growth of SM1240/Timetal-21S Metal Matrix Composites at Elevated Temperature," *Metallurgical and Material Transactions A*, Vol. 26A, pp. 2469-2478, 1995

[39] Ghonem, H., "Isothermal and Thermomechanical Fatigue Crack Growth in Metal Matrix Composites," Mechanics of Materials Laboratory, University of Rhode Island, Report: MML-95-4, March 1996

31

[40] Chan, K.S., "Effects of Interface Degradation on Fiber Bridging of Composite Fatigue Cracks," *Acta Metall. Mater.*, Vol.41, pp. 761-768, 1993

[41] Ananth, C.R. and Chandra, N., "Numerical Modeling of Fiber Push-out Test in Metallic and Intermetallic Matrix Composites - Mechanics of the Failure Process," *Journal of Composite Materials*, Vol. 29, No. 11, pp. 1488-1514, 1995

[42] Lerch, B.A., Hull, D.R., Leonhardt, T.A., "Microstructure of a SiC/Ti-15-3 composite", *Composites*, Vol. 21, No 3, pp.216-224, May 1990

[43] Rhodes, C.G., and Spurling, R.A., "Fiber/matrix Interface Reactions on Sic Reinforced Titanium Alloys", *Developments in Metal Matrix Composites*, Kamleshwar Upadhya, ed., The Minerals, Metals, and Materials Society, pp. 99-113, 1991

[44] Reeves, A.J., Dunlop, H., and Clyne, T.W., "The Effect of Interfacial Reaction Layer Thickness on Fracture of Titanium-SiC Particulate Composites" *Metallurgical Transactions A,* Vol. 23A, pp. 977-988, March 1992

[45] Yang, J.-M., Jeng, S.M., "Interfacial Reactions in Titanium-Matrix Composites", *Journal of Metals*, pp. 56-59, November 1989

[46] Morel, D.E., "Reaction Kinetics in Continuous Silicon Carbide Reinforced Titanium 15V-3Cr-3Al-3Sn", *Journal of Materials Engineering*, Vol.13, No.4, pp.251-255, 1991

[47] Gundel, D.B., Wawner, F.E., "Interfacial Reaction Kinetics of Coated SiC Fibers with Various Titanium Alloys", *Scripta Metallurgical et Material*, Vol. 25, pp. 437-441, 1991

[48] Watson, M.C., Clyne, T.W., "The Use of Pushout Testing to Investigate the Interfacial Mechanical Properties of Ti-SiC Monofilament Composites," 7th World Titanium Conference, San Diego, June 1992

[49] Zhang, T. and Ghonem, H., "Time-Dependent Fatigue Crack Growth in Titanium Metal Matrix Composites," *Fatigue and Fracture of Engineering Materials and Structures*, Vol.18, No. 11, pp. 1249-1262, 1995

[50] Takaku, A. and Arridge, RGC, "The Effect of Interfacial Radial and Shear Stress in Fibre Pull-out in Composite Materials," *J. Phys. D: Appl. Phys.*, Vol. 6, pp. 2038-2047, 1973

[51] Marshall, D., "Analysis of Fiber Debonding and Sliding Experiments in Brittle Matrix Composites," *Acta metall. mater.*, Vol. 40, No. 3, pp. 427-441, 1992

[52] Cho, C., Holmes, J., Barber, J., "Estimation of Interfacial Shear in Ceramic Composites from Frictional Heating Measurements," *Journal of the American Ceramics Society*, Vol. 74, No. 11, pp. 2802-2808, 1991

[53] Verma, R. Gosh, A.K., Merrick, H., Mukherji, T., "Measurement of interfacial shear properties of composites of Ti-1100 alloy reinforced with SCS-6 SiC monofilament fiber," *Materials Science and Engineering*, Vol A91, pp151-163, 1995

[54] Marshall, D.B., Shaw, M.C., Morris, W.L., Graves, J., "Interfacial Properties and Residual Stresses in Titanium and Titanium Aluminide Matrix Composites," *Workshop proceedings on Titanium Matrix Components*, P.R. Smith and W.C. Revelos, eds., Wright-Patterson AFB, OH, pp. 329-347, 1991

[55] Marshall, D.B., and Oliver, W.C., "Measurement of Interfacial Mechanical Properties in Fiber Reinforced Ceramic Composites," *Journal of American Ceramic Society*, Vol.70, No.8, pp. 542-548, 1987

[56] Yang, C.J., Jeng, S.M., Yang, J.-M., "Interfacial Properties Measurements for SiC Fiber-ReinforcedTitanium Alloy Composites," *Scripta Metallurgica et Materialia*, Vol. A24, pp. 469-474, 1990

[57] Mackin, T.J., Warren, P.D., Evans, A.G., "Effects of Roughness on Interfacial Sliding in Composites," *Acta metall. mater.*, Vol. 40, No.6, pp.1251-1257, 1992

[58] Williams, M.L. "The Stresses Around a Fault or Crack In Dissimilar Media," Bulletin of the Seismological Society of America 49-2, pp.199-204, 1959

[59] Sih64 & Rice

[60] England65

[61] Hutchinson, J.W., Mear, M.E., Rice, J.R., "Crack Paralleling an Interface Between Dissimilar Materials," *Journal of Applied Mechanics*, Vol.54, pp.828-832, Dec. 1987

[62] Rice, J.R., "Elastic fracture mechanics concepts for interface cracks," *ASME Journal of Applied Mechanics*, Vol..55, pp. 98-103, 1988

[63] He, M.Y., and Hutchinson, J.W., "Crack Deflection at an Interface Between Dissimilar Elastic Materials," *Int. J. Solids Structures*, Vol. 25, No. 9, pp. 1053-1067

[64] Needleman, ., "A Continuum Model for Void Nucleation by Inclusion Debonding, " *Journal of Applied Mechanics*, pp.525-531, Sept 1987

33

[65] Tvergaard, V., "Effect of Fibre Debonding in a Whisker-reinforced Metal,"
      Materials Science and Engineering, Vol. A125, pp. 203-213, 1989

[66] Tvergaard, V., "Fibre debonding and breakage in a whisker-reinforced metal,"
      Materials Science and Engineering, Vol. A190, pp. 215-222, 1995

CHAPTER 2: ELEVATED TEMPERATURE INTERPHASE BEHAVIOR

Abstract

An investigation has been conducted to determine the effect of temperature and thermal exposure on the interphase behavior of continuous fiber reinforced titanium metal matrix composites. The primary system considered is SCS-6/Timetal-21S, although limited work was also done on SM1240/Timetal-21S. First, an elevated temperature single fiber pushout apparatus was built to investigate the interfacial properties of fiber reinforced composites. Testing temperatures of up to 1000 °C in a vacuum of less than 10^{-6} torr can be obtained. Output includes applied load on the fiber and relative punch displacement. Next, elevated temperature fiber pushout test were conducted to determine the effect of test temperature on interphase shear properties. Corresponding variations of debonding shear strength and frictional shear stress with test temperature are presented and discussed. Effects of an initial stabilizing heat treatment have also been studied. Thermal exposure, in both a vacuum and an air environment, has been conducted on specimens, with temperatures up to 650 °C and exposure times of up to 100 hours. The resulting size and composition of the interphase has been examined and discussed. Fiber pushout tests were carried out at room and elevated temperature on the aged specimens. Results are discussed in terms of the influence of relaxation and oxidation on the debond shear strength. Additionally, transverse testing has been performed and, using a finite element procedure, the elevated temperature interface properties in the normal direction have been established.

2.1   Introduction

Fiber/matrix interphase behavior critically influences the thermo-mechanical behavior of fiber-reinforced composites. Both the bond strength and the fracture toughness of the interphase affect the overall behavior of the composite system. In composites consisting of strong fibers and a relatively weak matrix, the longitudinal strength depends on strong fiber-matrix bonding to promote efficient transfer of stress from the matrix to the fibers. Such bonding results in the longitudinal strength of the composite being on the order of the fiber strength. The interface region, or interphase, in addition to enabling this load transfer from matrix to fiber, should be able to accommodate the strain mismatch between the fiber and matrix and act as a crack blunting layer to minimize crack propagation [1]. However, due to the high stresses induced during consolidation and the brittle nature of the interphase constituents, this region can act as a site of crack initiation. Additionally, due to the directional nature of the reinforcement, good bond strength is necessary for the transverse strength of the composite, which will only be on the order of the matrix strength. In brittle matrix composites, toughness is achieved through energy absorption during frictional sliding and pullout of broken fibers, therefore a weak fiber matrix interface is desired. Stress is transferred to the fiber by frictional forces until the fully loaded fibers fail. The greater the frictional stresses, the more efficiently the fibers become loaded and the shorter the pullout lengths. In metal matrix composites (MMCs), which have strong fibers and a ductile matrix, strong interfacial bonding is generally desired although, in some cases such as in fatigue crack growth, frictional sliding and fiber pullout are important.

In order to optimize the damage resistance response of MMCs, it is essential that the properties of the fiber/matrix interface are understood in relation to influencing factors. The factors of most concern relate to the processing conditions, including consolidation

temperature, pressure and cooling rate, and the in use or testing temperature and environment. These variables result in alterations of the interphase properties, and therefore affect the subsequent behavior of the composite during loading.

In the foil-fiber-foil manufacturing technique, at the consolidation temperature for titanium metal matrix composites (Ti-MMCs), which is about 900 $^{\circ}$C [2, 3], a stress free condition exists within the composite. Upon cooldown, residual stresses arise due to the difference in coefficients of thermal expansion between the SiC fiber ($5x10^{-6}$ / $^{\circ}$C) and Ti alloy matrix ($11x10^{-6}$ / $^{\circ}$C) [4]. This difference causes an inherent residual compressive stress at the interface, in the normal direction. The extent of this compressive stress is dependent on the actual consolidation temperature and the cooling rate. A slower cooling rate allows a time dependent relaxation of the matrix material, which reduces the level of residual stress significantly. Mirdamadi, et al. [5] observed, in their work with SCS-6/Ti-15-3, that the cooling rate has a very significant effect on the radial stress at the fiber/matrix interface, while the effect of the consolidation pressure is only significant at cooling rates higher than about 1 $^{\circ}$C/s.

The high temperature and extended time necessary for consolidation also results in the formation of a brittle reaction zone between the fiber and/or fiber coatings and the matrix [6, 7, 8]. The effect of such aging on the properties of this interphase becomes important during long-term thermal exposure. Several authors have observed significant interphase growth under vacuum conditions, particularly at higher temperatures (600-1000 $^{\circ}$C) [9-11]. Due to the brittle nature of the interphase, defects and micro-cracks can form in this region which act as stress concentrations, leading to fiber and/or matrix crack initiation during the fiber bridging process [12-14]. Additionally, it is likely that interfacial reaction kinetics will change the residual stress characteristics of the fiber/matrix interface due to

37

volume changes associated with the growth and/or consumption of various constituents of the interphase. These changes could be seen as an increase in the frictional shear stress with increasing exposure time, such as that observed by Watson and Clyne [15] during room temperature fiber push out testing on SM1240/Ti-6Al-4V samples aged which were aged at 700 and 815 °C.

Loading conditions involving temperature, environment, and loading frequency also affect the properties of the interphase, and therefore the composite performance as a whole [16-19]. As temperature increases in the composite system, approaching the stress free consolidation temperature, the residual stresses at the fiber/matrix interface decrease. This effect is seen in the high frequency fatigue crack growth studies performed by Zheng and Ghonem [20], which have shown a decrease in the crack growth rate of bridging cracks in unaged SM1240/Timetal-21S specimens with increasing test temperature (from 24 - 650 °C). They interpreted these results in terms of increased interfacial crack length with temperature, which increases the matrix crack tip shielding force. Eldridge and Ebihara [21], using 0.28 - 0.48 mm thin slice push-out specimens, have noted a marked drop in the interfacial shear strength and frictional shear stress with increasing test temperatures from 300 to 825 °C in unaged SCS-6/Ti-24-11 intermetallic composite. Conversely, from 25-300 °C, a slight increase was seen in the debond strength with increasing temperature. Using finite element modeling of the fiber pushout test, Ananth and Chandra [22] showed an increase in the values of peak push out load, and therefore debond strength, with increasing temperature (25 °C to 200 °C) for 0.5 mm thick specimens.

In order to characterize the mechanical properties of the interphase and its response to various external influences, it is important to express these properties in terms of experimentally measurable parameters, such as interfacial debond strength, τ_d, frictional

shear stress, τ_s, and the energy release rate or fracture toughness of the Mode II interface crack. In this respect, the first two parameters, τ_d and τ_s, are used to describe a critical stress value for interface debonding and frictional sliding. The fracture toughness, G_{ic}, characterizes the propagation of an existing interphase crack.

Several experimental methods have been used in an attempt to establish these interfacial parameters in the longitudinal direction. Widely used among these methods are the fiber pullout [23, 24] and the fiber indention and "thin slice" single fiber pushout methods [21, 25, 2, 26, 27]. Each method has unique advantages and disadvantages. Fiber pullout, while most closely representing the actual conditions in a fiber and the surrounding matrix during loading, involves complicated specimen preparation, which may alter the composite stress state. Pushout methods, while difficult to perform, particularly at elevated temperatures under vacuum conditions, allow relatively easy specimen preparation, collection of a large data set from each specimen, and the ability, with the proper choice of specimen thickness, to preserve the composite stress state in the test specimen.

Less research has been done on interfacial properties in the transverse direction for unidirectional composites. Analytically, Folias [28] used a 3-D solution to show that the onset of fiber/matrix interface debonding will occur at a free surface. Lee et al [29], developed a mathematical model for transverse failure of a mono-fiber reinforced composite, and, using this model, studied the effect of fiber size on the failure behavior. They observed that an increase in fiber size, at both room and elevated temperatures, resulted in easier interfacial debonding. Zhal, et al [30] looked at the difference between modeling the composite with a hexagonal or square array fiber distribution, noting that the hexagonal array showed isotropic behavior, while the square array was much stronger in the direction of the nearest fibers, and weakest at 45° to this direction. Li and Wisnom

[31], in finite element modeling of SCS-6/Ti-6Al-4V showed that the fiber coating has a significant effect on the transverse debonding behavior. Experimentally, Nimmer [32] studied composite systems where the coefficient of thermal expansion for the matrix was larger than the fiber, and the interface was very weak, noting that the resultant force-displacement curve exhibited a bilinear nature, with the "knee" of the curve corresponding to interface failure. Marshall, et al,[33] in their study of several Ti_3Al composites, showed that the presence of brittle reaction products at the interface resulted in a weaker interface and a lower rupture strength in the transverse direction, but that strong interfacial bonding does not necessarily result in high transverse strength.

The purpose of this study is to characterize the elevated temperature interphase properties of Ti-MMCs in both the longitudinal and transverse direction. The effect of the standard heat treatment and post heat treatment thermal exposure on the size and mechanical properties of the interphase will be investigated. The parameters describing the mechanical properties of the interphase in the longitudinal direction are quantified using of an elevated temperature 'thin slice' fiber pushout testing technique. Temperature dependencies of the fiber/matrix debond shear strength and frictional shear stress are investigated through a series of room and elevated temperature fiber pushout tests for both vacuum aged and unaged conditions. . The interphase properties in the normal direction are evaluated through a set of transverse loading tests at various temperatures. A finite element procedure is used to take the global loads and extract the local normal interphase strength. Additionally, an environmental exposure study is conducted to identify the effects of oxidation on the interphase properties of this composite system.

2.2 Material and Specimen Preparation

The primary material considered in this study is a 6-ply SCS-6/Timetal-21S composite with an average fiber volume fraction of 0.32. The matrix of this composite consists of Timetal-21S, a metastable β titanium alloyed with 0.1 Fe, 16.0 Mo, 3.06 Al, 2.9 Nb, 0.2 Si. 0.22 C, 0.12 O, 0.005 N (wt %.) This alloy was developed in 1988 by TIMET for its unique combination of high strength, good elevated temperature properties and extraordinary environmental degradation resistance [34]. SCS-6 fibers have a 140 μm carbon cored SiC body with a 3 μm dual carbon coating. The unidirectional composite is fabricated for this study by vacuum hot pressing, using a foil/fiber/foil layup method. A detailed description of this material is given in the previous section Additionally, an SCS-6/Ti-15-3 composite was used in the aging study for comparison with published data.

'Thin slice' fiber pushout specimens (approximately 1 cm in length and 1.5 mm width) were sectioned to slightly larger than the desired thickness with a diamond wafering blade at a high speed/low load, with the fibers aligned parallel to the thickness of the specimen. Both sides of the specimen were ground with SiC paper to achieve the final thickness. Then a scratch-free surface was obtained by diamond polishing with increasingly smaller grit, through 1 μm.

Rectangular specimens measuring approximately 10.3 cm in length, 1.5 mm in width and 1.5 cm thickness were used in the transverse testing portion of this study. These were cut from larger plates of material with a diamond blade on a high speed saw, so that the fibers were aligned perpendicular to the length of the specimen. After initial cutting, approximately the center third of the specimen surfaces containing the fiber cross-sections were ground on increasingly finer grit SiC paper, then polished with a polycrystalline diamond suspension, from 9 μm to a final polish of 1 μm.

41

Specimens used for microstructural investigation were sectioned and polished similar to pushout specimens, then etched with Kroll's etchant in order to define the interphase boundaries. The etching time varied from 20 seconds to 80 seconds, depending on the testing and/or thermal exposure conditions of the specimen. Scanning Electron Microscopy (SEM), calibrated with Auger Electron Spectroscopy (AES), was used to identify the thickness of the reaction zone around the circumference of the fiber for each of the aged specimens. The average interphase thickness for a particular thermal exposure time/temperature condition was taken to be the mean of the measurements from all fibers examined.

2.3   Interface Tangential Behavior

2.3.1 Experimental Setup and Procedure

In order to characterize the interface under conditions representative of material applications, elevated temperature testing is necessary. Due to the low oxidation resistance of Ti-based alloys at high temperature, such elevated temperature testing requires a vacuum environment. Figure 2-1 is a photograph of the high temperature fiber pushout apparatus, modeled after the device designed by Jeffrey Eldridge at NASA Lewis Research Center in Cleveland, Ohio [25]. This device has the capacity to run at less than 10^{-6} torr vacuum and sample heating temperatures of at least 1000 °C, although for the tests described in this study, temperatures were limited to 650 °C.
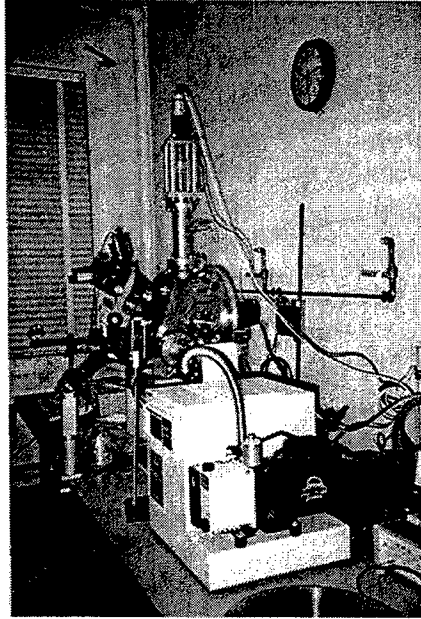
Figure 2-1   Elevated temperature fiber pushout apparatus

A labeled schematic of this device is shown in Figure 2-2. The sample and indentor are located inside a 12-inch diameter cylindrical stainless steel vacuum chamber with Conflat® ports on either end. A quartz window in each of these ports allows sample observation and heating as described below.   The test chamber is evacuated with the attached turbo pump in order to prevent significant oxidation of the sample during heating.
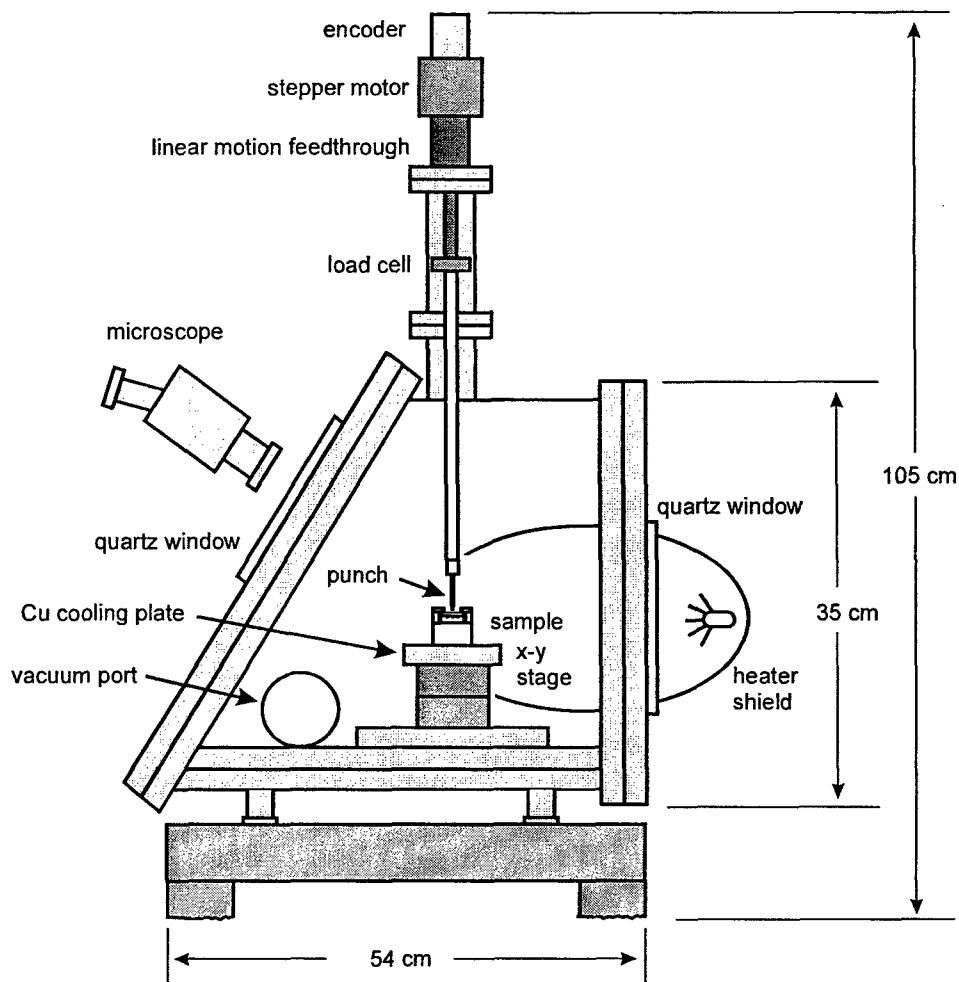
Figure 2-2   Schematic of the high temperature fiber pushout apparatus

Controlled indentor displacement is performed using a linear motion feedthrough driven by a stepper motor. The indentor is attached to a load cell, which is coupled directly to the shaft of the linear motion feedthrough. In order to avoid lateral play, the linear motion feedthrough was modified by placing a Teflon bushing around the shaft where it entered the vacuum chamber. Another Teflon bushing was located at the point where the stainless steel tube entered the vacuum chamber to stabilize the load train. The fiber is loaded in continuous single steps corresponding to a linear punch displacement of .0125

44

µm/step. The indentor used for load application is a conical tungsten carbide punch having a 30° included angle and a flat bottom. A punch having a 100 µm diameter flat bottom was used to push out the 140 µm SCS-6 fibers, while a 75 µm diameter flat bottom was used for the 100 µm SM1240 fibers. The specially designed conical shape of the indentor allows the punch to hold a higher load, without buckling, than a straight cylindrical punch, while the flat bottom distributes the applied load over a large portion of the fiber face and minimizes fiber damage by inhibiting penetration of the punch into the fiber.
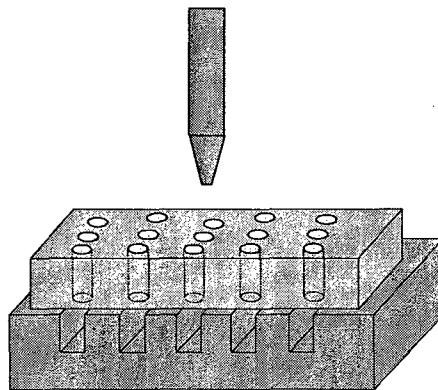
Figure 2-3   Schematic of fiber pushout base and punch

The sample support was designed for high-temperature exposure and thermal isolation. The specimen is mounted, using a clamping device, with fibers aligned over channels in a Ta support block. (See Fig. 2-3) A support block with 280 µm channels is used for testing SCS-6 reinforced samples, and a block with channels 200 µm wide is used for the SM1240 reinforced composite. These channel widths were chosen to be small enough to minimize sample bending, yet large enough to allow a reasonable amount of fibers to be tested without relacation of the composite sample. The Ta support block is mounted on a low-thermal-conductivity ceramic pedestal, for thermal isolation, and held in place by a hollow stainless steel fixture. The entire support base is secured inside the

45

vacuum chamber with two screws. This setup allows transfer of the support base to an optical microscope where fibers located over the grooves in the Ta block are marked on a corresponding micrograph. The fibers for pushout testing are later chosen from these indexed fibers. This sample holder assembly is then mounted on an x-y translation stage above a water-cooled Cu plate, ensuring that the x-y stage will not overheat.

Sample heating is achieved using a quartz halogen lamp inside an ellipsoidal reflector, with the lamp at one focal point and the sample at the other end, where the heating radiation is focused. The reflector is bisected by the chamber's vertical quartz window, so that the lamp itself remains outside the test chamber. The hot zone is a spot with a diameter of about 1.25 cm. Sample temperature is monitored by a thermocouple welded to the Ta support block.

Fiber/indentor alignment is performed remotely, using motorized actuators to control the motion of the translation stages, to bring the chosen fiber beneath the indentor. A quartz window tilted at an angle of 30° from vertical provides line-of-sight for a long working distance optical microscope located outside the chamber. The microscope is positioned so that the line-of-sight is perpendicular to the plane of the window in order to minimize distortion and multiple reflections.

A PC-controlled data acquisition system is used to collect data from the load cell and the encoder. Load and motor displacement data is stored on the computer hard drive, as well as being displayed, both graphically and numerically, on the monitor. As part of this research, a program was written in QuickBasic to link the PC with the stepper motor controller, via a RS-232 communication, allowing control of the motion of the indentor. A listing of this QuickBasic program is included in Appendix 1. Visual monitoring of the test is used to verify the occurrence of fiber sliding.

The specimen, once positioned in the vacuum chamber is heated to the required test temperature, and then monotonically loaded until fiber pushout occurs. Load and motor displacement are continuously recorded during the loading process. Characteristics of these load-displacement pushout curves for the material under examination will be discussed in detail in a subsequent section. Fiber pushout is later verified through SEM observations of the reverse side of the specimen. In addition, the surface morphology of the pushed out fibers, and the location of the debond crack is recorded.

It should be noted that all elevated temperature tests were conducted under vacuum conditions, while the room temperature tests were conducted in air. Some variation between values obtained in air and those obtained under vacuum may be expected based on a study that was carried out on intermetallic titanium composites [25]. In his room temperature study, the interphase shear strength was found to be 10 % lower in room air than in vacuum, but 30% higher in dry air than in vacuum. The frictional shear stress was more sensitive to moisture, being 87% lower in room air than in vacuum, and 20% lower in dry air than in vacuum. Similar data has not been published for SCS-6/Timetal-21S and is left for a future investigation.

In the current work, the interphase shear strength, τ_d, has been determined using the assumption of an average shear stress distribution along the interphase at the load level, P_d, corresponding to the initial debonding, as $\tau_d = P_d / (\pi d_f h)$, where d_f is the fiber diameter, and h is the specimen thickness (or fiber length). The interfacial frictional shear stress at any point after the initiation of debonding is calculated in the manner mentioned above, substituting the instantaneous load, P_i, for the debond load, P_d, and the remaining bonded length for the fiber length, h. The bonded length is considered to be (h-δ), where δ

is the sliding distance of the fiber. In this study, only the initial frictional shear stress, i.e the value corresponding to the load at the bottom of the debonding drop, is compared.

2.3.2 Pushout Test Results at Elevated Temperatures

Temperature affects many aspects of the fiber/matrix interphase debonding process. One notable effect can be seen in the comparison of a typical room temperature and high temperature fiber push-out curve. Fig. 2-4 shows the load displacement curves for fibers pushed out at several test temperatures. Note that the thicknesses are different for tests performed at different temperatures. A difference in curve shape is seen between the higher temperature curves (500 and 650 °C) and the room temperature curve. Additionally, the initial slope of the curves increase with increasing test temperature, indicating that the compliance of the composite system is increasing. This increase is due to the change in material proerties with increasing test temperature.
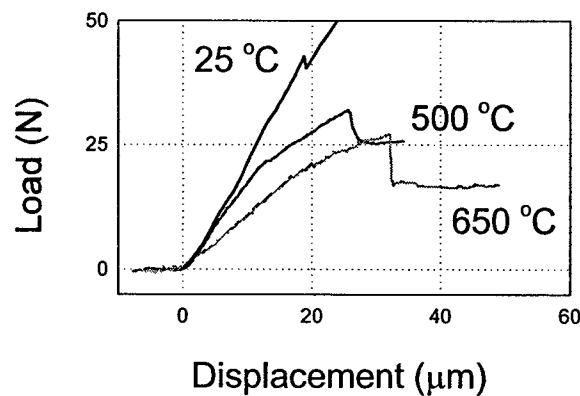
Figure 2-4   Typical elevated temperature pushout curves for SCS-6/Timetal-21S at
             room and elevated temperatures.   Note different specimen thicknesses:
             25 oC - 0.58 mm, 500 oC - 1.3 mm, 650 oC - 1.4 mm

For each fiber pushout curve, the onset of load application is indicated by the rise in load. Both curve shapes have an initial linear portion, as the load is increased but fiber debonding has not yet begun. A change in linearity indicates the onset of interphase debonding [35] . Beyond this point, the elevated temperature curves show increasing compliance with increasing load, in the form of a decreasing slope, as the debond crack propagates incrementally along the length of the interphase. This region of decreasing slope terminates in a load drop, with the maximum corresponding to the load at which the remaining bonded region has reached the minimum critical length, this portion debonds catastrophically, and the entire length of the fiber begins to slide. The force at the bottom of the drop, where the entire fiber begins to slide, is used to calculate the frictional shear stress of the interphase, τ_d, while the magnitude of the drop is a measure of the interfacial fracture toughness [35, 36]. Similarly shaped curves have been obtained for temperatures of 735, and 800 °C in vacuum.

The specimens tested at room temperature in air do not show the region of increasing compliance indicative of incremental debonding. The nature of the pushout curve and the corresponding SEM observations of specimens indicate that, at this temperature, the debonding is catastrophic. That is, the interface remains intact until the point just before the load drop occurs. Curves of similar shape were obtained in tests for pushout at temperatures of 160, 250 and 350 °C, even in thicker specimens (greater than 0.90 mm). The tests at temperatures rom 160 to 350 °C were conducted in vacuum, thereby ruling out the possibility that effects related to the air environment were the controlling factor in this type of push-out behavior.

This distinction between high and low temperature fiber push-out curves can be explained in terms of the effect of temperature on the deformation response of the matrix.

At lower temperatures, the matrix material behaves elastically. At temperatures above about 400 °C the ability of the matrix phase to flow under the applied stress is enhanced, thereby blunting the interface crack tip and inhibiting a catastrophic failure of the interface
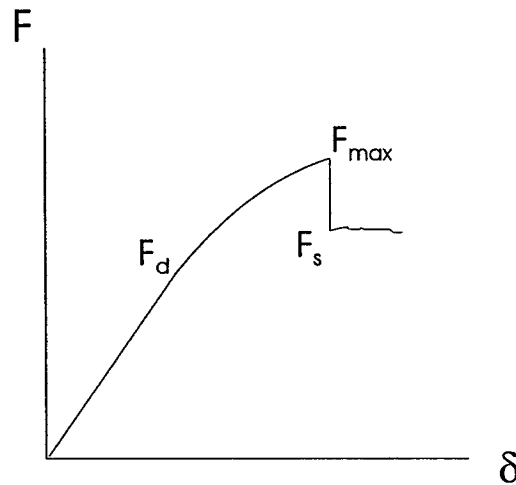
Figure 2-5   Schematic of a typical fiber pushout test

Fig. 2-5 shows a schematic of a typical fiber pushout test, with significant features labeled. In this study, the debonding load, F_d, is calculated at the first change in linearity of the force-displacement curve, corresponding to crack initiation, for specimens tested at high temperature (> 500 °C). The interphase shear strength is calculated from this debond load, as discussed previously. The maximum load, F_{max}, is the highest load achieved before complete debonding occurs. This maximum load value is significant in the calculation of the interphase fracture toughness, which will be discussed in a later chapter. At lower temperatures (< 400 °C), where no progressive debonding occurrs, the debond load is coincident with the maximum load, i.e., $F_d = F_{max}$ for the lower temperature tests.   The

firctional shear stress is calculated from the load at the bottom of the drop, F_s, which occurs at the point of complete debonding
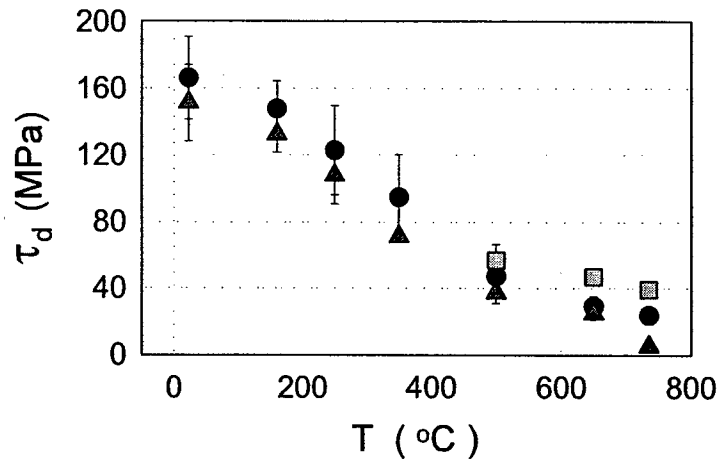
Figure 2-6   Interfacial shear properties for unaged SCS-6/Timetal-21S composite at various temperatures

The values of the debond shear strength, τ_d, and the interphase shear stress, τ_s are plotted in Fig. 2-6 for SCS-6/Timetal-21S for various test temperatures. Included also are values for the maximum load, τ_{max}, when it is different from τ_d (for temperature greater than 400 °C). As test temperature increases, both the interfacial shear strength and the frictional shear stress decrease. Both curves, but particularly the curve for τ_d, show a bilinearity with increasing temperature, with a transition point between 500 and 650 °C. This transition point is similar to that observed in the evolution pattern of residual stresses during the material cooldown from consolidation temperature to room temperature, which is discussed in detail in Chapter 3. This transition is interpreted as a point related to the onset of elastic response of the matrix material. Considerable scatter was seen in the fiber push-out data collected at the lower temperatures, presumably because, due to the non-

uniform distribution of fibers in the composite, the local radial residual stresses will vary

noticeably when the composite radial residual stresses are higher.
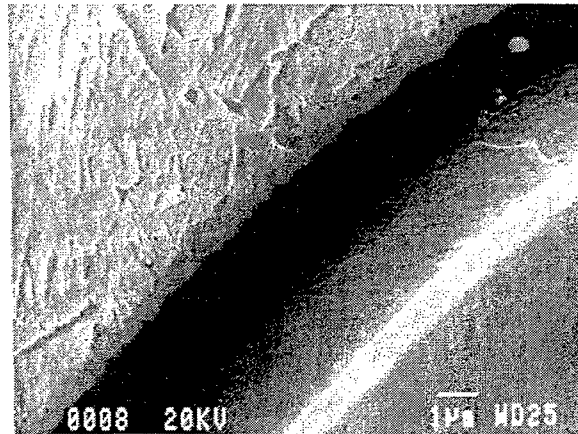
Figure 2-7   Micrograph of base of fiber after pushout testing showing: debonding
             between carbon layers

During fiber/matrix interface debonding, the location of the debond crack varies

somewhat within each specimen. SEM observation of the fibers after push-out shows that

the location of interfacial debonding for the SCS-6 reinforced composite is primarily

between layers of the C coating for all temperatures tested, as illustrated in Fig 2-7. This

figure is a micrograph of the base of a typical pushed-out fiber showing debonding within

the carbon layer near the fiber, with most of the carbon remaining on the matrix.

Occasionally, debonding is seen within the carbon layers adjacent to the matrix, where

most of the carbon remains adhered to the fiber after push-out. The two locations result in

similar interphase shear strength, but the magnitude of the load drop, corresponding to

interphase toughness [37,38] is slightly lower for debonding adjacent to the matrix. This

can be explained by the existence of a residual stress gradient that exists across the

interphase with lower values near the matrix due to the higher degree of matrix relaxation when compared to that of the fiber. Similar results for the location of debonding were found by Mukherjee, et al.[37] for the same material.

2.4 Interface Transverse Behavior

2.3.3 Experimental Setup

Prepared transverse loading specimens are mounted in an MTS load frame with the fibers in the 0° orientation with respect to the applied load., as shown schematically in Fig. 2-8. As a monotonic load is applied, an extensometer is used to measure displacement over a gage length of one inch, while the applied stress is determined by the load cell on the MTS testing frame. A long range microscope equipped with a video camera, allowing the picture to be displayed on a video monitor, is used for visual observation of the surface of the specimen during testing. Loading continues until separation of the fiber/matrix interface, in the transverse direction, is observed. Tests were carried out at several temperatures between room temperature and 650 ^{o}C. For the elevated temperature testing, heating was achieved using a quartz lamp, mounted in a split furnace setup. Temperature was monitored by thermocouples welded on either side of the specimen.
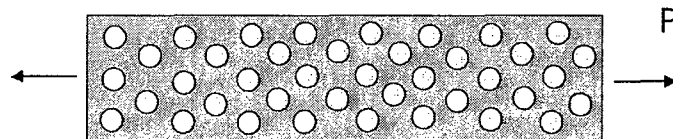
Figure 2-8   Transverse loading schematic

2.3.4 Transverse Loading Results at Elevated Temperature

Results of the transverse loading tests are shown in Fig. 2-9, as a plot of externally applied stress vs. strain during loading. The "knee' in the curve corresponds to interface separation. The stress at this point where the interface fails transversely will be denoted as σ_f.
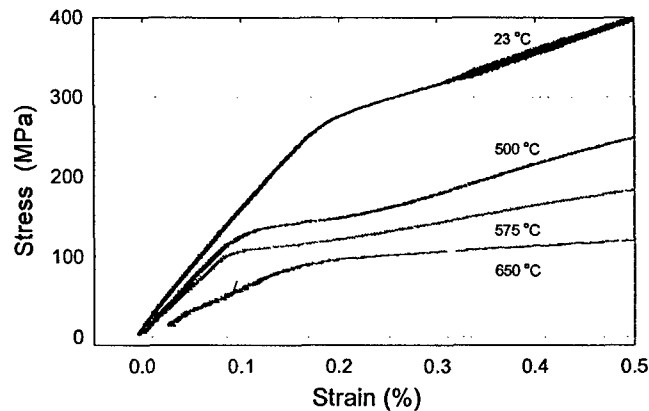
Figure 2-9   Transverse loading test results

The plot of the failure stress at various test temperatures for specimens of similar size, shown in Fig. 2-10, shows that σ_f decreases with increasing temperature. This behavior can be attributed to the relaxation of the compressive radial residual stress, which provides most of the interfacial bonding. σ_f is related to the transverse strength of the interface, but it is a global value, reflecting the separation of the interfaces of many fibers. A numerical approach for determining the transverse strength of the interface wil be discussed in detail in Chapter 5.

300

250

σ_f (MPa)

200

150

100

50

0   100 200 300 400 500 600 700

T (°C)
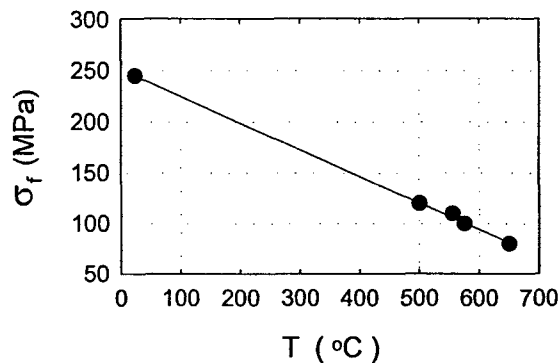
Figure 2-10   Failure stress for transversely loaded SCS-6/Timetal-21S
at various temperatures

2.5   Effect of Thermal Aging on Interface Tangential Behavior

In this section, the term "heat treatment" refers to vacuum exposure of the composite (after consolidation) to 621 °C for 8 hours, which is prescribed for this type of composite. The purpose of this heat treatment is to stabilize the β-phase of the titanium, and thus stabilize the mechanical locking effects induced by the matrix residual stress field, σ_{rr}, on the interphase region. The term "thermal exposure" or "thermal aging" is used to describe the process of holding the specimen at a fixed temperature for a prescribed period of time after the heat treatment. This can be environmental exposure in an air environment, or vacuum exposure in a vacuum of at least 10^{-6} torr. In this study, all specimens, unless otherwise noted, have been heat treated before any testing is conducted.

The temperature choices in this procedure are meant to simulate the conditions to which the composite will be exposed in typical applications; 500 °C as a relatively cold operating temperature, 650°C for a more typical operating temperature, and 800 °C for temperature spikes.   Under this type of thermal exposure, changes in composite constituents, particularly the matrix and interphase, would be expected.   Due to the

55

metastable nature of the β phase of the matrix, a second phase (usually α) is expected to precipitate in an amount proportional to the thermal exposure time [38]. The α-phase is a brittle phase that could affect the interface strength if precipitatates gather along the interface. A change in the interphase size and/or composition, as the constituents of the various phases react with one another, is expected and has been observed in several other titanium matrix composites [6, 7, 8, 39, 14, 10]. Corresponding to this interphase size could be a change in residual stress due to the associated volume changes at or near the interphase region. This change in residual stress could manifest itself as a change in the debond shear strength and interphase shear stress, which will be discussed further in the following section.

2.5.1   Experimental Setup and Procedure

Vacuum thermal aging was done in a continuous vacuum of approximately 10^{-6} torr. In order to achieve this vacuum, a specimen, previously sectioned, ground to the required thickness, and polished, is placed in the closed end of a quartz tube, while the open end is attached, through a specially designed fixture, to a vacuum turbo pumping system.

The closed end of the tube, which contains the specimen, is inserted into a furnace through a specially designed aperture. After evacuating the tube, the furnace, and hence the specimen, is heated at a rate of approximately 20 °C /min to the desired temperature and held for the required amount of time. Then, the furnace is shut down, and the specimen is furnace cooled under vacuum, until the temperature reaches 200°C. At this temperature, the vacuum is removed and the specimen is allowed to air cool to room temperature. Note that throughout the heat treatment process, the quartz tube is continuously evacuated and

the furnace temperature is verified using a thermocouple in the quartz tube, aligned with the specimen location.

Air thermal aging was done in the same furnace, without the vacuum setup. In this case, previously polished specimens were heated at a rate of approximately 20 °C /min to the required temperature. After thermal exposure for the desired time duration, the specimens were removed from the furnace and air-cooled.

2.5.2 Effects of Thermal Exposure in Vacuum

The influence of thermal exposure in vacuum on heat treated SCS-6/Timetal-21S was investigated using a vacuum level of at least 10^{-6} torr. Measurements of the interphase region were taken using Scanning Electron Microscopy (SEM), both before and after the aging procedure. Figure 2-11 is a micrograph of a typical interface region. SEM measurements of specimens subject to various aging conditions showed that no significant interphase growth occurs for exposure times of up to 100 hours for temperatures up to 650 °C in vacuum. The interphase thickness was approximately 0.8 µm for all exposure conditions. At 800°C, for 100 hours of thermal exposure, a slight increase in interphase thickness is observed, with the interphase measuring approximately 1.0 µm.
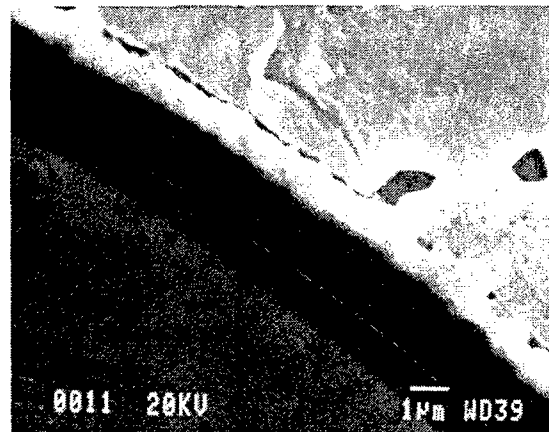
Figure 2-11   Micrograph of interface region of unaged SCS-6/Timetal-2S

The SEM observations of interphase size were verified using Auger Electron Spectroscopy (AES). This procedure was carried out by analyzing points in a line across the fiber, coating, interphase and matrix. A plot was then constructed of element concentration vs. distance along this line, relative to an arbitrary starting point on the fiber near the interphase. Figure 2-12 shows an example of such a plot for the unaged condition of SCS-6/Timetal-21S. Similar plots were obtained for exposure conditions through 650 $^\circ$C, which indicated that no significant depletion of elements occurs during thermal exposure at or near the fiber/matrix interphase.
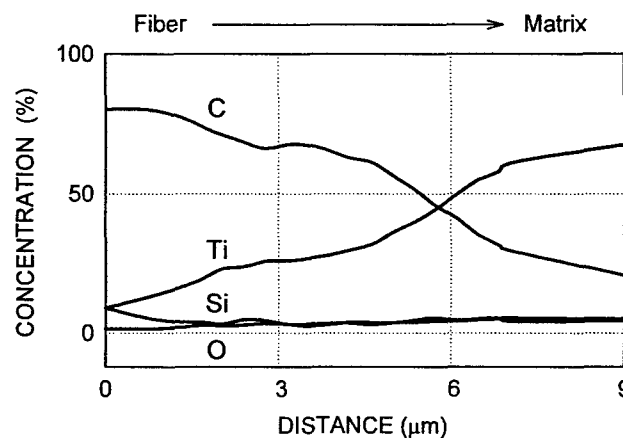
Fiber ————————————→ Matrix

Figure 2-12   Auger Electron Spectroscopy compositional data for unaged
SCS-6/Timetal-21S fiber/matrix interphase

The results found for interphase sizes in this study are different from those reported by several authors in their studies of thermal exposure in other Ti matrix composite systems [10,11, 9]. Some of these results are shown in Fig. 2-13. The closest material to those included in this study is the composite system SCS-6/Ti-15-3-3 (Ti-15V-3Al-3Cr-3Sn is a metastable beta Ti alloy with properties similar to Timetal-21S, although inferior oxidation resistance). For this composite, Gundel and Wawner [11] observed an interphase

size of 1.5 μm after 1000 hours of thermal exposure at 700 °C in vacuum. They also observed that below 925 °C the reaction rates for Timetal-21S were lower than those of Ti-15-3, although no long-term experimental results were quoted for the SCS-6/Timetal-21S composite system. At the higher temperature of 1000 °C Gundel and Wawner [11] measured the interphase thickness to be approximately 12 μm after 100 hours of thermal exposure for this SC-6/Ti-15-3, and about 11.5 μm for SCS-6/Timetal-21S. Yang and Jeng [9] measured interphase thicknesses of approximately 4.5 μm after 44 hours at 850 °C and 8 μm after 11 hours at 950 °C in Ti 15-3.

1	1000 °C	SCS-6/Ti-6-4	(G&W)
2	1000 °C	SCS-6/Ti-15-3	(G&W)
3	1000 °C	SCS-6/Beta21S	(G&W)
4	850 °C	SCS-6/Ti-15-3	(Y&J)
5	950 °C	SCS-6/Ti-15-3	(Y&J)
6	850 °C	SCS-6/Ti-25-10	(Y&J)
7	950 °C	SCS-6/Ti-25-10	(Y&J)
8	850 °C	SCS-6/Ti-24-11	(Y&J)
9	950 °C	SCS-6/Ti-24-11	(Y&J)
10	500 °C	SCS-6/Timetal21S	(O&G)
11	650 °C	SCS-6/Timetal21S	(O&G)
12	750 °C	SCS-6/Timetal21S	(O&G)
13	875 °C	SCS-6/Timetal21S	(O&G)
14	900 °C	SCS-6/Ti-15-3	(O&G)
15	1100 °C	SCS-6/Ti-15-3	(O&G)
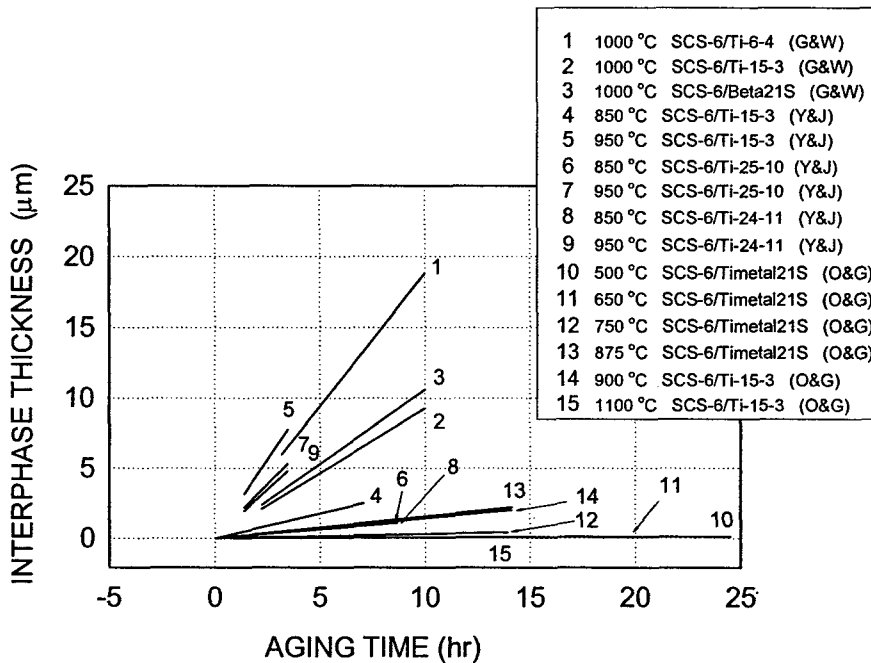
Figure. 2-13   Relationship between interphase thickness, d, and square root of thermal aging for different composite systems published by various authors

The higher interphase growth rates quoted in some of these studies could be explained in terms of oxidation. Morel [10] and Yang & Jeng [9] maintained a vacuum level of only 10^{-3} torr in their thermal exposure experiments, which may not be enough to prevent surface oxidation of the interphase region. In the work of Andrieu, et al.[40] on a

59

Ni based superalloy, it was shown that for a vacuum range of 10^{-4} torr sufficient oxygen exists to cause oxidation in that material at elevated temperatures. It has also been noted that beta titanium alloys easily show surface oxygen contamination, even in supposed vacuum heat treatments [38].

One effect of high temperature oxidation of SCS-6/Timetal-21S has been observed in a different part of this study, as a large growth of the reaction zone, particularly at the higher temperature investigated (875 °C). In part of this study, a specimen was thermally exposed in air after the interphase was debonded, allowing penetration of oxygen along the length of the fiber. Initial observation of a slice taken from the center of this specimen shows a fairly large interphase, approximately 3.5 μm thick (Fig. 2-14a) Closer examination of this interphase (Fig 2-14b) suggests that the carbon coating has oxidized completely. AES confirms this premise, identifying only Ti and O (not C) in the interphase region. In the current study, the vacuum level of 10^{-6} torr used for thermal exposure is assumed sufficient to avoid such oxidation effects.
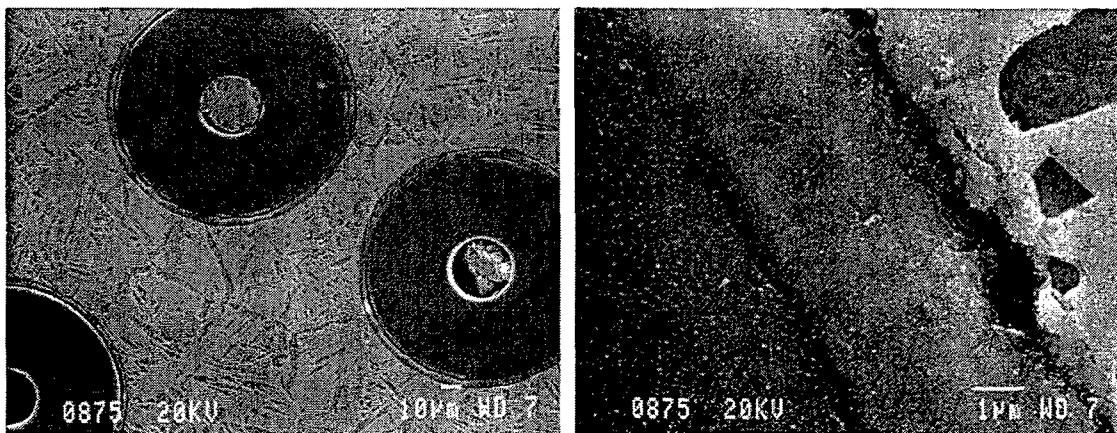
(a) several fibers   (b) closeup of fiber/matrix interface

Figure 2-14   Micrograph of large interphase growth observed in SCS-6/Timetal-21S
that was aged after interface debonding

In order to verify that this difference in interphase growth observed by other authors and in the current study is due to vacuum conditions during thermal exposure and not an inherent material difference between SCS-6/Timetal-21S and SCS-6/Ti-15-3, a vacuum aging study was performed on SCS-6/Ti-15-3. Specimens of this material were thermally exposed in vacuum, at 900 and 1100 °C. As with the Timetal-21S composites, no significant growth was observed at 900 °C. After 200 hours at 1100 °C, an interphase thickness of 3 μm was observed, accompanied by a marked deterioration of the carbon coating. This interphase growth of approximately 200% is still significantly smaller than that reported at a vacuum level of 10^{-3} torr, suggesting that the lower vacuum level is an important factor in the large interphase growth.

The effect of the thermal exposure on the debond shear strength and frictional shear stress was investigated using fiber push-out testing. A series of push-out tests were conducted on specimens which were thermally exposed at two temperatures (500 and 650 °C) in vacuum, then pushed out at their respective exposure temperatures. The results of this study are presented in Fig. 2-15(a-c) as plots of the interphase shear strength, τ_d, frictional shear stress, τ_s, and maximum shear stress, τ_{max}, as a function of temperature. Data is included for specimens in the unaged condition as a baseline reference. As a comparison, note that τ_d for unaged specimens pushed out at room temperature is 161.2 MPa. Since the focus of this investigation is on practical in-use conditions for this material, thermally exposed specimens were not tested at room temperature. The results illustrated in these figures suggest that the residual stresses, which were "locked in" during cooldown of the composite after consolidation have relaxed during the thermal exposure process. Although it takes 100 hours of thermal exposure in order to relax these stresses at 500 °C, this relaxation is almost instantaneous at 650 °C. This can be seen by the fact that

61

at 650 °C, the debond shear stress, τ_d, is almost identical for the unaged, 50 hour and 100

hour thermally exposed specimens. Therefore, the test temperature has a more significant

effect on τ_d than the prolonged thermal exposure at this temperature.

a) interphase shear strength, τ_d b) frictional shear stress, τ_s
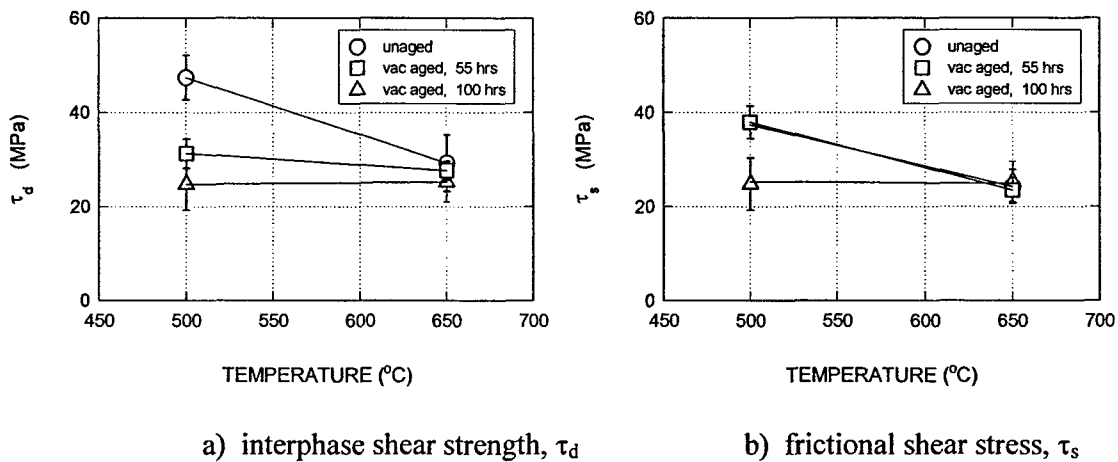
Figure 2-15(a-b)   Effect of thermal aging in vacuum on interphase properties at several
temperatures. Note: Fiber pushout was conducted at aging
temperature. (at 23 oC, τ_d = 166.4 MPa)

c) maximum shear stress, τ_{max}
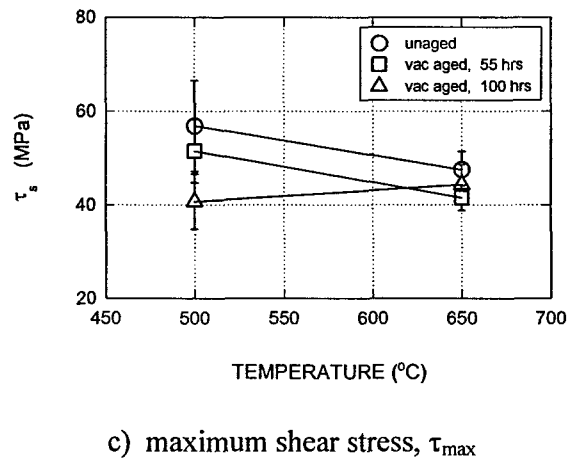
Figure 2-15(c)   Effect of thermal aging in vacuum on interphase properties at several
temperatures. Note: Fiber pushout was conducted at aging
temperature. (at 23 oC, τ_d = 166.4 MPa)

2.5.3 Effects of Thermal Exposure in Air

In actual use, composites exposed to elevated temperatures will also be exposed to the effects of oxidation, if only at the component surface and along a propagating crack. During elevated temperature crack bridging, the debonded region of the fiber/matrix interphase is exposed to the effects of oxidation, as well. For this reason, it is necessary to investigate the effect of extended high temperature oxidation on the interphase shear properties. This was done by thermally exposing, in air, polished specimens of SCS-6/Timetal-21S, at temperatures of 500 and 650 $^\circ$C for time durations of up to 100 hours. The specimens were then lightly polished in order to remove the surface oxidation and observed for interphase changes using SEM. Fiber push-out testing was conducted in vacuum at the corresponding exposure temperature.
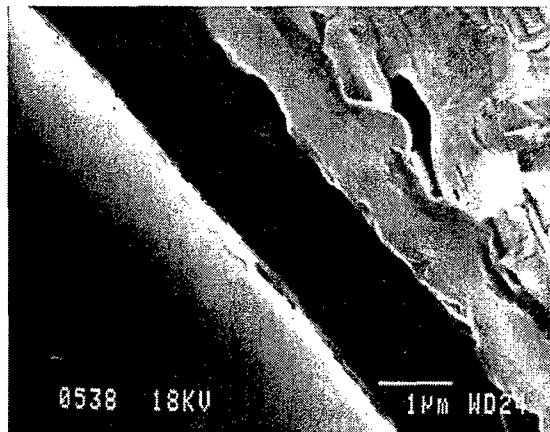
Figure 2-16   Micrograph of carbon layer after thermal exposure in air at 500 $^\circ$C for 100 hours
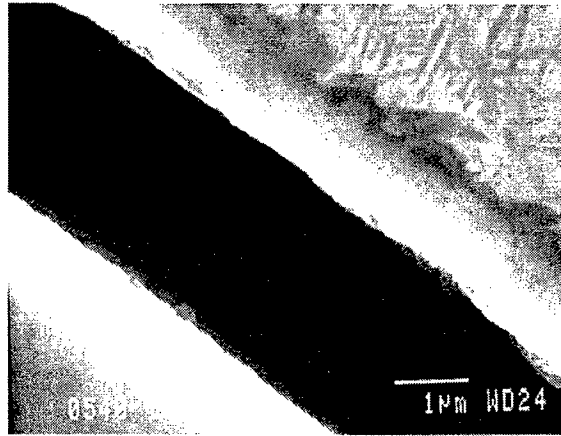
Figure 2-17   Micrograph of carbon layer after thermal exposure at 650 °C for 100 hours

Prior to push-out testing, specimens were examined under the SEM to determine possible changes in the interphase size or appearance after thermal exposure in air. Observation show that the carbon layer remains intact in the 500 °C/55 hr sample, while 100 hours of exposure at the same temperature causes some degradation of the carbon layer (Fig. 2-16). In the 650 °C/100 hour sample, the carbon is almost completely depleted, leaving a crevice around the circumference of the fiber (Fig. 2-17). In order to more closely examine the extent of the oxidation, additional 650 °C air aged specimens were prepared by polishing them parallel to the fiber direction. Examination of these specimens showed a crevice along the length of the fiber. Closer examination of the carbon layer at the center of the fiber length, left by the removal of a fiber, showed features consistent with oxides (Fig 2-18a), suggesting that oxidation had indeed taken place along the entire length of the fiber (.97 mm). This surface is distinctly different from the carbon layer in the 6518°C/100 hour vacuum exposed specimen, which exhibits a morphology typical of the unoxidized carbon surface (Fig. 2-18b).
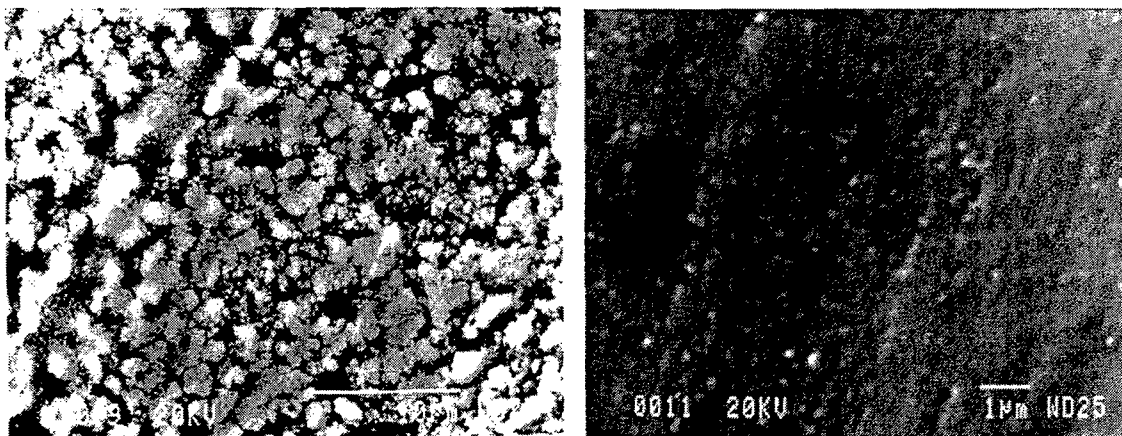
a) air exposure   b) vacuum exposure

Figure 2-18   Morphology of fiber surface after pushout from a specimen
that had been thermally aged at 650 °C in air and in vacuum

Results of the fiber push-out tests on specimens which were thermally exposed in air are summarized in Fig. 2-19, a plot of the interphase shear strength, τ_d , as a function of temperature for various air exposure times, and for the unaged condition. Thermal exposure of 55 hours in air at 500 °C causes a slight increase in the interphase shear strength. This increase may be related to a volume change in the interphase or the carbon layer in the early stages of the oxidation process. This would increase the compressive radial residual stress, thereby increasing τ_d. Continuing to age to 100 hours reduces this value by approximately 50%. This drop can be explained by the degradation of the carbon layer after 100 hours of thermal exposure. In the 650 °C/100 hr air exposure condition, the interfacial shear stress drops to a negligible level. A negligible load is required to push out this fiber. This observation is expected, based on the complete carbon layer depletion previously discussed under SEM observations. Since the carbon layer has disappeared, leaving a crevice, no radial residual stress would be present at the fiber/matrix interface. In fact, some of the fibers actually fell out during specimen handling.
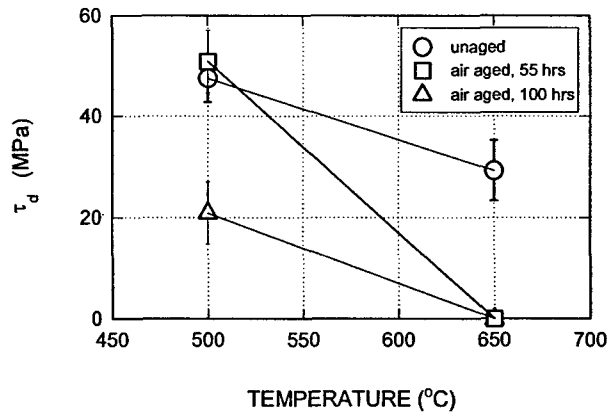
Figure 2-19   Effect of thermal exposure in air on interphase shear strength, τ_d, at several temperatures. Fiber pushout was conducted in vacuum at exposure temperature. (At 23 oC, $\tau_d = 161.2$ MPa)

2.6   Summary and Conclusions

The work in this paper focuses on the influence of temperature and thermal exposure on the interphase properties of continuous SiC fiber reinforced Ti matrix composites, primarily SCS-6/Timetal-21S. The work consists of an investigation into the effects of test temperature, heat treatment, and vacuum and air thermal exposure on the size and composition of the interphase of SiC/Ti composite systems. An elevated temperature fiber pushout apparatus has been built and used for vacuum testing at temperatures to 650 °C and exposure times to 100 hours were considered. Elevated and room temperature fiber pushout testing on the thermally exposed specimens as well as specimens with various fiber volume fractions were conducted to determine interphase properties in the tnagential direction. Transverse loading tests at elevated temperatures, coupled with numerical modelling were used to determine the interphase properties in the transverse direction. An

66

thermal exposure study conducted in air showed the effect of oxidation on the interphase properties of this composite system. These tests yielded the following results:

1. A difference exists in the response of the interfacial debonding between specimens tested at 500 °C and those tested below 400 °C. At the higher temperatures, the initiation of interphase decohesion was followed by incremental debonding, leading to complete interphase failure and fiber sliding. At lower temperatures the initiation of debonding was coincident with complete interphase failure.

2. The variation of τ_d and τ_s with increasing temperature follows the bilinear trend of the compressive radial residual stress, with a transition point near 650 °C, the temperature corresponding to the onset of plastic behavior in the matrix material.

3. For transverse loading, the interphase failure stress, σ_f, decreases with increasing temperature due to the decrease in compressive radial residual stress at elevated temperatures.

4. Thermal exposure under vacuum conditions results in no noticeable increase in the interphase size or composition. The values of τ_d and τ_s for these thermally exposed specimens were determined through the use of fiber pushout in vacuum at temperatures representative of typical in-use conditions. These tests indicate that the effect of thermal exposure is not as significant as the test temperature at 650 °C, where there is little difference in the τ_d or τ_s between unaged and vacuum exposed conditions to 100 hours. At 500 °C, however, vacuum exposure decreases τ_d by approximately 50 % and τ_s by over 30 %. Thermal exposure testing in air at 650 °C, even for exposure times as low as 55 hrs, show the carbon layer surrounding the fiber is depleted along the entire length of the fiber, leading to no interphase shear

strength or frictional shear stress along the interphase. At 500 °C, the carbon layer is

degraded but not completely oxidized.

2.7   References

[1] Agarwal, B.D., Broutman, L.J., Analysis and Performance of Fiber Composites, John Wiley & Sons, Inc., New York, NY, 1990

[2] Yang, J.M., Jeng, S.M., Yang, C.J., "Fracture Mechanisms of Fiber Reinforced Titanium Alloy Matrix Composites, Part I: Interfacial Behavior," *Materials Science and Engineering*, Vol. A138, pp. 155-167, 1991

[3] Sohi, M., Adams, J., Mahapatra, R., "Transverse Constitutive Response of Titanium-Aluminum Metal Matrix Composites," Constitutive Laws for Engineering Materials, C.D. Desai, ed., ASME Press, New York, NY, pp. 617-626, 1991

[4] Davidson, D.L., "The Micromechanics of Fatigue Crack Growth at 25 °C in Ti-6Al-4V Reinforced with SCS-6 Fibers," *Metallurgical Transactions*, Vol. 23A, pp. 865-879, 1992

[5] Mirdamadi, M., Johnson, W.S., Bahei-El-Din, Y.A., and Castelli, M.G., "Analysis of the Thermomechanical Fatigue of Unidirectional Titanium Metal Matrix Composites," *Fatigue and Fracture, ASTM Spec Publ*, No. 1156, pp. 591-607, 1993

[6] Reeves, A.J., Dunlop, H., and Clyne, T.W., "The Effect of Interfacial Reaction Layer Thickness on Fracture of Titanium-SiC Particulate Composites" *Metallurgical Transactions A*, Vol. 23A, pp. 977-988, March 1992

[7] Rhodes, C.G., and Spurling, R.A., "Fiber/matrix Interface Reactions on Sic Reinforced Titanium Alloys", *Developments in Metal Matrix Composites*, Kamleshwar Upadhya, ed., The Minerals, Metals, and Materials Society, pp. 99-113, 1991

[8] Lerch, B.A., Hull, D.R., Leonhardt, T.A., "Microstructure of a SiC/Ti-15-3 composite", *Composites*, Vol. 21, No 3, pp.216-224, May 1990

[9] Yang, J.-M., Jeng, S.M., "Interfacial Reactions in Titanium-Matrix Composites", *Journal of Metals*, pp. 56-59, November 1989

[10]   Morel, D.E., "Reaction Kinetics in Continuous Silicon Carbide Reinforced Titanium 15V-3Cr-3Al-3Sn", *Journal of Materials Engineering*, Vol.13, No.4, pp.251-255, 1991

[11]   Gundel, D.B., Wawner, F.E., "Interfacial Reaction Kinetics of Coated SiC Fibers with Various Titanium Alloys", *Scripta Metallurgical et Material*,   Vol. 25, pp. 437-441, 1991

[12]   Metcalfe, A.G. and Klein, M.J., "Composite Materials," A.G. Metcalfe, ed., Academic Press, New York and London, Vol. 1, 1974

[13]   Imai, Y., Shinohara, Y., Ikeno, S., Shiota, I., "Deterioration Factor of SiC/Ti Alloy Composite after Heat Treatment," *ISIJ International*, Vol. 32, No. 8, pp. 917-922, 1992

[14]   Kantzos, P., Ghosn, L. and Telesman, J., "The Effect of Degradation of the Interface and Fiber Properties on Crack Bridging," *HITEMP Review*, Vol. 2, Cleveland, OH, pp. 32-1 - 32-14, 1992

[15]   Watson, M.C., Clyne, T.W., "The Use of Pushout Testing to Investigate the Interfacial Mechanical Properties of Ti-SiC Monofilament Composites," 7th World Titanium Conference, San Diego, June 1992

[16]   Cox, B.N., Marshall, D.B., "Overview No. 111: Concepts for Bridged Cracks in Fracture and Fatigue," *Acta. metall. mater.*, Vol. 42, No. 2, pp. 341-363, 1994

[17]   Zheng, D., Ghonem, H., "High temperature/High Frequency Fatigue Crack Growth Damage Mechanisms in Titanium Metal Matrix Composites," in *Life Prediction Methodology for Titanium Matrix Composites, ASTM STP 1253*, W.S. Johnson, J.M. Larson and B.N. Cox, eds., American Society for Testing and Materials, Philadelphia, PA, 1995

[18]   Campbell, M.D., Cherry, B.W., "Fatigue Crack Propagation in Fibre Reinforced Composite Materials," Fracture Mechanics and Technology proceedings

[19]   Walls, D., Bao, G., Zok, F., "Fatigue Crack Growth in a Ti/SiC Composite," *Fatigue of Advanced Materials*, pp. 343-356, January 1991

[20]   Zheng, D. and Ghonem, H. "Fatigue Crack Growth of SM1240/Timetal-21S Metal Matrix Composites at Elevated Temperature," *Metallurgical and Material Transactions A*, Vol. 26A, pp. 2469-2478, 1995

[21]   Eldridge, J.I., Ebihara, B.T., "Fiber Pushout Testing Apparatus for Elevated Temperatures," *Journal of Materials Research*, Vol. 9, No. 4, pp. 1035-1042, 1994

[22]   Ananth, C.R. and Chandra, N., "Numerical Modeling of Fiber Push-out Test in Metallic and Intermetallic Matrix Composites - Mechanics of the Failure Process," *Journal of Composite Materials*, Vol. 29, No. 11, pp. 1488-1514, 1995

[23]   Takaku, A. and Arridge, RGC, "The Effect of Interfacial Radial and Shear Stress in Fibre Pull-out in Composite Materials," *J. Phys. D: Appl. Phys.*, Vol. 6, pp. 2038-2047, 1973

[24]   Hsueh, C-H., "Interfacial Debonding and Fiber Pull-out Stresses of Fiber-reinforced Composites," *Materials Science ansd Engineering*, Vol. A123, p. 1-11, 1990

[25]   Eldridge, J.I., "Elevated Temperature Fiber Pushout Testing," Materials Research Society Fall Meeting, Boston, MA, Nov. 1994

[26]   Hsueh, C-H., "Effects of Interfacial Bonding on Sliding Phenomena During Compressive Loading of an Embedded Fibre," *Journal of Materials Science*, Vol. 25, pp. 4080-4086, 1990

[27]   Mackin, T.J., Warren, P.D., Evans, A.G., "Effects of Roughness on Interfacial Sliding in Composites," *Acta metall. mater.*, Vol. 40, No.6, pp.1251-1257, 1992

[31]   Li, D.S., Wisnom, M.R., Micromechnaical Modeling of SCS-6 Fiber Reinforced Ti-6Al-4V under Transverse Tension – Effect of Fiber Coating," *Journal of Composite Materials*, V.30, No. 5, pp 561-588, 1996

[34]   Fanning, J.C., "Timetal®21S Property Data,"Beta Titanium Alloys in the 90's, D. Eylon, R.R Boyer and D.A. Koss, eds., The Minerals, Metals, and Materials Society, pp. 3-14

[35]   Kerans, R. J., and Parthasarathy, T.A., "Theoretical Analysis of the Fiber Pullout and Pushout Tests," *Journal of the American Ceramic Society*, Vol. 74, pp.1585-1596, 1991

[36]   Chan, K.S., "Failure Diagrams for Unidirectional Fiber Metal-Matrix Composites," *Metallurgical Transactions A*, Vol. 24A, pp. 1531-1542, July 1993

[38]   Bania, P.J., "Beta Titanium Alloys and Their Role in the Titanium Industry," Beta Titanium in the '90s, D. Eylon, R.R. Boyer and D.A. Koss, eds, The Minerals, Metals, and Materials Society, pp 397-410

[39]   Chan, K.S., "Effects of Interface Degradation on Fiber Bridging of Composite Fatigue Cracks," *Acta Metall. Mater.*, Vol.41, pp. 761-768, 1993

CHAPTER 3: EFFECT OF PROCESSING-RELATED PARAMETERS ON INTERFACE PROPERTIES

Abstract

This study deals with the influence of processing–related parameters on the shear strength of the fiber/matrix interphase in a SiC/Ti MMC. The effect of variation of several parameters which effect composite residual stress were investigated, including the use of various material properties in modeling, applied temperature-pressure profile during consolidation, heat treatment, and fiber volume fraction. A numerical model is introduced through which the evolution of residual stress fields in each composite is calculated, during cool down from consolidation to room temperature, using a finite element approach. In this analysis, the material behavior, including the relaxation characteristics of the residual stresses at elevated temperature and their effects on the stress field at room temperature are identified. The effect of the change in residual stress in each case is related to the change in interface debonding properties using data obtained from fiber pushout tests.

3.1 Introduction

The various types of damage modes observed in a unidirectional metal matrix composite, MMC, subjected to fatigue loading include matrix cracking, fiber/matrix interface debonding, delamination, and fiber fracture [1, 2, 3]. In an unnotched MMC specimen, matrix cracks are initiated from the interphase region causing stress localization and delamination along the fiber/matrix interface. In a transverse loading of the composite, this damage mode results in a decrease in the composite modulus and a consequent decrease in strength. In the presence of a dominant matrix crack propagating perpendicular to the fiber orientation, unbroken fibers in the crack wake bridge the crack surfaces. Crack bridging,

71

which is an important toughening mechanism in a unidirectional MMC, is based on the ability of the fiber to carry the evolving stress caused by the relative displacement between the fiber and the matrix. In a MMC with strong fiber/matrix interface such as the B_4C-B/Ti-6Al-4V composite, limited relative displacement results in an early fiber fracture [4]. On the contrary, the relatively weak fiber/matrix interface in a SiC/Ti MMC allows for interface debonding to occur with a corresponding increase in the crack opening displacement. The initiation of damage in this interphase layer is affected by the localization of stresses as the matrix crack tip approaches the interface.

Both delamination and interface debonding modes of fracture, have been shown to be influenced by the fiber/matrix interphase strength [5, 6, 7]. The strength of the interphase dictates the extent of interface failure that, in turn, determines the durability of a composite system. In a SiC/Ti-MMC, the chemical bonding has been shown to be insignificant or nonexistent [8, 9]. The strength of fiber/matrix interphase region, therefore, is derived from mechanical clamping on the fiber due to the residual stress field. The residual stress states in each constituent of the composite are the results of fabrication method and post-processing heat treatment procedures. The interphase strength could then be viewed as a processing by-product parameter that can be tailored to optimize the resistance of the composite to fatigue failure. In addition, the strength is influenced by the growth kinetics and thermal aging characteristics of the interphase region. While direct measurement of the interphase strength is difficult to obtain, information leading to the determination of the strength values could be extracted from results of fiber pullout or pushout test of the composite samples. The influence of temperature and its consequent modification of the damage mechanism in a SiC/Ti MMC has not been studied. In the present work, the authors have examined the idea that the interphase strength is influenced

by the composite processing approach where the nature of the interface region and the internal stress field both define this strength.

Processing procedures, which vary for different composites, subject the material to a variety of time/temperature/pressure conditions. One of the most common processing procedures for fabricating metal matrix composites with continuous fiber reinforcement is the foil/fiber/foil layup method. This method involves alternating layers of matrix material, in the form of thin metal foils, with mats of ceramic fibers. A vacuum hot pressing technique is used to consolidate the layers of fiber and foil into the composite material. Another method for composite fabrication involves deposition of Ti on the SCS-6 fibers through a physical vapor deposition (PVD) process. The fibers are then consolidated in a sheath of the same Ti alloy by hot isostatic pressing (HIP). In either fabrication procedure, during the hot pressing procedure, the temperature and pressure are such that the matrix material experiences a viscoplastic deformation and flows around the fiber, resulting in a fully consolidated composite material upon cooling. Unlike the foil/fiber/foil layup method, this fabrication process allows for an easy means of varying the fiber volume fraction, while maintaining an even fiber distribution.

At the consolidation temperature, above 900 °C, a stress-free condition exists within the composite. Upon cooldown, residual stresses arise due to the large difference in coefficients of thermal expansion between the SiC fiber (5×10^{-6} / °C) and the Ti matrix (11×10^{-6} / °C). This difference causes an inherent residual compressive stress at the fiber/matrix interface, in both the radial and axial direction. The extent of the residual stress is dependent on the actual consolidation temperature and cooling rate, as well as the volume fraction of fibers in the composite.

Effects of different processing variables and post-processing heat treatment on the

residual stress field in the interphase region of a SiC/Ti MMC are studied in this chapter. Numerically, the residual stress states obtained by using various material behaviors in the computation of the residual stress state in the composite are compared. By varying the temperature-pressure profile during consolidation of composite specimens, the effect of the variation of these parameters is investigated. Additionally, the effect of a post-processing heat treatment is studied. The effect of fiber volume fraction on the debond shear stress and the debonding type in fiber reinforced metal matrix composites at elevated temperatures is also investigated. The effect of test temperature on these characteristics was considered for the temperature ranges of 20 °C through 650 °C. Fiber pushout procedures and numerical calculations of the associated stress field in thin-slice specimens cut from these composites are utilized to assess the interphase shear strength of a SiC/Ti MMC as function of test temperatures.

3.2   Material and Experimental Procedures

The experimental portion of this study focuses on two unidirectional fiber reinforced titanium composites, SCS-6/Timetal-21S and SCS-6/Ti-6242, manufactured by different processing techniques. These tw composite systems have a different titanium alloy matrix, but the same fiber reinforcement. The SCS-6 fiber is a 140 μm carbon cored SiC fiber with a 3 μm dual carbon coating. Timetal-21S is a metastable β titanium alloyed with 0.1 Fe, 16.0 Mo, 3.06 Al, 2.9 Nb, 0.2 Si. 0.22 C, 0.12 O, 0.005 N (wt %.) [10]. The SCS-6/Timetal-21S composite is fabricated using a foil/fiber/foil layup method, consolidated through vacuum hot pressing.   Variation in the processing parameters is possible by adjusting the temperature-pressure profile during the consolidation process and adding or eliminating a post-processing heat treatment.

A 6-ply SCS-6/Timetal-21S composite with an average fiber volume fraction of 0.32 was also used in this study. Ti-6242 is a near-α titanium alloyed with 0.06 Al, 0.02 Sn, .04 Zr, and .02 Mo. The SCS-6/Ti-6242 composite is manufactured through a process where the Ti is deposited on the SCS-6 fibers through a physical vapor deposition (PVD) process, then the coated fibers are consolidated in a sheath of the same Ti alloy by hot isostatic pressing (HIP).

This process allows complete consolidation at volume fractions much higher than those obtained using the foil/fiber/foil method, while maintaining regular fiber spacing, as seen in Fig.3-1, a micrograph of the crossection of a SCS-6/Ti-6242 composite with $V_f = 0.57$. SCS-6/Ti-6242 composite samples with average fiber volume fractions of 0.23, 0.30 and 0.57 were used to investigate the effect of fiber volume fraction on the interface debonding behavior of Ti MMCs.
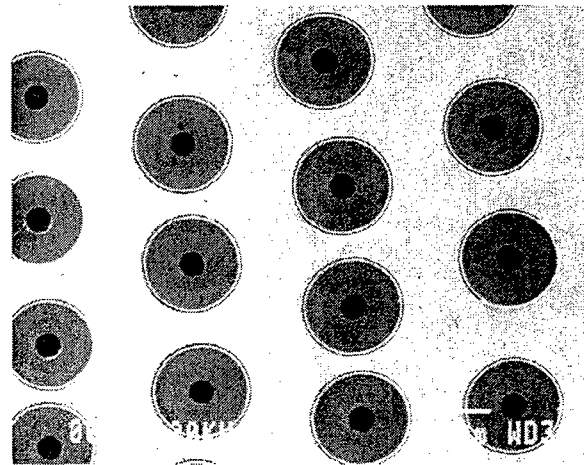
Figure 3-1   Micrograph of SCS-6/Ti6242 composite

Specimens were sectioned to the desired thickness with a diamond wafering blade at a high speed/low load, ground on SiC paper on both sides until the desired thickness was

75

attained, then diamond polished through 1 μm grit. Specimens were mounted in the specimen holder of the fiber push out apparatus and a low magnification optical micrograph was taken of each specimen. Fibers aligned with grooves in the pushout base of the test apparatus were chosen and marked on the micrograph for ease of identification during testing. The specimen holder is mounted on a removable assembly including an x-y stage with motorized actuators for remote alignment of the chosen fiber with the punch. The carbide punches used in this study are tapered at a 30° included angle (for added strength) with a beveled edge flat tip of 100 μm diameter for the SCS-6 fibers. A detailed description of the pushout apparatus is given in the previous chapter.

Vacuum testing was performed in a chamber which is evacuated to approximately 10^{-6} torr.. The specimen, once positioned in the vacuum chamber was heated to the required test temperature, and then monotonically loaded until fiber pushout occurs. Load and motor displacement are continuously recorded during the loading process. Characteristics of these load-displacement pushout curves for the material under examination were discussed in detail in the previous chapter. Fiber pushout is verified through SEM observations of the reverse side of the specimen. In addition, the surface morphology of the pushed out fibers, and the location of the debond crack is recorded.

As discussed previously, the interphase shear strength, τ_d, has been determined using the assumption of an average shear stress distribution along the interphase at the load level, P_d, corresponding to the initial debonding, as $\tau_d = P_d / (\pi\, d_f\, h)$, where d_f is the fiber diameter, and h is the specimen thickness (or fiber length). The interfacial frictional shear stress at any point after the initiation of debonding is similarly calculated, substituting the instantaneous load, P_i, for the debond load, P_d, and the remaining bonded length for the fiber length, h. The bonded length is considered to be (h-δ), where δ is the sliding distance

76

of the fiber. In this study, only the initial frictional shear stress, i.e. the value corresponding to the load at the bottom of the debonding drop, is compared.

3.3 Numerical Procedure - Two phase model for generation of residual stresses

Significant levels of thermal residual stresses are induced in the composite due to mismatches in the coefficients of thermal expansion of the constituent phases. A concentric two-phase cylinder model of a fiber embedded in the matrix phase is utilized in this work to calculate the evolution of stress fields along the interface during the consolidation process, and the stress variations in the prepared test specimen. This idealization of the composite is possible due to the hexagonal fiber array exhibited in this composite, as shown in Fig. 3-2.
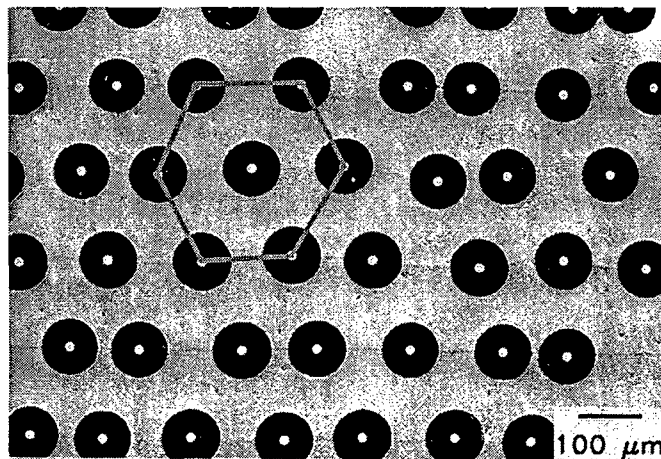
Figure 3-2 Micrograph showing hexagonal fiber array exhibited in a metal matrix composite fabricated through the F-F-F layup method.

A hexagonal unit cell is idealized as concentric fiber and matrix cylinders, as shown in Fig 3-3, where the radius of the matrix cylinder is determined by the physical radius of

the fiber and the composite fiber volume fraction. The interface can be represented by a

mathematical plane of zero thickness, since interface debonding has been observed to occur

along the carbon-rich coating, which is a thin layer in relation to the fiber or matrix

dimension. This interface plane is assumed to accommodate radial and shear stress

components. In an infinitely long composite where the free surface effect is negligible, and

perfect bonding is assumed to exist, the shear stress component diminishes and the

mechanical bonding is provided by the compressive radial stress only.
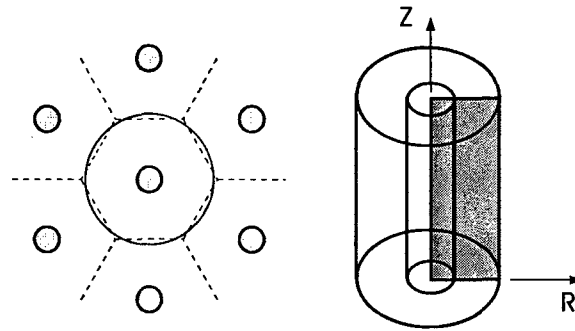
Figure 3-3 Schematic showing hexagonal unit cell idealized as a concentric fiber
and matrix cylinders, and axisymmetric plane used in finite element
modeling.

The meshing in the finite element model used for evaluation of the residual stresses

for this portion of the study is shown in Figure 3-4. Due to the axisymmetric geometry of

the model, only a longitudinal plane of the composite cylinder needs to be analyzed This

axisymmetric model consists of 480 fiber elements and 840 matrix elements. The element

size is biased with smaller elements adjacent to the interface on both the fiber and matrix

side, allowing greater accuracy in critical locations in the model without increasing the

number of elements dramatically.

A constraint of constant radial displacement is imposed on the outer surface of the

modeled cylinder to acknowledge the existence of surrounding fibers. An isostrain condition is imposed on one end of the cylinder to represent the generalized plane strain condition, while the other end is fixed for investigation of the residual stress state in the bulk composite. In order to represent the cutting of a specimen slice for fiber pushout testing, the isostrain condition on the end of the composite cylinder is released. This represents the free surface that is formed in the composite specimen.

fiber matrix
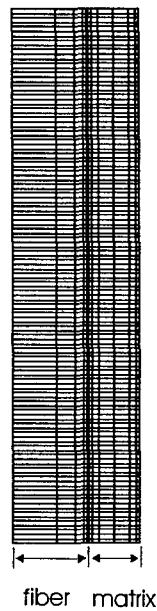
Figure 3-4   Finite element model showing mesh used for evaluation of residual stresses in
                       SCS-6/Timetal-21S composite system

3.4   Effect of modeling using various material behaviors

Numerical generation of residual stresses in a composite requires input of material properties of the composite constituents. This study examines the dependency of the residual stresses on the type of material behavior used to generate the stresses. The fiber, composed predominantly of SCS-6, a silicon carbide ceramic, exhibits elastic behavior for

temperatures within the recommended range of use of the composite.. For this reason, the focus of this study will be on the matrix material, Timetal-21S, a metastable beta titanium. The residual stresses generated modeling the matrix material behavior as elastic, elastic-plastic, and viscoplastic will be investigated.

The mechanical and physical properties of the SiC SCS-6 fiber and the titanium alloy Timetal-21S are obtained from several publications [11, 12, 13]. The fiber is assumed to behave elastically at all loading conditions, while the matrix behavior for this study has been modeled using several different material properties, including elastic, elastic-perfectly plastic and viscoplastic. All the constituent phases are considered isotropic, and a uniform thermal distribution across all layers is assumed. The variation with temperature of the modulus of elasticity (Young's modulus) and CTE of SCS-6 and Timetal-21S are presented graphically in Fig. 3-5(a-b) respectively. Poisson's ratio, which is not temperature dependent, is 0.34 for the SCS-6 and 0.25 for the Timetal-21S. The viscoplastic behavior of the matrix is modeled using a unified visoplastic theory [14, 15].

(a) Modulus of Elasticity (E)   (b) Coefficient of Thermal Expansion (CTE)
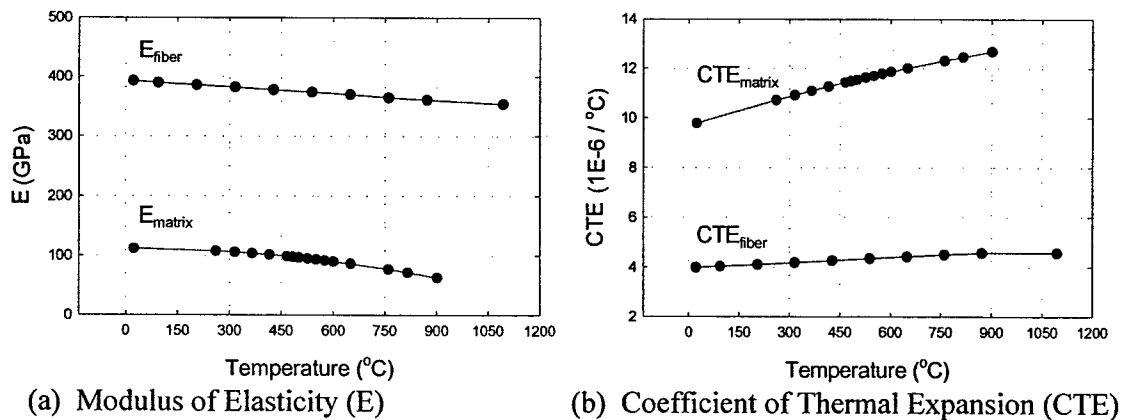
Figure 3-5   Variation of material properties with temperature for the SCS-6 fiber
              and the Timetal-21S matrix

80

In each case, the process-induced residual stress field is established in the composite by a procedure involving cooling down from a stress-free temperature (815 °C) to room temperature. The fiber and matrix phase are subjected to compressive and tensile residual axial stresses, respectively, during cool down because the coefficient of thermal expansion, CTE, of the SiC fiber (4.0 X 10^{-6} /°C at 25 °C) [16] is less than of the titanium alloy matrix (9.8 X 10^{-6} /°C) [16]. The interphase region is a highly stressed region in the composite since it experiences the effect of both thermal strain due to CTE mismatches and mechanical strain due to differences in the Poisson ratios between the fiber and the matrix phase.

The evolution of the residual stresses in the matrix phase adjacent to the fiber/matrix interface for purely elastic material properties is shown in Fig. 3-6. At room temperature, the locked-in residual stresses are as follows: σ_{11} is 357 MPa in compression, σ_{22} is 587 MPa and σ_{33} is 762 MPa, both in tension. Since no relative displacement occurs between the fiber and matrix due to the boundary conditions that simulate an infinitely long composite, there is no shear stress along the interface.
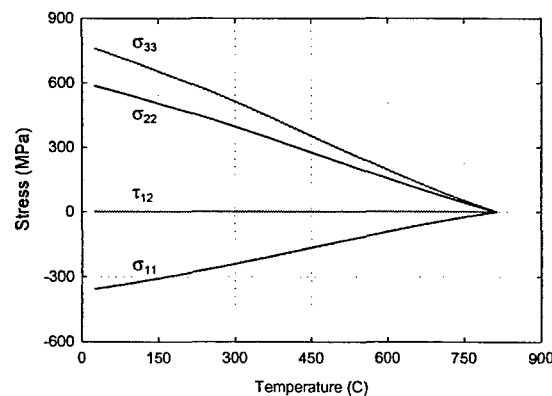
Figure 3-6   Evolution of residual stresses in the matrix adjacent to interface in SCS-6/Timetal-21S during cooldown using elastic matrix properties

81

Similar evolution curves occur for cooldown using elastic- perfect plastic properties

for the Timetal-21S matrix, as illustrated in Figure 3-7. A slight difference is seen in the

room temperature values of σ_{22} and σ_{33}, the tensile components of the residual stresses.

When plasticity is included in the model, a change occurs at approximately 300 $^\circ$C, when

the stresses are high enough to cause some plastic deformation of the matrix material. This

deformation reduces the amount of residual stresses in the matrix by approximately 7%. In

this case, the room temperature stresses are as follows: σ_{22} = 543 MPa and σ_{33} = 705 MPa.
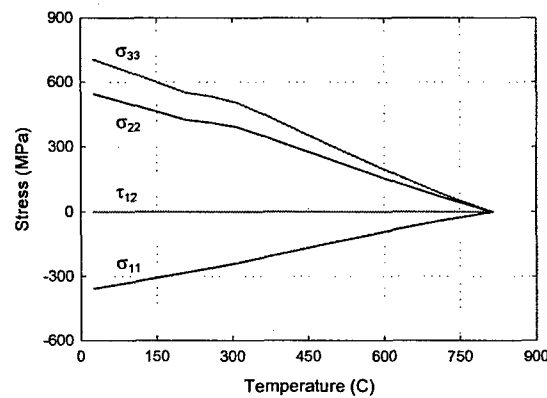
Figure 3-7   Evolution of residual stresses in matrix adjacent to interface in
             SCS-6/Timetal-21S during cooldown using elastic-pure plastic
             matrix properties

Figure 3-8 shows that the room temperature residual stresses are greatly reduced

when viscoplastic material properties are used for the matrix. In this case, σ_{11} = -105

MPa, σ_{22} = 171 MPa and σ_{33} = 214 MPa, showing a 100% drop in radial and over 70%

drop in both axial and hoop stress when compared to the purely elastic situation. These

values compare favorably to an interactive experimental/mathematical technique which

determined the axial component of residual stress in a SCS-6/Timetal-21S composite at 25

$^\circ$C to be 160 and 174 MPa following a simulated cooling rate of 0.05 and 0.5 $^\circ$C/sec,

respectively [17]. This data suggests that the viscoplastic simulation generates the most

reasonable values for the internal stress field in the composite.
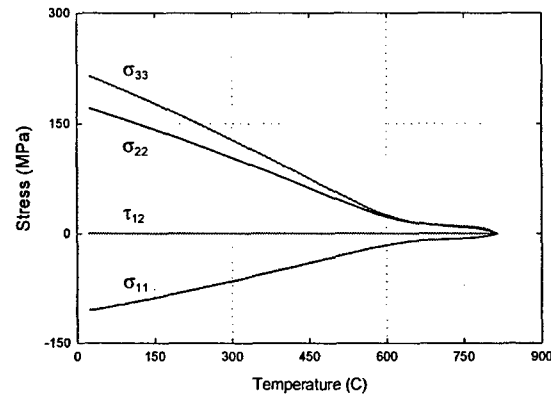
Figure 3-8   Evolution of residual stresses in matrix adjacent to interface in
SCS-6/Timetal-21S during cooldown using viscoplastic matrix
properties

The curves generated in these simulations indicate that while the elastic portion of
the evolution curve is controlled by the mismatches in the coefficients of thermal expansion
between the fiber and the matrix, the stress magnitude is set by the degree of inelastic flow
permitted in the viscoplastic affected range, from consolidation to about 600 °C.

3.5   Effect of processing parameters

3.5.1   Experimental setup and Procedure

The material used in this study is a unidirectional SCS-6/Timetal-21S composite.
Two composites, denoted as C1 and C2, are fabricated from identical materials, in the
Mechanics of Materials Laboratory (MML) at the University of Rhode Island using a
foil/fiber/foil lay-up consolidated through a vacuum hot pressing technique. The third
composite was provided by Timet.. The nominal fiber volume fraction in all cases is 0.35.
Each composite is fabricated with a unique set of processing variables to generate different

processing-related properties. The temperature and applied pressure histories employed during post-fabrication cooldown are illustrated in Figs. 3.9(a) and (b), respectively. The first two temperature profiles include an 8-hour heat treatment in vacuum at 650 °C. The third composite was subjected to a separate 8-hour heat treatment prior to testing. These temperature-pressure profiles were chosen to be considerably different, while still allowing for full consolidation of the composite.

(a) temperature profile   b) pressure profile
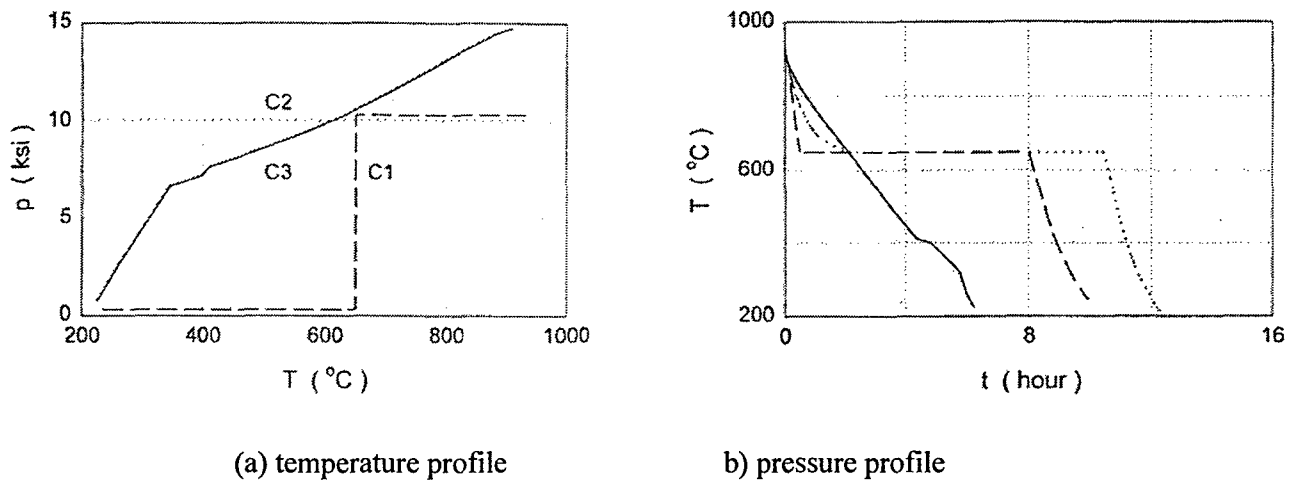
Figure 3-9 Temperature and pressure profiles used for consolidation of test composites.

The cross section of each of the composite samples exhibit a staggered array of fiber arrangement with full consolidation taking place around the fiber and at the foil/foil interfaces. Fig 3.10 shows an example of one of the composites fabricated in the MML, which has been prepared for fiber pushout testing.

84
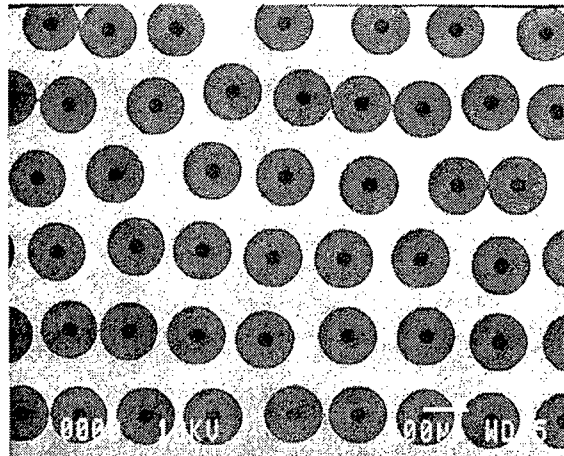
Figure 3-10   Micrograph of composite, C1, fabricated for this study

3.5.2   Fiber Pushout Results

Fiber pushout tests are performed at ambient temperature and 500 °C, which is the expected operating temperature of this composite system. The fiber pushout apparatus and procedure are detailed in Chapter 2. The pushout test matrix is shown in Table. 3-1, where H is the specimen thickness, P_d is the load at the initiation of debonding, P_s is the initial shear load required to push the fiber after complete debonding, and τ_d is the interfacial shear strength, calculated from P_d and the thickness, as discussed in Chapter 2.

Data for Composite 3 are available at several temperatures from the work presented in Chapter 2, while Composite 1 and 2 were tested at room temperature, 500 and 650 °C. Figure 3-11 is a plot of the change in interfacial shear strength, τ_d, with temperature, for each of the three composites. There is no significant difference in τ_d between the composites at any of the temperatures tested suggesting that processing parameters do not significantly effect the interfacial shear strength of this system. In order to explain these results, an investigation was undertaken to study the effects of the processing parameters

85

on the residual stress state in the composite.
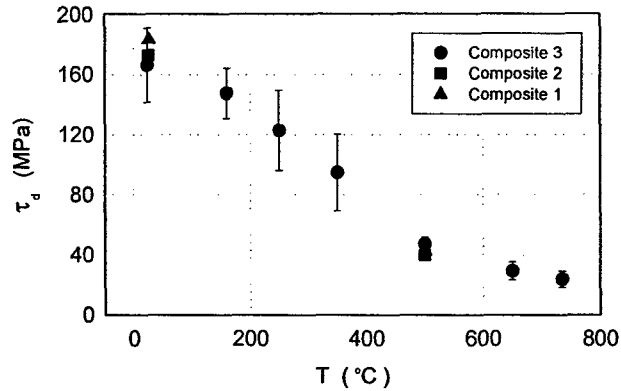
Figure 3-11   Interfacial shear strength for SCS-6/Timetal-21S composites with varying processing parameters at several temperatures

Table 3-1   Test matrix for fiber pushout tests of SCS-6/Timetal-21S composites.

ID	T ($^{\circ}$C)	H (mm)	P_s (N)	P_d (N)	T_s (MPa)	τ_d (MPa)
C1	25	0.50	32.0	38.0	145.5	172.8
C1	500	0.91	13.6	16.0	34.0	40.0
C2	25	0.50	35.0	40.3	159.2	183.3
C2	500	0.91	10.3	17.0	25.7	42.5
C3	25	0.50	37.5	46.0	170.6	191.0
C3	163	0.52	23.9	31.0	104.5	135.5
C3	250	0.91	40.0	50.0	100.0	124.9
C3	350	1.10	28.0	44.0	57.9	90.9
C3	500	1.40	25.5	23.0	41.4	34.1
C3	650	1.40	17.9	20.5	29.1	30.9
C3	735	0.95	2.5	12.0	6.0	28.7

3.5.3 Residual Stress Analysis

The process-induced residual stress is established in each composite by a procedure involving cooling down from a stress-free temperature, as described previously, with the corresponding temperature history shown in Fig. 3-9(a). The applied fabrication pressure, however, has not been modeled in the simulation due to the selection of the representative volume element. As explained in the previous section, the magnitude of the residual stresses upon cooldown is set by the degree of inelastic flow permitted in the range affected by viscoplasticity, from consolidation to about 650 °C. However, the relaxation of the residual stress in this temperature range is limited due to its small magnitude as shown in Fig. 3-12. In addition, the evolution curves for all three composite samples considered in this study are practically identical, thus, the residual stress contribution to mechanical strength of the interphase is expected to be correspondingly similar.
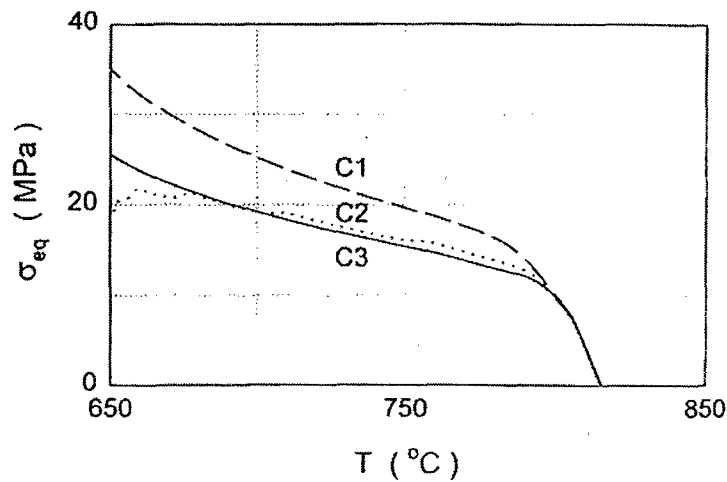
Figure 3-12   Portion of evolution curve showing small magnitude of region that determines the amount of relaxation of the residual

These observations explain the results from the previous section that showed that the various temperature-pressure profiles applied during consolidation had no significant effect on the interfacial shear strength of the composite at the room temperature, 500 and 650 °C. The interfacial shear strength is predominantly affected by the clamping force provided by the radial residual stress in the composite at the operating temperature. Since then variation of processing parameters have limited ability to change the residual stresses in the composite, it follows that the effect on the interfacial shear stress would be similarly limited. Additionally, as temperature is increased, this effect will be smaller, since the residual stresses decrease with increasing temperature, as discussed in Chapter 2.

3.6   Effect of Post-Processing Heat Treatment

The effect of post-processing heat treatment, or thermal aging, is discussed in detail in Chapter 2.5.2 and 2.5.3. Briefly, thermal exposure under vacuum conditions results in no noticeable increase in the interphase size or composition. The values of τ_d and τ_s for these thermally exposed specimens were determined through the use of fiber pushout in vacuum at temperatures representative of typical in-use conditions. These tests indicated that the effect of thermal exposure is not as significant as the test temperature at 650 °C, where there is little difference in the τ_d or τ_s between unaged and vacuum exposed conditions to 100 hours. At 500 °C, however, vacuum exposure decreases τ_d by approximately 50 % and τ_s by over 30 %

Thermal exposure testing in air at 650 °C, even for exposure times as low as 55 hrs, show the carbon layer surrounding the fiber is depleted along the entire length of the fiber, leading to no interphase shear strength or frictional shear stress along the interphase. At 500 °C, the carbon layer is degraded but not completely oxidized

3.7 Effect of Fiber Volume Fraction

3.7.1 Experimental setup and Procedure

The experimental setup for this part of the study was identical to that described in Section 3-5-1, with one exception. The SCS-6/Ti-6242 specimens, fabricated as described in Section 3-2 (Material and Experimental Procedures) have a round crossection, unlike the SCS-6/Timetal-21S specimens which come in a flat sheet. In order to fit these specimens in the test apparatus and used the same fiber alignment procedure, the specimens were ground on two opposing edges, creating a specimen with parallel sides.

3.7.2 Pushout results

In order to study the effect of variation of fiber volume fraction on the interphase properties of a Ti/SiC composite system, elevated and room temperature fiber pushout tests were performed on several SCS-6/Ti6242 composite samples with two fiber volume fractions. These had an average fiber volume fraction of 0.57 and 0.30 or 0.23 samples and were between 540 and 680 μm thick. Attempts to test thicker specimens failed due to the high debond shear strength of this composite. Employing a procedure similar to that used for the Timetal-21S composite, the interphase shear strength and frictional shear stress were calculated for these composite specimens at 23, 500 and 650°C. The results are shown in Fig. 3-13 as a comparison of τ_d for the high and low fiber volume fraction. It can be seen that this composite has a stronger fiber/matrix interphase than the Timetal/21S interphase, possibly due to the different processing procedure.

89

350
300
250
200
150
100
50

τ$_d$ (MPa)

0   100   200   300   400   500   600
TEMPERATURE (°C)

■ V$_f$ = .57, 650 μm
◆ V$_f$ = .57, 580 μm
▲ V$_f$ = .30, 680 μm
▼ V$_f$ = .24, 540 μm
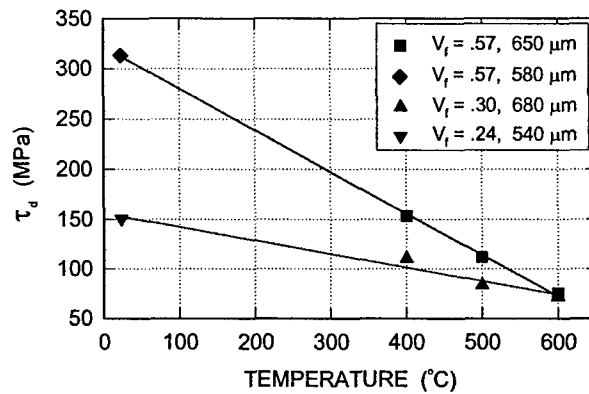
Figure 3-13   Comparison of interphase shear strength, $\square_d$, for specimens with fiber volume fractions Vf = 0.57 and Vf = 0.23 or 0.30 in SCS-6/Ti6242

Both specimens displayed a fairly linear decrease in interfacial shear strength with increasing temperature. The samples with the higher fiber volume fraction show a higher interphase shear strength than those with the lower fiber volume fraction at each temperature. with the variation between high and low fiber volume fraction most prominent at room temperature, where the difference in residual stresses would be highest. At elevated temperatures, the residual stresses will relax with increasing temperature, allowing the high and low fiber volume fraction samples to display similar debonding strengths.

Additionally, in this portion of the study, the type of debonding behavior was investigated. Guichet et al. [18], in room temperature fiber pushout tests on SCS-6/Ti-6242, have identified two types of debonding behavior, which they have denoted as Type I and Type II, drawn schematically in Fig 3-14. In type I debonding, the initiation of debonding is indicated by either a change in linearity or a small load drop, followed by an increasing slope during continued load application. A maximum gradually occurs, followed by a slow decrease in slope as the fiber slides. Type II debonding exhibits a linear increase in load until a maximum is reached, followed by a sudden load drop as the

interface debonds catastrophically. At the bottom of this load drop, the load either remains

steady or very gradually decreases.
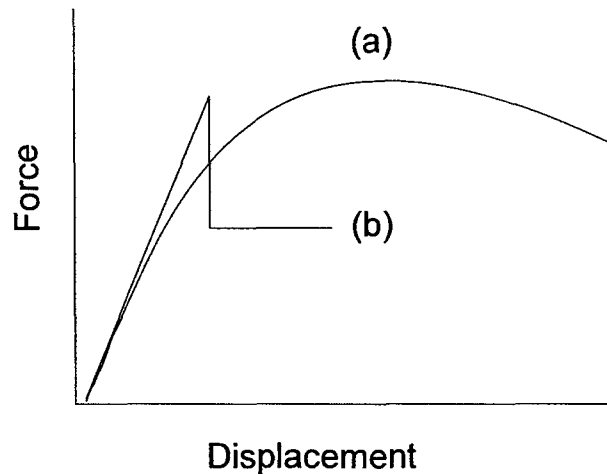
Figure 3-14   Schematic of two distinct types of debonding, (a)Type I and (b)Type II

Similar, but not identical, behavior has been found in the current elevated

temperature study of the Ti6242 composite, with two distinct debonding types observed.

Figure 3-15 shows typical fiber pushout curves for the 0.24 volume fraction SCS-6/Ti6242

composite at room temperature. In order to avoid exceeding the fracture strength of the

punch used for fiber pushout, it was necessary to terminate the test before reaching a

maximum load for this thickness. Previous testing on thinner specimens provided

verification that, after the small load drop, the curve gradually increases to a maximum and

then slowly decrease as shown in our schematic for Type I debonding. This type of

debonding behavior is similar to that observed in the SCS-6/Timetal -21S composite

system for room- and low temperature testing, as discussed in detail in Chapter 2. At

elevated temperatures below 400 °C, both the high and low fiber volume fraction

specimens exhibited only this type of debonding behavior.

91
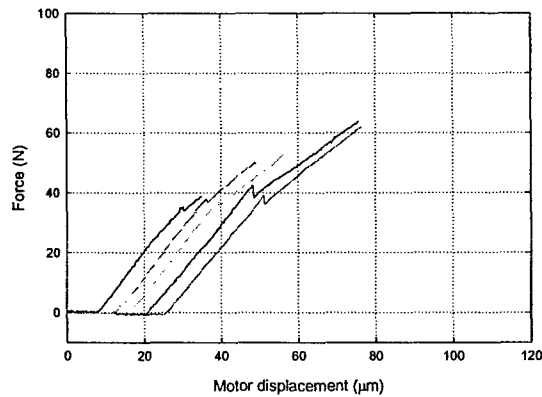
Figure 3-15   Fiber pushout curves: SCS-6/Ti-6242, 23 °C, Vf = 0.24, h = 0.58 mm

At higher temperatures, a second type of debonding was observed, similar to Guichet's Type II debonding, where the load rises linearly, then a change in linearity occurs where debonding initiates, followed by a region of increasing compliance as the debonding length increases. This stage is terminated by a sudden, large load drop where complete debonding occurs, followed by a frictional sliding portion where the load either remains approximately constant or gradually decreases. An example of this is shown in Figure 3-16, for the 0.57 fiber volume fraction specimen tested at 610 °C.
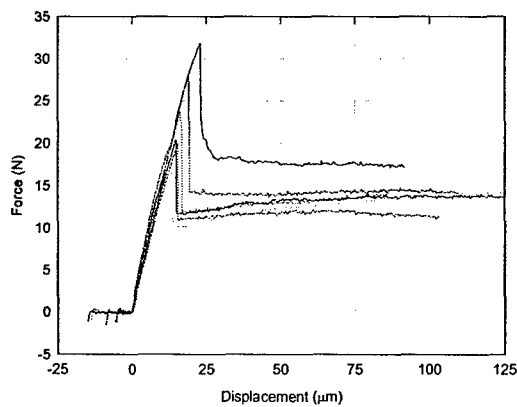
Figure 3-16   Fiber pushout curves: SCS-6/Ti-6242, 610 °C, Vf = 0.57, h = .70 mm

92

Guichet, et al. [18] have attributed this difference in pushout behavior to the location of the debond crack. For Type I debonding, they observed that the decohesion occurs between the carbon layers, resulting in fractured particles of carbon adhering to the surface of the fiber. Conversely, the decohesion was observed to occur strictly between the fiber coating and the reaction zone for the Type II debonding, with an intact carbon layer, and a smooth fiber sliding surface. In the current study, the observation of both types of debonding within the same 0.57 fiber volume fraction specimen at room temperature (Figure 3-17) supports the premise that debonding location affected debonding type. Additionally, the fact that both debonding types occurred in the same sample indicates that at the higher fiber volume fraction, the debonding behavior is susceptible to the differences in local residual stress fields. The surfaces of the fibers pushed out at elevated temperatures were studied using SEM, and compared to the type of debonding observed during pushout. The results of this comparison show that the roughness of the fiber surface is a factor in determining the debonding type. At room temperature for Type II debonding, decohesion occurs between the carbon layer and the interphase. At elevated temperatures, however, Type II behavior was found to correspond to decohesion that occurs between carbon layers also. In this case, the fiber surface was smooth, probably due to the lower debond shear strength, as a result of the relaxation of the clamping force on the fiber at elevated temperature. Type I decohesion occurred when the fiber surface was rough, primarily between carbon layers, at all temperatures.
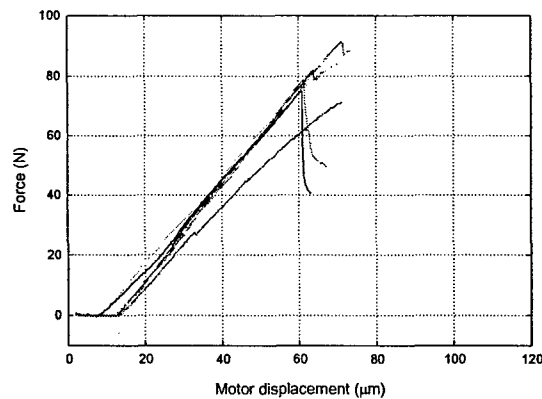
Figure 3-17   Fiber pushout curves: SCS-6/Ti-6242, 23 °C, Vf = 0.57, h = .540 mm

Note that the difference in the characteristics of the two debonding types between the work of Giuchet, et al and the current study can be attributed to the thickness of the specimens used in each study. As previously discussed, in order to accurately represent the behavior of the bulk composite in a thin slice specimen, the cut sample must be thick enough to preserve the residual stresses in the bulk composite, at least along the center of the specimen. This minimum thickness was not maintained in the study by Guichet, et al. that could lead to some variation in the characteristics of the fiber pushout curve in that study. However, the basic shapes of the curve remain similar and a comparison is possible.

3.7.3   Numerical Analysis

Variation in fiber volume fraction will affect the residual stresses generated in the composite upon cooldown. In order to correlate these changes in residual stress to the changes in the interphase properties of a Ti/SiC composite system, the two-phase finite element model previously described was applied to composites with several different fiber volume fractions. It has previously been shown that in order to accurately model the

94

residual stress state in a Ti/SiC composite, a viscoplastic analysis is necessary. Since the state variables for use in a numerical model are available for the SCS-6/Timetal-21S system, while at the time of the analysis, they did not exist for the SCS-6/Ti-6242 composite system, the numerical work will be carried out on the SCS-6/Timetal-21S system. Due to the similarities in the two composites, the trend in residual stress distribution should be similar in both systems.

During the cooldown process, the residual stresses build up at the fiber/matrix interface. A plot of the residual stress as a function of fiber volume fraction at various temperatures, are presented in Figures 3-18(a)-(c). Note the difference in scale for the stress axis. These plots show that as the fiber volume increases, the radial, axial and hoop stresses all increase. That is, the axial and hoop stresses become increasingly tensile, while the radial stress becomes less compressive. Additionally, as the temperature increases, the residual stresses decrease for all fiber volume fractions. Note that in an infinitely large composite the shear stresses are always negligible.

(a) 23 °C   (b) 500 °C
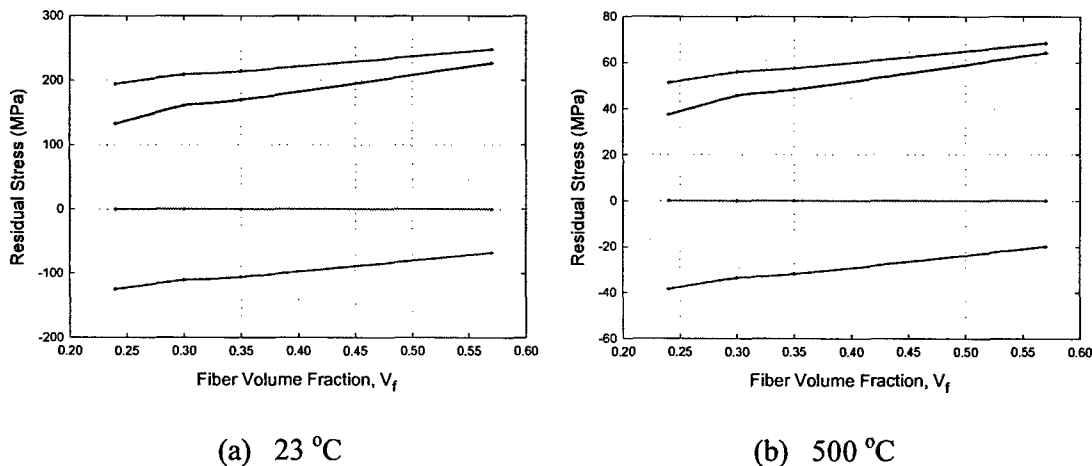
Figure 3-18(a-b)   Residual stress as a function of fiber volume fraction at various temperatures
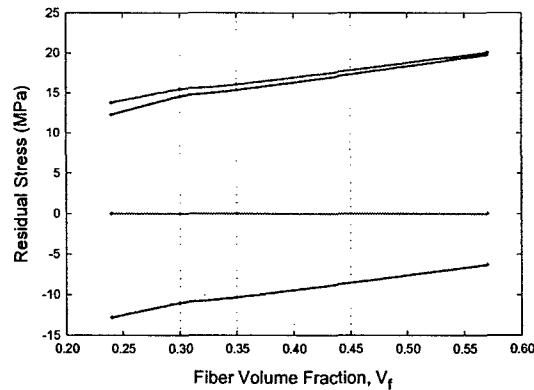
c) 650 °C

Figure 3-18(c)   Residual stress as a function of fiber volume fraction at various temperatures

When the composite specimen is cut, the residual stresses are redistributed due to the free surface along the cut edges. Figure 3-19 shows the radial residual stress distribution at room temperature for several fiber volume fractions in specimens 1.0 mm thick. The values of stress near the center of the specimen length are indicative of the stresses in the bulk composite. For a majority of the length of the interface, neglecting the edge effects, the radial, axial and hoop stresses, σ_{11}, σ_{22} and σ_{33} respectively, increase with increasing fiber volume fraction. Also note that as the fiber volume increases, the residual stress distribution becomes increasingly less sensitive to edge effects.
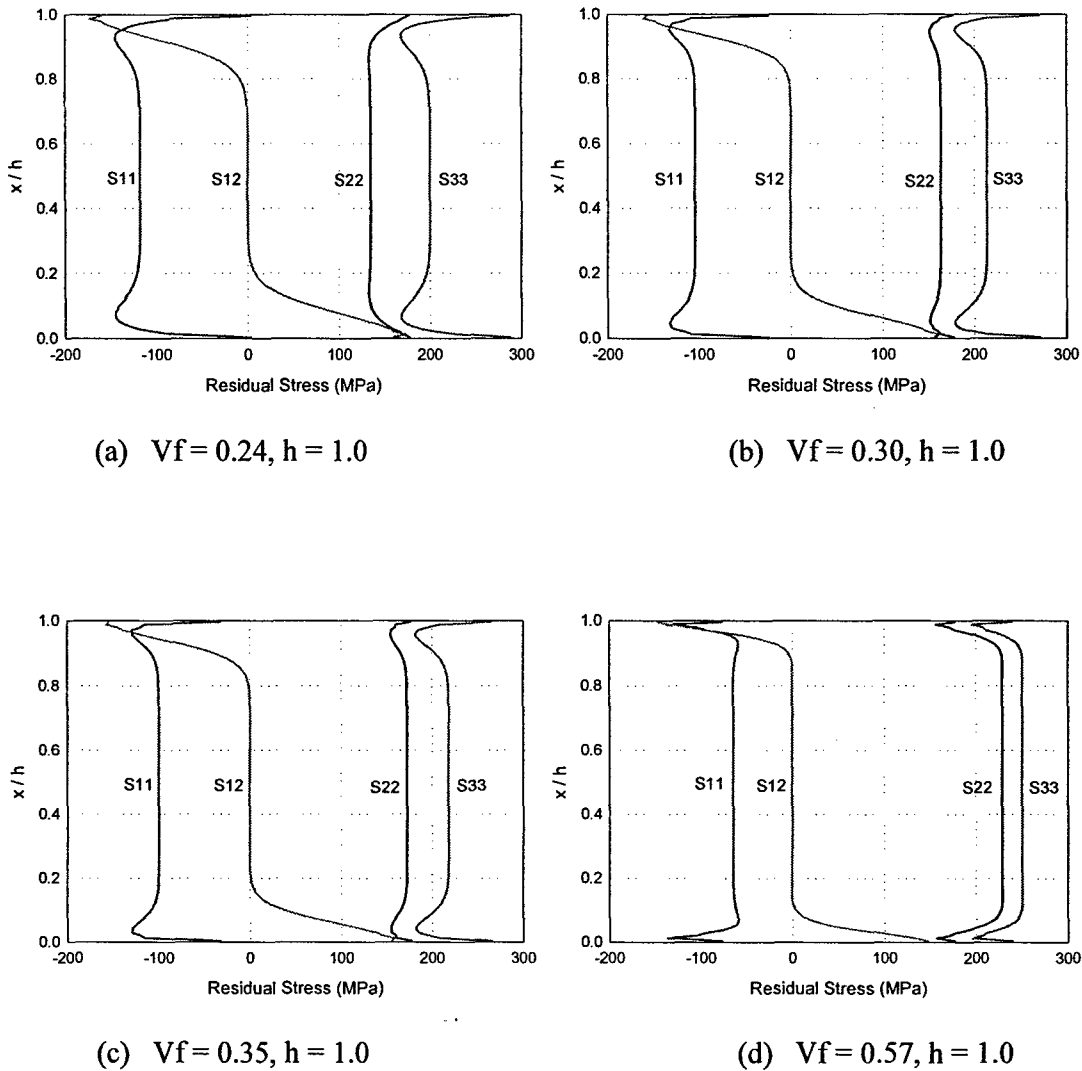
Figure 3-19   Residual stress distribution at room temperature in composite specimens
with thickness h=1 and various fiber volume fractions

Experimental results show that the interfacial shear stress increases with increasing
fiber volume fraction, while numerical results show that in the bulk composite, the radial
residual stress decreases with increasing fiber volume fraction. According to previous
observations (see Chapter 2), if the radial residual stresses in the bulk composite is the
controlling factor in determining the level of interfacial shear stress, the interfacial shear
stress should increase as the radial residual stress increases.   It has been noted by

researchers [19] working on alumina glass composites that the fiber volume fraction that can be modeled accurately with a simple two- phase model is limited by the fiber volume fraction which allows interaction between the stress fields of neighboring unit composites. In order to eliminate the possibility of inaccuracies due to this stress field interaction, the concentric cylinder model was modified to include a surrounding bulk composite region. The properties of this bulk composite region were calculated using a the rule of mixtures for Young's Modulus and Poisson's ratio, and a modified rule of mixtures [20] for the coefficient of thermal expansion. These properties are plotted in Figure 3-20 for the range of temperatures and fiber volume fractions under consideration.

(a) Modulus of Elasticity (E)   (b) coefficient of thermal expansion (CTE)
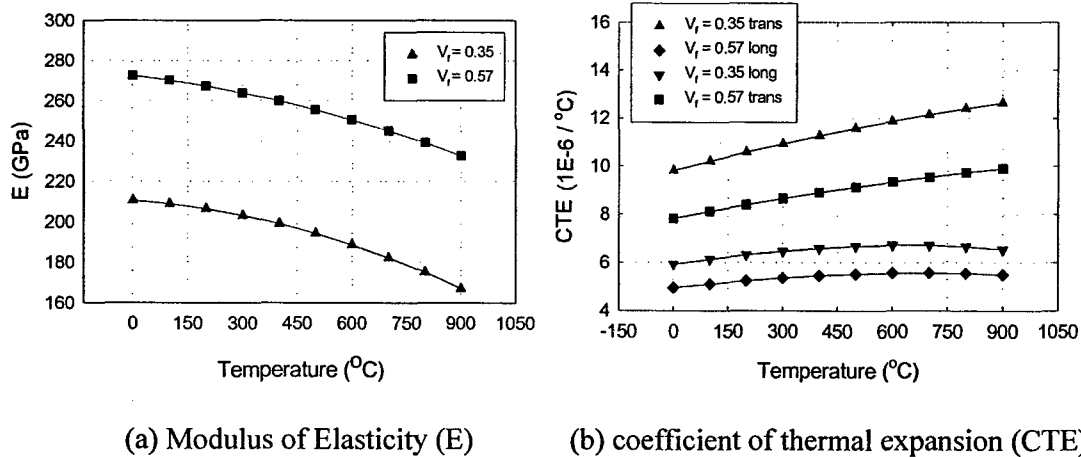
Figure 3-20   Material properties (in longitudinal and transverse directions) for numerical modeling of SCS-6/Timetal-21S using the equivalent composite cylinder

This three-phase model was used to generate the residual stresses in the composite slice during cooldown to room temperature and after "slicing" the composite to a thickness identical to the fiber pushout specimen. The inclusion of the third phase of bulk composite changes the stress state significantly, as shown in Figure 3-21, a plot of the residual stress state in a thin slice composite specimen calculated using a three-phase concentric cylinder

model. Notably, the radial residual stresses, σ_{11}, are considerably more compressive than in the previous calculations, although the trend of decreasing compressiveness with increasing fiber volume fraction is the same in both simulations.

(a)   Vf = 0.35, h = 0.65   (b)   Vf = 0.57, h = 0.65
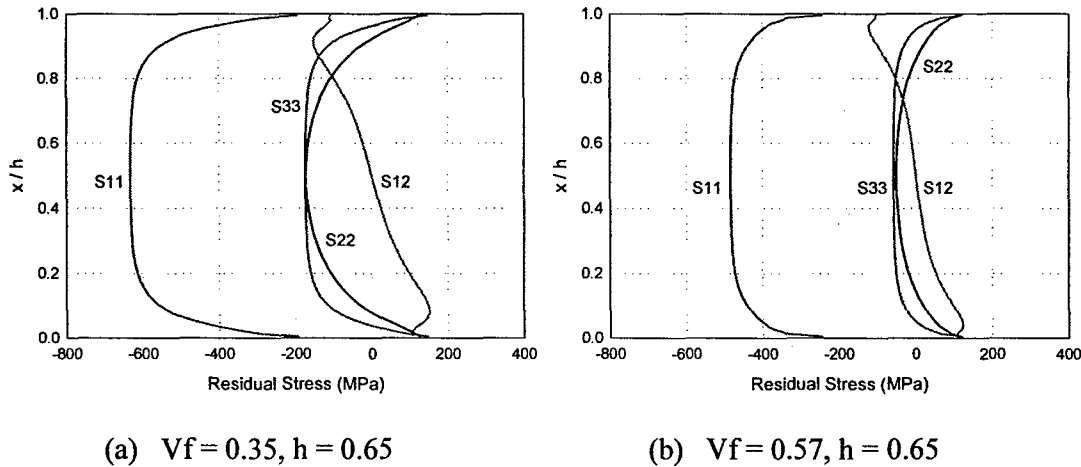
Figure 3-21   Residual stress distribution at room temperature in composite specimen using 3-cylinder modeling approach for two fiber volume fractions

Looking at the role of edge effects on the residual stress distribution, it is apparent that, although in the center of the composite slice the radial residual stress, σ_{11}, increases with increasing fiber volume fraction, along the edges of the specimen, the radial stress becomes more compressive as the fiber volume fraction increases, requiring a higher applied load for intial debonding and a higher calculated interfacial shear stress. This trend is also seen in the two-phase model

. A major difference between the two- and three-phase models is the distribution of the axial stress, σ_{22}. In the two-phase model, in which the effect of the bulk composite is ignored, the axial stress is tensile for all fiber volume fractions under consideration (Fig. 3-19), with the σ_{22} higher in the highest fiber volume fraction sample. In the three-phase model calculations, in both fiber volume fractions, the axial residual stress is compressive

and increases with increasing fiber volume fraction, i.e. the axial residual stress becomes less compressive with increasing fiber volume fraction. Note that the residual stresses are in the matrix phase adjacent to the fiber/matrix interface. (The residual stresses in the fiber will be in the opposite direction). In this portion of the study, the location of the initiation of debonding was not investigated. It is assumed that the debonding takes place from the top of the specimen, as observed for SCS-6/Timetal-21S in the work detailed in Chapter 2. Based upon this assumption, an increase in the compressive stress in the matrix adjacent to the interface corresponding to an increase in the residual tensile stress in the fiber, as seen in the change from high to low fiber volume fraction, would add to the tendency of the fiber to debond when a compressive load is applied during fiber pushout testing. This result suggests that the radial axial stress is a key controlling factor in the interfacial shear strength in fiber reinforced metal matrix composites.

Additionally, although, as previously discussed, no residual shear stress exists in the semi-infinite bulk composite, cutting changes this stress state due to the new surfaces that are created. After cutting, the residual shear stress varies from zero at the middle of the specimen to a maximum along the cut edges. The low fiber volume fraction specimen exhibits a slightly higher residual shear stress just below the cut surface than the high fiber volume fraction. Since the debonding originates along the free surface, it follows that a higher shear stress along the surface in the higher volume fraction sample would result in higher values of interphase shear strength.

3.8   Summary and Conclusions

The work in this chapter focuses on the influence of various processing-related parameters on the interfacial shear stress in SiC/TiMMC at several practical temperatures.

The effect of variation of processing conditions including variation of fiber volume fraction and of the time-temperature-pressure profile during consolidation of the composite are examined, as well as the effect of the post-processing heat treatment. Thin-slice fiber pushout tests are used to find the interfacial shear strength of the composite systems under investigation. A concentric cylinder model is introduced to numerically obtain the compsite residual stress state both in a semi-infinte composite, and a thin-slice specimen. This residual stress state is discussed in relation to the experimental results. Additionally, the effect on the calculation of residual stresses using various matrix material properties, including elastic, elastic-pure plastic and viscoplastic is examined.

The following results were obtained from this work:

1. The difference in residual stress generated using an elastic and an elastic pure-plastic matrix material model is only about 7%. When viscoplastic material properties are used for the matrix, residual stresses are reduced by as much as 100% for radial and 70 % for axial and hoop stresses at room temperature.

2. While the elastic portion of the stress evolution curve is controlled by the mismatches in the coefficients of thermal expansion between the fiber and the matrix, the stress magnitude is set by the degree of inelastic flow permitted in the temperature range affected by the viscoplasticity, from consolidation to about 600 °C.

3. An increase in the fiber volume fraction increases the interfacial shear stress at all temperatures, with the most noticeable difference at room temperature. This

increase is possibly due to the decrease in compressive axial residual stress in the matrix adjacent to the interface with increasing fiber volume fraction.

4.   Fiber pushout tests of low (23-35%) and high (57%) fiber volume fraction specimens yield two different types of fiber pushout curves . Although these curves are similar to those obtained in Chapter 2 for temperature variation, they depend on fiber volume fraction as well as temperature.

5.   Variation of the time-temperature-pressure curves during consolidation of the SCS-6/Timetal-21S composite yields an insignificant change in the interfacial debonding behavior of this composite. This observation is due to the small amount of relaxation of residual stresses possible in the inelastic portion of the cooldown from the consolidation temperature to 600 °C.

3.9   References

[1]   P. Bowen, A. R. Ibbotson, and C. J. Beevers, Fatigue of Advanced Materials, R. O. Ritchie, R. H. Danskardt and B. N. Cox, eds., Materials and Component Engineering Publications Ltd., UK, 379 (1991)

[2]   S. M Jeng, P. Allassoeur and J. M. Yang, Materials Science and Engineering, A154, 11(1992)

[3]   D. Zheng and H. Ghonem, Metallurgical and Materials Transactions A, 26A, 2469(1995).

[4]   D. L. Davidson, R. M. Arrowood, J. E. Hack, G. R. Leverant, and S. P. Clough,, in Mechanical Behavior of Metal Matrix Composites, J. E. Hack and M. F. Amateau, eds., TMS-AIME, Warrendale, PA, 117(1981)

[5]   M. L. N. McCartney, Proceedings of The Royal Society London, 409A, 329(1987)

[6]   M. D. Sensmier, and P. K., Wright, Fundamental Relationships Between Microstructure and Mechanical Properties of Metal Matrix Composites, M. N. Gungor and P. K. Liaw, eds., The Mineral, Metal and Materials Society, Warrendale, PA, 441 (1990)

[7]   R. M. McMeeking and A. G. Evans,Mechanics of Materials, 9, 217 (1990)

[8]   D. C. Phillips, Journal of Material Science, 9, No. 11, 1847 (1974)

[9]   K. M. Prewo and J. B. Brennan, Journal of Material Science, 15, No. 2, 463 (1980)

[11]   Y. Le Petitcorps, M. Lahaye, R. Pailler and R., Naslain, Composites Science and Technology, 32, 31 (1988)

[12]   P. L. Martin, W. H. Bingel and M. Mahoney, Workshop Proceedings for Titanium Matrix Components, P. R. Smith and W. C. Revelos, eds., Wright-Patterson AFB, Ohio, WL-TR-92-4035, 277(1992)

[13]   H. Ghonem, Y. Wen, D. Zheng, M Thompson and G. Linsey,Materials Science and Engineering, 161, 45(1993)

[14]   S. R. Bodner and Y. Partom, Journal of Aplied Mechanics, 42, 385 (1975)

[15]   R. W. Neu and S. R. Bodner, Contributive Research and Development- 6, Prepared for Wright-Patterson AFB, Ohio, Sept 1995

[17]   Ghonem, H., Wen, Y. and Zheng, D., "An Interactive Simulation Technique to Determine the Internal Stress States in Fiber Reinforced Metal Matrix Composites", *Material Science and Engineering*, Vol. A177, 1994, pp. 125-134

[18]   Guichet, B., Sangleboeuf, J-C, Vassel, A. and Bretheau, T., "Study of Push-out Micromechanical Test. Response of SCS-6/Ti6242 Composite," CMMC conference, 1996

[20]   Agarwal, B.D., Broutman, L.J., Analysis and Performance of Fiber Composites, John Wiley & Sons, Inc., New York, NY, 1990

CHAPTER 4: HIGH TEMPERATURE INTERPHASE PROPERTIES AND THEIR INFLUENCE ON COMPOSITE DAMAGE MECHANISMS

Abstract

The damage mechanisms of the Ti metal matrix composite SCS-6/Timetal-21S are investigated in this study at both ambient temperature and elevated temperatures. The debond shear strength and interfacial shear stress are identified through the use of elevated temperature thin-slice fiber pushout tests at temperatures ranging from 24 to 650 °C. The debond shear strength of the interface was found to decrease with increasing test temperature. The effect of these temperature variable properties on the failure modes of the SCS-6/Timetal-21S composite has been used to establish a temperature dependent damage map for this composite system, which describes the failure modes as a function of the stress intensity factor and temperature.

4.1 Calculation of Damage Mechanism Boundaries

Fiber reinforced composites are promising materials for elevated temperature applications, since the properties of these materials can be tailored for the particular loading conditions. The key properties of fiber-reinforced composites rely on the characteristics of the fiber/matrix interphase, including brittleness, bond strength and chemical reactions between matrix and fiber constituents. In order to optimize properties of MMCs for particular applications, it is essential that the properties of the fiber/matrix interface be well understood, as well as the many factors that influence these properties. The factors of most interest relate to the processing conditions, particularly consolidation temperature, pressure and cooling rate, and the in-use or testing conditions such as

104

temperature and environment. These variables result in alterations of the interphase properties, and therefore influence the subsequent behavior of the composite during loading.

Processing procedures, which vary for different composite types, subject the material to a variety of time/temperature/pressure conditions. The foil-fiber-foil technique is one of the most common methods for fabricating metal matrix composites with continuous fiber reinforcements. This method involves alternating layers of matrix material, in the form of a thin rolled foil, with layers of fibers. Two methods are used in maintaining the alignment and spacing of the fibers prior to consolidation. These fibers can be rolled on a drum and held in place by an organic binder that will be burned off during consolidation, then cut into sheet form. Alternately, sheets of fibers are woven with a thin metal wire, typically molybdenum for Ti matrix composites, which will be chemically integrated into the matrix phase upon composite consolidation. In either case, a vacuum hot pressing technique is used to consolidate the layers of fiber and foil into the composite material. During this hot pressing procedure, the temperature and pressure are such that the matrix material experiences a plastic deformation, and flows around the fibers, resulting in a fully consolidated material upon cooling

At the consolidation temperature, above 900 $^{\circ}$C for Ti-MMCs [1,2], a stress free condition exists within the composite. Upon cooldown, residual stresses arise due to the large difference in coefficients of thermal expansion between the SiC fiber (5×10^{-6} / $^{\circ}$C) and Ti alloy matrix material (11×10^{-6} / $^{\circ}$C) [3]. This difference causes a compressive radial residual stress in the matrix adjacent to the interface, which acts as a clamping force on the fiber. Since the chemical bonding in these types of composites is minimal, this clamping force provides most of the interfacial debonding. The extent of this compressive stress is

dependent on the actual consolidation temperature and the cooling rate. Bahei-El-Din, et al. [4] observed, in their work with SCS-6/Ti-15-3, that the effect of the consolidation pressure is only significant at cooling rates higher that about 1 ^{O}C/s, while the cooling rate has a very significant effect on the radial stress at the fiber/matrix interface. For viscoplastic materials, such as Ti alloys, a slower cooling rate allows a time dependent relaxation of the material, which reduces the level of residual stress significantly.

The high temperature necessary for consolidation also results in the formation of a brittle reaction zone between the fiber and/or fiber coatings and the matrix, and a corresponding increase in the compressive residual stress in this area. Due to the brittle nature of the interfacial reaction zone, and the strain mismatch between the reaction zone, fiber and matrix constituents, it is probable that micro cracks will form in this region during composite processing. Also, the porous nature of the carbon coatings makes it likely that small defects will exist in this area. These defects, which can be thought of as notches, can act as stress concentrations in the composite, leading to fiber and/or matrix crack initiation [5].

In use, or test conditions, such as temperature, loading frequency and environment, also affect the properties of the interphase, and therefore the behavior of the composite as a whole. As temperature increase in the composite system, approaching the stress free consolidation temperature, the residual stresses at the fiber/matrix interface decrease. High frequency fatigue crack growth studies performed by Zheng and Ghonem [6] have shown a decrease in the crack growth rate of unaged SM1240/Timetal21S samples during the initial crack bridging stage, corresponding to an increase in crack tip shielding, with increasing test temperature (from 24 - 650 ^{O}C). Eldridge and Ebihara [7] have noted a marked drop in the experimental values of interfacial shear strength and frictional shear stress with

increasing test temperatures (from 300 to 825 ^{O}C) in unaged SCS-6/Ti-24-11 intermetallic composite for thin slice push out samples (0.28 - 0.48 mm thick). Conversely, from 25 - 300 ^{O}C, a possible slight increase was seen in the debond stress with increasing temperature. Ananth and Chandra [8] also calculated an increase in the values of peak push out load, and therefore debond strength, with increasing temperature (25 ^{O}C to 200 ^{O}C) for 0.5 mm samples using finite element modeling of the fiber push out test. These results show that the properties of the interface are indeed temperature dependent.

In composites consisting of strong fibers embedded in a relatively weak matrix, the longitudinal strength relies extensively on strong fiber-matrix bonding to promote efficient transfer of stress from the matrix to the fibers. Such bonding will result in the longitudinal strength of the composite being on the order of the fiber strength. The interface region, or interphase, in addition to enabling this load transfer from matrix to fiber, can accommodate the strain mismatch between the fiber and matrix and act as a crack blunting layer to minimize crack propagation [9]. However, as mentioned previously, due to the high stresses induced during fabrication and the brittle nature of the interphase constituents, this region can also act as a site of crack initiation [10]. Additionally, due to the directional nature of the reinforcement, good bond strength is necessary for the transverse strength of the composite, which will only be on the order of the matrix strength. Conversely, in some composite systems, a weak fiber matrix interface is desired. For example, toughness is achieved in brittle matrix composites through energy absorption during frictional sliding and pullout of broken fibers. Stress is transferred to the fiber by frictional forces until the fully loaded fibers fail according to the weakest link statistics [11]. The greater the frictional stresses, the more efficiently the fibers become loaded and the shorter the pullout lengths. In metal matrix composites (MMCs), which have strong fibers and a ductile

matrix, strong interfacial bonding is generally desired, although in some cases, such as in fatigue crack growth, frictional sliding and fiber pullout are important. The fatigue crack growth rate at elevated temperature for these types of materials under fiber bridging conditions has been found to decrease with increasing crack length, contrary to the material's monolithic counterparts [12-14]. This phenomena is a result of the behavior of the crack when it encounters the fiber reinforcement. The interface tends to debond under the stress field caused by the approaching crack tip, allowing the intact fiber to bridge the crack. Matrix crack propagation is retarded when the bridging fibers carry some of the applied load, thus reducing the crack tip driving force.

This fiber bridging in MMCs is a direct result of fiber/matrix debonding behavior under the applied stress conditions. This debonding consists of two stages: debond crack initiation and propagation of the debond crack after initiation. When the matrix crack approaches a fiber, a large interfacial shear stress is induced by the crack opening displacement. This stress results in the initiation of a debond crack along the interface. The initial debond length will be a function of the fiber stress and the properties of the interphase at that temperature. In SiC/Ti MMCs, compressive residual forces are present at the interface, induced by the effect of cooling from the composite consolidation temperature on the matrix and fiber, which have a large difference in coefficients of thermal expansion. These compressive forces cause the now free surfaces of the debond crack to make contact with one another, introducing a frictional sliding force along the debonded surfaces. Propagation of the debond crack is then a function of both the debond strength of the interface and the frictional sliding stress along the debond crack surfaces. Studies have shown that such sliding results in wear of surface asperities and deterioration

of the interface [15,16]. This interfacial degradation is followed by fiber breakage and pullout.

In order to characterize the interphase and its response to the various influencing factors, specific interphase parameters must be identified. The properties of the interface can be defined according to various combinations of parameters such as physical, chemical, microstructural, etc. It is convenient to choose the parameters with which to describe these properties according to the material characteristics under consideration. When investigating the macrostructural properties of the composite, such as strength, toughness or fatigue crack growth rate, it is useful to express the properties of the fiber-matrix interface in terms of the experimentally obtained values of interfacial debond strength and frictional shear stress. These parameters, the debond shear strength, τ_d, and the frictional sliding stress, τ_s, are used to describe a critical stress value for interface debonding and frictional sliding.

Several experimental methods have been used in an attempt to establish these interfacial parameters, including fiber pullout, fiber indention, and "thin slice" individual fiber pushout. Each method unique advantages and disadvantages. Single fiber pullout, while most closely representing the actual conditions in a fiber and the surrounding matrix during loading, involves complicated specimen preparation which may keep the composite from being truly representative of the composite stress state. Conversely, pushout methods allow relatively easy sample preparation, the ability to obtain several data points from one sample, and the ability, with the proper choice of sample thickness, to preserve the true composite stress state in the sample. This method has been chosen for use in this study.

During cyclic loading at elevated temperatures, three possible failure processes can occur: fiber fracture, crack deflection, and fiber bridging. A combination of the properties of the fiber, matrix and fiber-matrix interface zone will determine the presence and/or

109

dominance of each of these fracture processes. Generally, failure of composite systems having strong interfaces and relatively weak fibers are generally dominated by fiber fracture, while high temperature failure of systems with weak interfaces is dominated by interface cracking. For example, in the composite systems, FP/ZE41A [17] and B4C-B/Ti-6Al-4V [18], both having strong interfaces and comparatively weak fibers, fiber fracture will be the dominant failure mode with fracture of the fibers occurring ahead of the crack tip and the resulting micro-cracks linking with the main crack. Conversely, composite systems such as SiC/Ti, having relatively low interface strength but high fiber strength can exhibit fiber bridging at room and elevated temperatures under certain combinations of stress ratio and applied stress range.

During the fiber pushout process, as in actual composite debonding, propagation of the Mode II debond crack can be modeled as a crack running along an interface between two dissimilar materials (the fiber and the matrix). Analysis of cracks in bi-material interfaces show that the different elastic constants possessed by the fiber, matrix and interface results in a mixed mode stress state, even when loading is uniaxial. [19] Consequently, the fracture mechanics description of this type of crack is more complicated than that required to describe crack propagation in a homogeneous material, where only one parameter, the critical stress intensity factor, K_{ic}, is needed. The additional complexities arise from the shearing of the crack surfaces due to the modulus mismatch. In such a case, the parameter K is scale sensitive. However, the critical strain energy release rate, G_{ic}, is not, and is therefore a convenient parameter by which to describe the debonding process. He and Hutchinson [20] have devised a delamination diagram based on calculated values of the energy release rate for deflection, G_d, compared with the energy release rate for penetration, G_p. A recent paper by Chan [21] has refined this work to include fiber

110

fracture, interface fracture, and fiber bridging, using as the controlling parameters the interfacial properties, τ_d, and τ_s. Expanding upon the work of He and Hutchinson [20], he has shown that the critical ratio τ_d / σ_f, where σ_f is the fiber strength, can be used to predict the failure modes of fiber reinforced composites. The effect of temperature on these properties and subsequent influence on these damage modes, however, was not addressed.

The purpose of this study is to characterize the elevated temperature damage mechanisms of MMCs, particularly those of the fiber/matrix interface, and to identify the effect of these properties on the failure modes of the composite under fatigue loading conditions. Using an optimized sample thickness, the parameters necessary to describe the debonding behavior of the composite system will be investigated with respect to typical in-use temperatures. Temperature dependency of the fiber/matrix interface debond shear strength, τ_d, and the frictional shear stress, τ_s, will be investigated through a series of room temperature and elevated temperature fiber pushout tests. These parameters are used to predict the controlling failure mode in the MMC systems during loading. The criterion for establishing the boundaries between these failure modes is based on work done by Chan [21], but is expanded to include elevated temperature effects and will be applied to the SCS-6/Timetal-21S composite system.

4.2   Material and Experimental Procedures

The material considered in this study is a 6 ply Timetal-21S/SCS-6 composite, although this technique could be used for any continuous fiber-reinforced metal matrix composite. The matrix of the composite consists of Timetal-21S, a metastable β titanium alloyed with 0.1 Fe, 16.0 Mo, 3.06 Al, 2.9 Nb, 0.2 Si. 0.22 C, 0.12 O, 0.005 N (wt %.) SCS-6 fibers have a 140 μm carbon cored SiC body with a 3 μm dual carbon coating. The

samples received a stabilization heat treatment of 8 hours at 621 °C in vacuum. Specimens were sectioned to the desired thickness with a diamond wafering blade at a high speed/low load, ground on SiC paper, then diamond polished through 1 μm grit.

Push-out specimens were polished on both sides until an appropriate thickness was attained. The sample was mounted in the specimen holder of the fiber push out apparatus and a low magnification optical micrograph was taken of each sample. Fibers aligned with grooves in the pushout base were chosen and marked on the micrograph for ease of identification during testing.

The fiber pushout apparatus consists of a load train and a specimen holder assembly incorporated into a 12" cylindrical vacuum chamber (Fig. 2-1). Loading is applied by a stepper motor with an attached encoder that reads motor displacement. The motor shaft is coupled with a linear motion feedthrough at the vacuum chamber. A load cell is mounted between the feedthrough shaft and a hollow stainless steel tube to which the punch assembly is attached. The carbide punches used in this study are tapered at 30° included angle with a flat tip of 100 μm diameter for the SCS-6 fibers and 75 μm diameter for the SM1240 fibers. The specimen holder is mounted on a removable assembly including an x-y stage with motorized actuators for remote alignment of the chosen fiber with the punch.

After the chosen fiber was aligned with the punch, the fiber was monotonically loaded at the sample's corresponding aging temperatures under vacuum conditions until fiber pushout occurred. The general shape of an elevated temperature fiber pushout curve is shown in Fig. 4-1. At elevated temperatures, a change in linearity such as that occurring at point A, which has been described as the onset of fiber debonding [22], is fairly evident. The interface debond strength, τ_d, was taken to be the stress corresponding to this change in linearity, while the initial drop in the pushout curve (B), occurring when the debond crack

propagates completely through the thickness of the sample and slip occurs, was also noted. This drop is evident at all temperatures. The frictional shear stress, τ_s, was considered to be the value of stress at the bottom of the load drop (C), where the fiber will stop sliding due to frictional resistance. Fiber pushout was verified through SEM observations of the reverse side of the sample. In addition, the surface morphology of the pushed out fibers were compared for the various aging and test temperature combinations.
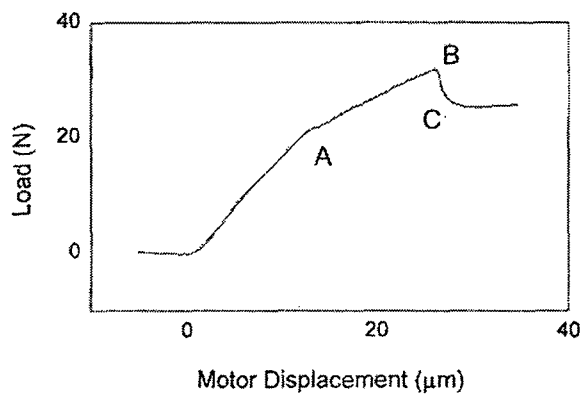
Figure 4-1   General shape of an elevated temperature fiber pushout curve

4.3   Calculation of Damage Mechanism Boundaries

For the case of a crack approaching a bimaterial interface, comparisons of the energy release rate, G_d, to the energy release rate for interface penetration, G_p, have shown that the ratio G_d/G_p is independent of the crack length, a [20]. Deflection of the crack when it reaches the bimaterial interface will take place if this ratio is greater than the ratio of interface toughness, G_i to the Mode I toughness of the fiber, G_f, i.e,

$$\frac{G_i}{G_f} < \frac{G_d}{G_p}$$

since interface propagation will require a lower load than for penetration across the interface [20]. The interface toughness at complete debonding can be expressed as

$$G_i = \frac{B_2 \, R_f}{E_f} \left[\frac{(\tau_d - \tau_f)l}{R_f} \right]^2$$

where

$$B_2 = \frac{(1 + v_f)\,(1 - 2v_f)\,E_m + (1 + v_m)\,E_f}{(1 - v_f)\,E_m + (1 + v_m)\,E_f}$$

and

$$G_f = \frac{(1 - v^2)\,\sigma_f^2\,\pi\,a_f}{E_f}.$$

In these equations, v_f, v_m, E_f and E_m are the Poissons ratio and Young's modulus of the fiber and matrix respectively, σ_f is the fracture strength of the fiber and a_f is the fiber crack length. The ratio of G_i/G_f is found to be proportional to $[(\tau_d - \tau_f)/\sigma_f]^2$ [21]. From this result, it was hypothesized that the critical ratio for describing the failure mechanisms in MMCs is τ_d/σ_f. Using this critical ratio, Chan established a failure diagram that considers bridging, limited and extensive interfacial debondiing, and matrix yield, based on room temperature material and interfacial properties

Good agreement was obtained through a comparison of this criterion with experimental results, by plotting a delamination diagram and comparing the relative placement of the experimental data either below or above the delamination line. This analysis was restricted to interface delamination and penetration of a crack only. It has been established experimentally that when the ratio of G_i/G_f is high, fiber bridging accompanies the interface decohesion, while when this ratio is low, fiber fracture is the accompanying mechanism [21]. Due to the proprtionality between G_i/G_f and τ_d/σ_f, it can be assumed that these observations hold for this critical ratio also.

114

4.3.1 Matrix Failure

Through the analysis of matrix yielding by a concentrated slip model, Chan et al [23], have shown that matrix slip lowers the normal stress directly in front of the fiber crack tip for $x/L \leq 0.1$ only. Therefore, the stress in a fiber (with diameter D) located directly in front of the crack tip ($y=0$, $x=D/2$) can be written based on the K field of a semi-infinite mode I crack [24] as

$$\sigma_{yy} = \frac{K}{\sqrt{\pi D}}$$

At the onset of fiber fracture, $\sigma_{yy} = \sigma_f$ so that

$$\sigma_f = \frac{K}{\sqrt{\pi D}}$$

A criterion for matrix yielding, based on the critical ratio τ_d / σ_f, can be written as

$$\frac{\tau_d}{\sigma_f} > \frac{\tau_y}{\sigma_f}$$

That is, matrix yielding followed by fiber fracture will occur prior to interface debonding if the critical ratio τ_d / σ_f exceeds the ratio of yield strength of the matrix material in shear to the fracture stress of the fiber, σ_f,

$$\frac{\tau_d}{\sigma_f} > \frac{\sigma_y}{\sqrt{3}} \frac{\sqrt{\pi D}}{K}$$

Recognizing that the debond strength of the interface, τ_d and matrix yield strength, σ_y are temperature dependent, the equation for the boundary of the matrix yielding region can be rewritten as

$$K > \frac{\sigma_y}{\tau_d} \left[\sigma_f \frac{\sqrt{\pi D}}{\sqrt{3}} \right]$$

115

where the proportionality factor between the stress intensity factor and the temperature dependent material parameters, τ_d and σ_y, is the constant function of temperature independent material parameters in the parenthesis.

4.3.2 Fiber Bridging

For fiber bridging, the fiber stress in the bridging zone can be described [21] as

$$\sigma_{yy} = C \; \tau_s^{1/2} \left(\frac{K_{tip}}{D}\right)^{1/2} r^{1/4}$$

where

$$C = \frac{4}{(1-v_f)}\left[\frac{2(1-v^2)E_c}{\sqrt{2\pi}\;(b_2' + b_3')\;A\;E_m}\right]^{1/2}$$

with

$$E_c = v_f\;E_f + (1-v_f)\;E_m$$

where v_f is the fiber volume fraction, A is the orthotropy factor described by Budiansky & Amazigo [25], E_m is the Young's modulus of the matrix, $v = v_f = v_m$ is the Poisson's ratio of the both the fiber and matrix, K_{tip} is the local stress intensity factor at the crack tip, and r is the distance behind the crack tip. The parameters b_2' and b_3' are non-dimensional coefficients that are functions of the elastic properties of the fiber, matrix and composite, which have been defined by Hutchinson and Jensen [26] as follows:

$$b_2' = \frac{(1+v)\;E_m\;\left\{(1-v)^2\;E_f + (1-2v)\;[1-v+\rho(1+v)]\;(E_m - E_f)\right\}}{(1-v)E_f\;[(1+v)\;\bar{E} + (1-v)\;E_m)]}$$

$$b_3' = \frac{\rho(1+v)\;\left\{(1-\rho)(1+v)(1-2v)(E_f - E_m) + 2(1-v)^2\;E_m\right\}}{(1-v)(1-\rho)[(1+v)\;\bar{E} + (1-v)\;E_m]}$$

where

$$\bar{E} = \rho\;E_m + (1-\rho)\;E_f$$

and the area fiber fraction, $\rho = (R_f / R)^{1/2}$, R_f is the radius of the fiber and R is the radius of the cylindrical shell of composite used in the model. At the onset of fiber bridging, $K = K_{tip}$ and $r = D/2$ for a bridging zone the size of one fiber diameter behind the crack tip.

Noting that $\sigma_{yy} = \sigma_f$ in the bridging zone, the above equation can be expressed in terms of the critical ratio, τ_d / σ_f as

$$\frac{\tau_d}{\sigma_f} = \frac{\tau_d D^{1/2}}{C \ \tau_f^{1/2} \ K^{1/2} \ r^{1/4}}$$

Separation of the temperature dependent components, τ_s and C (which is a function of the fiber Young's modulus) leads to a description of the boundary for fiber bridging at any temperature

$$K < \frac{1}{C^2 \ \tau_s} \left(1.416 \ \sigma_f^2 \ \sqrt{D} \ \right)$$

4.3.3 Interface debonding

Between the boundaries of matrix yielding and fiber bridging on the damage process map is the interface debonding region, where fiber fracture will follow debonding before significant bridging will occur.

4.4 Results and Discussion

Typical high temperature push out curves for unaged samples of Timetal-21S/SCS-6 are shown in Figure 4-2 for room temperatures, 500, and 650 °C. The slope of the loading portion of the curve increases with increasing temperature due to the increasing material compliance. The change from linearity seen in the two elevated temperature plots corresponds to the initiation of the interfacial debond crack [22]. As noted on the diagram,

117

these samples (at 500 and 650 °C) are approximately the same thickness and can be compared directly, while, due to maximum force limitations, the room temperature sample is thinner. Comparison of the elevated temperature curves shows increasing compliance with temperature, in the form of a decreasing slope, as the debond crack propagates along the length of the interphase. This slope change is terminated with a load drop, with the maximum (point B), corresponding to the load at which the remaining bonded region has reached the minimum critical length, this portion debonds catastrophically, and the entire length of the fiber begins to slide. The value of shear strength corresponding to the bottom of the drop, where the interphase is completely debonded, is taken to be the frictional shear stress of the interphase, while the magnitude of the drop is an indication of the interfacial fracture toughness [21,22].
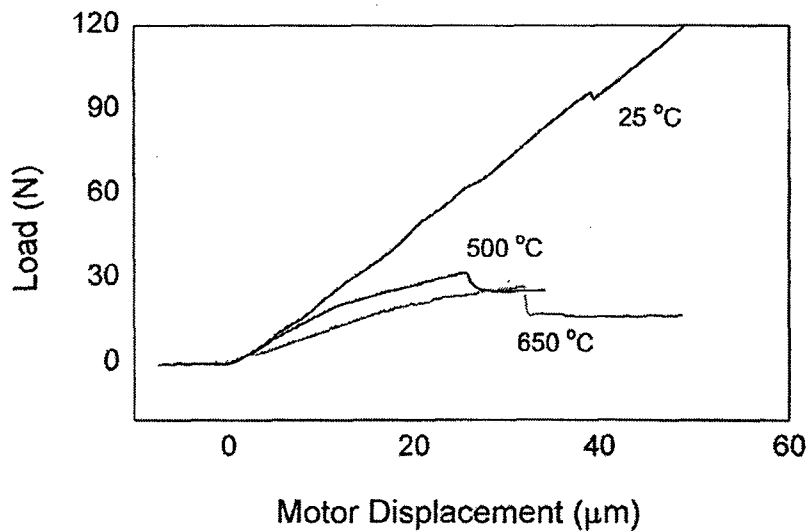
Figure 4-2 Typical curves for fiber pushout at room temperature, 500 and 650 °C. (Note sample thicknesses: 23 oC .63 mm, 500 oC 1.07 mm, 650 oC 1.10 mm)

The samples tested in ambient temperature do not show the region of increasing sample compliance indicative of incremental debonding. The nature of the pushout curve

and the corresponding SEM observations of samples indicate that at this temperature, the debonding is catastrophic along the entire length of the specimen. Similar shaped curves were obtained for the testing at 160, 250 and 350 °C, even in thicker samples (greater than 0.90 mm). This observation is consistent with the effect of temperature on the elastic properties of the matrix material. At the lower temperatures, the matrix material behaves elastically. Higher temperatures, above about 400 °C, enhance the ability of the matrix phase to flow under the applied stress, thereby blunting the crack tip and inhibiting a catastrophic failure of the interface.

For this study, the debonding load is taken to be point A in Figure 4-1, where the debond crack initiates, for high temperature tested samples, and at the maximum point (B in Figure 4-1) for those tested at lower temperatures. The interphase shear strength has been determined using the assumption of an average shear stress distribution along the interphase at this load level. The average values of the debond shear strength, τ_d, and frictional shear stress, τ_s, determined using this average shear stress assumption are listed in Table 4-1 for SCS-6/Timetal-21S for the above mentioned temperatures. The decrease in τ_d and τ_s with increasing temperature is due to the relaxation of the compressive residual stress at the interface with elevated temperature, as discussed in the Chapter 2. This relaxation will reduce the force necessary to push the fiber out, and reduce the effect of friction on the sliding surfaces once the fiber has completely debonded and begins to slide.

Table 4-1   Interface properties of SCS-6/Timetal-21S at various temperatures

	τ_d (MPa)	τ_s (MPa)
25 °C	221	149.2
500 °C	160.5	41.2
650 °C	138.6	20.6

The calculation of damage characteristics requires the knowledge of the temperature dependence not only the interfacial shear strength and frictional shear stress shown in Table 4-1, but also the fiber strength and various properties of the matrix such as yield strength and Young's modules. The yield strength of Timetal-21S has been established by several authors as a decreasing function of temperature [27,28]. These matrix material properties are listed in Table 4.1 as a function of temperature. For this analysis, the Poisson ratios of the fiber and matrix materials are considered equivalent, and the fiber strength, σ_f, is considered constant for the temperature range investigated. The values for these have been obtained from existing literature [30] and are listed in Table 4.2 and 4-3.

Table 4-2   Properties of SCS-6 fibers (no temperature dependence)

E_f (GPa)	v_f	σ_f (MPa)
400	0.25	3600

Table 4-3   Properties of Timetal-21S matrix at various temperatures

T (^{O}C)	E_m (GPa)	v_m	σ_m (MPa)
24	98.2		1043
204	90.3		779
316	84.8	0.32	696
482	76		589

Application of the experimentally obtained interfacial properties allows the establishment of a temperature dependent map of the damage mechanism occurring in the composite system. Figure 4-3 shows the damage map for the system SCS-6/Timetal-21S.

120

The boundaries are calculated from experimentally obtained shear strength and interfacial shear stress data up to 650 °C and extrapolated to higher temperatures based on the assumption that above the stress free consolidation temperature, no distinction will occur between any of the failure modes.
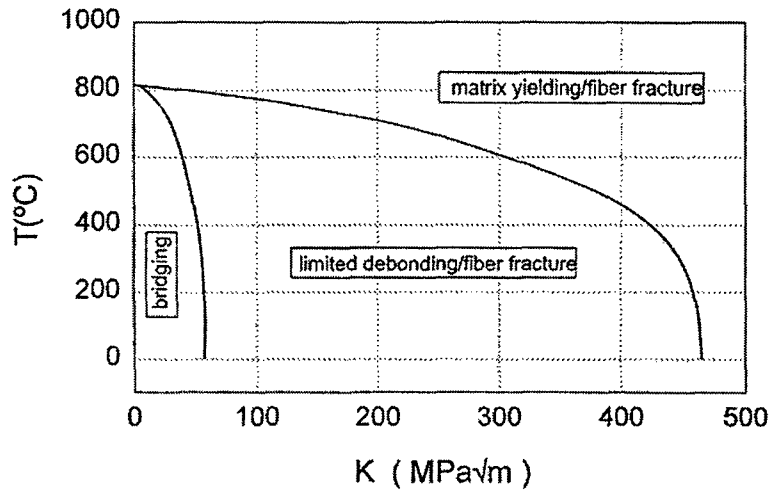
Figure 4-3 Temperature dependent composite failure map for SCS-6/Timetal-21S

The boundary that describes fiber bridging at any temperature can be written as

$$ K < \left(1.416 \, \sigma_f^2 \, \sqrt{D} \ \right) \frac{1}{C^2 \, \tau_s} $$

where the temperature dependent components are τ_s and C (which is a function of the Young's modulus of the matrix), K is the stress intensity factor, σ_f is the fiber strength, and D is the fiber diameter. As indicated by the equation of this line, along the boundary between fiber bridging and interfacial debonding, K_{max} is inversely proportional to the square of C, which is an inverse function of the matrix Young's modulus, and of τ_d, the interfacial debond strength. As temperature increases, the Young's modulus of the matrix decreases, causing C to increase, slowly at lower temperatures, and more rapidly at higher

121

temperatures. In the same temperature range, the frictional shear stress along the interface is decreasing. The net effect of the temperature variation of these parameters is to decrease the size of the fiber bridging region with increasing temperature. It should be noted that the effect of temperature on the matrix is more significant to the determination of the failure mode than that of the interfacial shear stress.

Similarly, the equation which describes the boundary of the matrix yielding region can be written as

$$ K > \left(\sqrt{\frac{\pi D}{3}} \, \sigma_f \right) \frac{\sigma_y}{\tau_d} $$

where the proportionality factor between the stress intensity factor and the temperature dependent material parameters, τ_d, the debond strength, and σ_y, the yield strength of the matrix, is the constant function of temperature independent material parameters in the parenthesis. Therefore, the boundary between interfacial debonding and matrix yielding is governed by the ratio of τ_d/σ_y. The stress intensity factor, K_{max}, is a function of temperature, since it is directly proportional to τ_d, and inversely proportional to σ_y, both of which decrease with temperature. The net effect of these parameters causes a small change with temperature until 400 °C, after which a large increase is observed in this parameter sum. This causes the region of interfacial debonding on the damage map (Fig. 4-4) to decrease rapidly at temperatures above 400 °C.

Between these two boundaries, one delineating matrix yielding, the other fiber bridging, lies a region where limited interfacial debonding is expected to occur followed by fiber failure.

Since K values exceeding 100 MPa $\sqrt{m}$, and temperatures above the melting point of the matrix material, Timetal-21S, are unrealistic, the map will be redrawn with these

122

limits, in Fig. 4-4. It is clear from this composite diagram that for the temperature range for which this system has been developed (<650 °C), matrix yielding will never be the dominant failure mode. This observation is as expected, since the interface is relatively weak compared to the strength of the fiber.
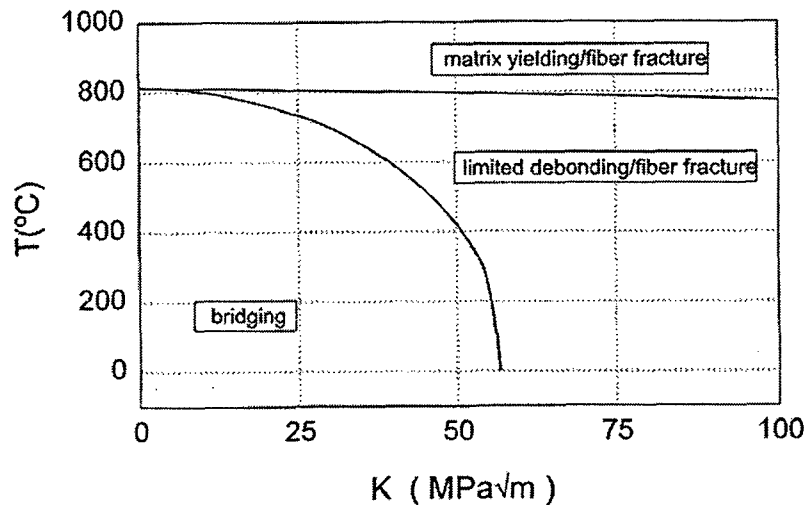
Figure 4-4   Temperature dependent composite failure map for SCS-6/Timetal-21S showing region of practical application

A composite damage map, such as the one generated in the study, can be used to predict the failure mode of a composite system under particular loading conditions. Fiber bridging is generally desirable for reduction in fatigue crack growth in fiber reinforced MMCs in order to increase damage tolerance. This failure diagram indicates that in order to stay within the desired fiber bridging zone, as temperature is increased, the stress intensity factor must be lowered in order to avoid crossing into the region of interfacial debonding followed by fiber fracture. In addition, optimization of a composite system is possible for a required application through the modification of the key interphase properties, according to this failure diagram. Comparison of such damage maps for

123

materials with different reinforcing fibers, or similar fibers with different processing conditions, and therefore different values of τ_d and τ_s, can be used to distinguish the effect of these variables on the loading conditions required to obtain failure through a particular damage mechanism.

4.5   Summary and Conclusions

High temperature interfacial properties have been established experimentally for the MMC composite system SCS-6/Timetal-21S.   These properties were used to derive equations for the boundaries of a high temperature composite damage map that describes the dominant failure mode as a function of the temperature and stress intensity factor during loading. The results of this study can be summarized as follows:

1.   The debond shear strength and frictional shear stress, τ_d and τ_f, for this system, decrease with increasing temperature, due to the relaxation of the clamping force at elevated temperatures.

2.   The interface properties derived from fiber pushout experiments can be used to derive equations for the boundaries of a high temperature composite damage map which describes dominant failure modes as a function of the stress intensity factor and the temperature.

3.   Matrix yielding followed by fiber fracture cannot be the dominant failure mode for SCS-6/Timetal-21S, based on the established composite failure diagram and the service temperature of this composite.

4.   The boundary between fiber bridging and interface debonding, for the composite system SCS-6/Timetal21S, occurs at decreasing K_{max} with increasing temperature.

4.6   References

[1]   Yang, J.M., Jeng, S.M., Yang, C.J., "Failure Mechanisms of Fiber Reinforced Titanium Alloy Matrix Composites, Part I: Interfacial Behavior," *Materials Science and Engineering*, Vol. A138, pp. 155-167, 1991

[2]   Sohi, M., Adams, J., Mahapatra, R., "Transverse Constitutive Response of Titanium-Aluminum Metal Matrix Composites," Constitutive Laws for Engineering Materials, C.D. Desai, ed., ASME Press, New York, NY, pp. 617-626, 1991

[3]   Davidson, D.L., "The Micromechanics of Fatigue Crack Growth at 25 °C in Ti-6Al-4V Reinforced with SCS-6 Fibers," *Metallurgical Transactions*, Vol. 23A, pp. 865-879, 1992

[4]   Bahei-El_Din, Y.A., Dvorak, G.J., "Mechanics of Hot Isostatic Pressing of a Densified Unidirectional SiC/Ti Composite," *Acta metall. Mater.* Vol. 43, No. 7, pp. 2531-39, 1995

[5]   Metcalfe, A.G. and Klein, M.J., "Composite Materials," A.G. Metcalfe, ed., Academic Press, New York and London, Vol. 1, 1974

[6]   Zheng, D., Ghonem, H., "High temperature/High Frequency Fatigue Crack Growth Damage Mechanisms in Titanium Metal Matrix Composites," in *Life Prediction Methodology for Titanium Matrix Composites, ASTM STP 1253*, W.S. Johnson, J.M. Larson and B.N. Cox, eds., American Society for Testing and Materials, Philadelphia, PA, 1995

[7]   Eldridge, J.I., Ebihara, B.T., "Fiber Pushout Testing Apparatus for Elevated Temperatures", *Journal of Materials Research*, Vol. 9, No. 4, pp. 1035-1042, 1994

[8]   Ananth, C.R. and Chandra, N., "Numerical Modeling of Fiber Push-out Test in Metallic and Intermetallic Matrix Composites - Mechanics of the Failure Process," *Journal of Composite Materials*, Vol. 29, No. 11, pp. 1488-1514, 1995

[9]   Agarwal, B.D., Broutman, L.J., Analysis and Performance of Fiber Composites, John Wiley & Sons, Inc., New York, NY, 1990

[11]   Thouless, M.D., Evans, A.G., "Effects of Pull-out on Toughness of Reinforced Ceramics," *Acta metall mater.*, Vol. 36, No. 3, pp. 517-522, 1988

[12]   Zhang, T. and Ghonem, H., "Time-Dependent Fatigue Crack Growth in Titanium Metal Matrix Composites," *Fatigue and Fracture of Engineering Materials and Structures*, Vol. 18, No. 11, pp. 1249-1262, 1995

[13]   Cotterill, P.J. and Bowen, P., "Fatigue Crack Growth in a Fiber-Reiforced Titanium MMC at Ambient and Elevated Temperatures," *Composites*, Vol. 24, No. 3, pp. 214-221, 1993

[15]   Kantzos, P., Ghosn, L., Telesman, J., "The Effect of Degradation of the Interface and Fiber Properties on Crack Bridging," HITEMP Review,Vol. 2, Cleveland,OH, pp. 32.1-32.14, 1992

[16]   Warren, P.D., Mackin, T.J., Evans, A.G., "Design , Analysis and Application of an Improved Push-Through Test for the Measurement of Interface Properties in Composites", *Acta. metall. mater.*, Vol. 40, No. 6, pp. 1243-1249, 1992

[17]   Davidson, D.L., Chan, K.S., McMinn, A., and Leverant, G.R., "Micromechanics and fatigue crack growth in an alumina-fiber-reinforced magnesium alloy composite" *Metallurgical Transactions A*, pp. 2369-2378, 1989

[18]   D. L. Davidson, R. M. Arrowood, J. E. Hack, G. R. Leverant, and S. P. Clough,, in Mechanical Behavior of Metal Matrix Composites, J. E. Hack and M. F. Amateau, eds., TMS-AIME, Warrendale, PA, 117(1981)

[19]   Rice, J.R., Sih, G.C., "Plane Problems of Cracks in Dissimilar Media", *Journal of Applied Mechanics*, pp.418-423, June 1965

[20]   He, M.Y., and Hutchinson, J.W., "Crack Deflection at an Interface Between Dissimilar Elastic Materials," *Int. J. Solids Structures*, Vol. 25, No. 9, pp. 1053-1067

[21]   Chan, K.S., "Effects of Interface Degradation on Fiber Bridging of Composite Fatigue", *Acta. metall. mater.*, Vol. 41, No. 3, pp. 761-768, 1993

[22]   Kerans, R. J., and Parthasarathy, T.A., "Theoretical Analysis of the Fiber Pullout and Pushout Tests," *Journal of the American Ceramic Society*, Vol. 74, pp.1585-1596, 1991

[23]   Chan, K.S., He, M.Y., Hutchinson, J.W., "Cracking and Stress Redistribution in Ceramic Layered Composites," *Mater. Sci Eng.*, A167, pp. 57-64, 1993

[24]   Irwin, G.R., *Trans. ASME, J. Appl. Mech.*, Vol. 24, pp, 361-364, 1956

[25]   Budiansky, B. and Amiziago, J.C., "Toughness by Aligned Frictionally Constrained Fibers," *J. Mech. Phys. Solids*, Vol. 37, pp. 93-109, 1989

[26]   Hutchinson, J.W., and Jensen, H.M., "Models for Fiber Debonding and Pullout in Brittle Matrix Composites with Friction," *Mechanics of Materials*, Vol. 9, pp. 139-163, 1990

[27]   Neu, R.W., and Bodner, S.R., "Determination of Material Costants of Timetal-21S for a Constitutive Model," *Contributive Research and Development*, Vol. 6, Prepared for Wright-Patterson AFB, Ohio

[28]   Ghonem, H., Wen, Y., Zheng, D., Thompson, M. and Lindsey, G., "Effect of Temperature   and Frequency on Fatigue Crack Growth in Ti-β21S Monolithic Laminate," *Material Science   and Engineering*, Vol. 161, pp. 45-53, 1993

CHAPTER 5:   **INTERFACE DECOHESION IN SiC-TITANIUM**
                   COMPOSITES AT ELEVATED TEMPERATURES

Abstract

During loading of fiber reinforced metal matrix composites (FRMMCs), the debonding of the interphase plays a critical role in the overall composite behavior. The process of fiber debonding can be represented as independent decohesion in two directions, longitudinal (along the length of the fiber), and transverse (normal to the fiber surface). In order to model this behavior, an experimental/numerical study has been undertaken to identify the parameters governing the decohesion process of the interphase in SiC-Ti composites in both the normal and tangential direction. These parameters, the maximum interface traction, maximum separation, and cohesive energy, are established for various temperatures based on matching finite element simulations of the decohesion process with debonding experiments. Results indicate that

5.1 Introduction

Metallic and intermetallic matrix composites (MMCs and IMCs) are considered as potential material systems of choice for advanced propulsion systems of future air and space crafts because of their high stiffness and strength. A critical issue in the successful application of these composites is the mechanical characteristics of fiber-matrix interfaces. Interfaces are narrow regions separating well-defined domains and are primarily responsible for a range of key properties including stiffness, strength, and fracture behavior [1]. The role of interface is very vital to the stress transfer between the fiber and matrix;

and the interfaces influence mechanical performance and fracture behavior of the composites under various loading conditions [2-4].

Interfaces have been modeled in a number of ways, e.g., a narrow region of continuum with graded properties, an infinitely thin surface separated by springs, and cohesive zones with specific traction-separation laws. One of the fundamental research issues is, what is the best way to characterize interfaces within the framework of continuum mechanics.. Recently, Chandra et al. [5] simulated the interfacial mechanical behavior of thin-slice push-out tests incorporating the spring layer model and fracture mechanics approach. They analyzed both the initiation and propagation of interfacial failure to explain many of the experimental observations of push-out behavior at room and elevated temperatures [6]. In the spring layer model [7], a stress based criterion for debonding, and a frictional resistance based criterion for interfacial sliding have been used to capture debonding and sliding. Debonding is postulated to occur under the combined action of normal tensile stress (mode I) and shear stress (mode II) failures at the interface. In the fracture mechanics approach strain energy release rate at the tip of the interface cracks are computed using the equivalent domain integral method [8]. In this approach a critical strain energy release rate is used as the criterion to determine the extension of the crack.

In recent years, cohesive zone approaches are finding increasing use in describing failure and fracture behavior of interfaces (both internal and external) in a number of material systems. CZM have been used in the past to study crack tip plasticity, creep under static and fatigue loading conditions, crazing in polymers, adhesively bonded joints, interface cracks in bimaterials, crack bridging due to fibers and ductile particle in composites. CZM was originally proposed by Barenblatt [9,10] as a possible alternative to the concept of fracture mechanics in perfectly brittle materials. CZM avoided the presence

of singularity at the tip of a sharp crack, which obviously could not be sustained in real materials. In a perfectly brittle material there is no scope for any form of inelastic deformation, which could account for reduction of stresses to an acceptable value. Barenblatt adopted the atomic binding energy variations at the tip of the crack and postulated a zone ahead of the crack tip where stresses are lowered through the atomic rearrangements. A narrow zone ahead of the crack tip was termed process zone where energy was consumed during this rearranging process. Barenblatt proposed the concept of traction force varying with the increasing atomic separation for perfect brittle materials and then extended the concept to quasi-brittle materials undergoing small-scale plasticity. The intensity of traction was based on intermolecular forces and reached a peak value of nearly $E/10$ where E is the young's modulus of material (in tens of GPa) and separation distance was of the order of interatomic distance (a few angstroms). Later, Dugdale [11] extended this concept to perfectly plastic materials by postulating the existence of a process zone at the crack tip. He used a constant cohesive force equal to the yield stress of the material opposing the opening of crack in this process zone. Based on these Dugdale and Barenblatt models, Hillerborg and co-workers [12] (Jan 1996). proposed the Fictitious Crack Model (FCM) for analyzing crack growth in cementitious composites. FCM has made a rapid strides in the analysis of concrete structures in the field of civil engineering.

CZM has spawned a plethora of modeling efforts in the fracture of metals, ceramics, polymers and their composites in the field of engineering mechanics [13-15]. Needleman was one of the first to use polynomial and exponential type of traction-separation law to simulate the particle debonding in metal matrices [13,16-19] further used the above model to study the void nucleation at the interface of particle and matrix material; and fast crack growth in brittle material under dynamic loading; and dynamic crack growth at the

130

interface of bimaterials. Tvergaard [20] and Tvergaard and Hutchinson [21] used a trapezoidal shape of the traction-separation law to calculate the crack growth resistance. Camacho and Ortiz [22] employed a linear cohesive-law fracture model to propagate multiple cracks along arbitrary paths during impact damage in brittle materials. Geubelle et al. [23] have utilized a bilinear cohesive law to simulate the spontaneous initiation and propagation of transverse matrix cracks and delamination fronts in thin composite plates subjected to low-velocity impact. In all the cohesive zone models (except Dugdale's model; refer Table 5-1) the traction-separation laws for the interfaces are such that with increasing interfacial separation, the traction across the interface increases, reaches a maximum, decreases and eventually vanishes, permitting a complete decohesion. The main difference lies in the shape and the parameters of functional constants that describe that shape. Additionally the magnitude of the parameters varies widely ranging from MPa to GPa for tractions, Joules to Kilo Joules for energy and nanometers to micrometers for the separation distance. Table 5-1 describes the details of those popular models mentioned above with specific attention focused on the shape and the values of the model parameters.

The purpose of this study is to determine cohesive zone parameters to describe decohesion in the normal and tangential direction in a sample MMC. A numerical simulation of debonding was performed on two separate models, each consisting of fiber and matrix phases attached by decohesion elements, one a concentric cylinder model and the other a transverse model. These models incorporate a cohesive zone describing interface decohesion into finite element models representing the material behavior of a MMC, and simulating loading, either normal and tangential to the fiber direction. In this work, the fiber-matrix interface in the composite, SCS-6/Timetal 21S, has been studied using an binomial form of the cohesive zone model.

Table 5-1. Various Cohesive Zone models and their parameters

Year and author	Proposed Model	Model parameters	Problem solved	Model constants	Comments
1959, 1962 Barenblatt, G.I.	*(figure: f vs y, y=b)*	$K = \int \frac{G_i(t)dt}{\sqrt{t}} = \sqrt{\frac{\pi ET}{1-\nu^2}}$ (ductile) $= \sqrt{\frac{\pi ET_i}{1-\nu^2}}$ (brittle) $T = T_e + T_i$ T_i = work of separation for britt. mater T_n = work of plastic deformation	Perfectly brittle materials		The first to propose the cohesive zone concept
1960 Dugdale, D.S.	*(figure: $\hat{\tau} = \sigma_y$, δ)*	$\frac{s}{a} = 2 \sin^2(\frac{\pi}{4}\frac{T}{Y})$ For small value of T/Y $\frac{s}{l} = 1.23\left(\frac{T}{Y}\right)^2$	Yielding of thin ideal elastic-plastic steel sheets containing slits	Plastic zone ranges from 0.042 to 0.448 (in.)	Cohesive stress equated to yield stress of material
1987 Needleman	*(figure: Polynomial fit, Linear fit; T_n vs u_n, T_t vs u_t)*	ϕ_{sep} = wk. of Sep. δ = normalizing Par. σ_{max} = Max. Stress	Particle-matrix decohesion	$\delta = 10^{-9}$ to 10^{-8} m Cohesive Energy 1 to 10 J/m² σ_{max} = 1000 MPa	Phenomenological model. predict normal separation
1989 Rice & Wang	*(figure: σ vs δ; Model based on atomic fit of the type $(1+x)e^{-x}$, σ_{max})*	E_o = Init. Young's mod h = normalizing Par. σ_{max} = Max. Stress $\alpha = \mathrm{cons}\tan t(\frac{E_o h}{a^2} = 2\gamma)$	Solute segregation		Ascending part is equated to E_o. Normal separation Ignores shear separation
1990 Needleman	*(figure: T_n vs Δ_n/δ; Exponential fit for Tn. Linear fit for Ts, Polynomial, Exponential)*	ϕ_{sep} = wk. of Sep. δ = normalizing Par. σ_{max} = Max. Stress	Particle-matrix decohesion	$\delta = 10^{-9}$ to 10^{-8} m	predict normal separation
1990 Needleman	*(figure: T_n, ϕ_n vs u_n; Exponential fit for normal Tn, Trignometric fit for shear Ts)*	ϕ_n = wk. of Nor. Sep. ϕ_t = wk. of Shr. Sep. δ_n, δ_t = critical displacements. σ_{max} = Max. Stress	Decohesion of interface under hydrostatic tensiom	$\delta_n = \delta_t = 2\times10^{-8}$ to 2×10^{-9} m $J/\phi_n = 0.57 \sim 2.59$ $\sigma_{max}/\sigma_o = 2,3$	Periodic shear traction to model Pieriels shear stress due to slip
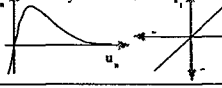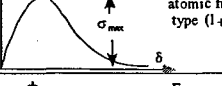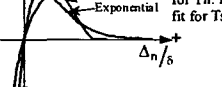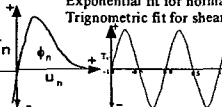
Year and author	Proposed Model	Model parameters	Problem solved	model constants	Comments
1992 Tvergaard & Hutchinson	*(figure: σ(λ) vs λ, trapezoidal)*	▮ wk. of Separation. ▮ = critical displ. ▮ Peak nor. trn/int.face str. ▮ factors governing shape of sep	Crack growth in elasto-plastic material, peeling of adhesive joints	▮/▮, ▮ 0~10. (▮ Pl wk.), ▮/▮ = 1 ▮ 0~14 ▮ 0.15, 0.5 ▮/E 1/300	Claims shape of separation law are relatively unimportant
1993 Xu & Needleman	*(figure: Exponential fit for both Tn and Tt; T_n, ϕ_n vs Δ_n, T_t, ϕ_t vs Δ_t)*	▮ wk. of Nor. Sep. ▮ wk. of Shr. Sep. ▮ = critical displacements ▮ Max. Stress	Particle-matrix decohesion	$\delta_n, \delta_t =$ 2×10^{-10} to 2×10^{-9} m	Predicts shear and normal separation
1990 Tvergaard	*(figure: T_n vs u_n, T_t vs u_t)*	▮ = critical displacements. ▮ Max. Stress	Interfaces of whisker-reinforced metal matrix composites	▮, ▮ = 1X10⁻⁹m. E=60GPa(Young's mod) ▮/E 0.005 ▮/▮ 5~9	Linear Model
1996 Camacho and Ortiz	*(figure: σ vs δ, τ)*	▮, ▮ Nor. and Shr stress at fracture initiation ▮ crit. nor.opening and shr. opening displ. G_c = Fracture energy	Impact	Alumina: σ_0= 400 MPa ▮ 1.7 10⁻⁷ m Steel: ▮ 1500 MPa ▮ 2.7 10⁻⁶ m	Predicts failure by both shear and normal separation in tension and by shear separation in compression
1997 Gaubelle & Bayler	*(figure: T_n, T_t bilinear)*	Φ_n, Φ_t: Work of normal and tangential separation Δ_n, Δ_t: Normal and Tangential displacement jump δ_n, δ_t: Normal and tangential interface characteristic-length	delamination by low-velocity impact	▮ = E/10 Critical normal displacement jump ▮ =10⁻⁵-10⁻⁴m	Bilinear model Ascending curve can be matched to initial stiffness of the material
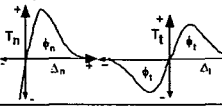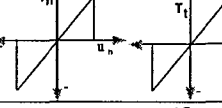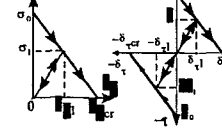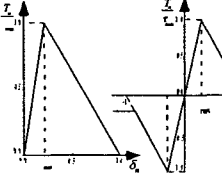
The purpose of this study is to determine cohesive zone parameters to describe decohesion in the normal and tangential direction in a sample MMC. A numerical simulation of debonding was performed on two separate models, each consisting of fiber and matrix phases attached by decohesion elements, one a concentric cylinder model and the other a transverse model. These models incorporate a cohesive zone describing interface decohesion into finite element models representing the material behavior of a MMC, and simulating loading, either normal and tangential to the fiber direction. In this work, the fiber-matrix interface in the composite, SCS-6/Timetal 21S, has been studied using an binomial form of the cohesive zone model.

5.2   Material and Experimental Procedures

The material considered in this study is a 6 ply Timetal-21S/SCS-6 composite, which is described fully in Chapter 2.

The experimental portion of this work is described in detail in Chapter 2. Briefly, it consists of two separate types of test, each performed at temperatures ranging from 23 to 650 °C. Fiber pushout tests consist of applying an increasing load to the fiber surface of a thin-slice of the composite, until the fiber slides out of the matrix. Results describe the force-displacement relationship during fiber debonding in the tangential (or longitudinal) direction, with respect to the fiber direction, at each of the test temperatures (Fig. 5-1). The transverse loading tests, carried out in order to determine the transverse decohesion characteristics, involve loading perpendicular to the fiber axis, until separation of the interface and the onset of yielding in the matrix phase of the composite (Fig. 5-2). These tests result in applied stress-strain curves at the test temperatures
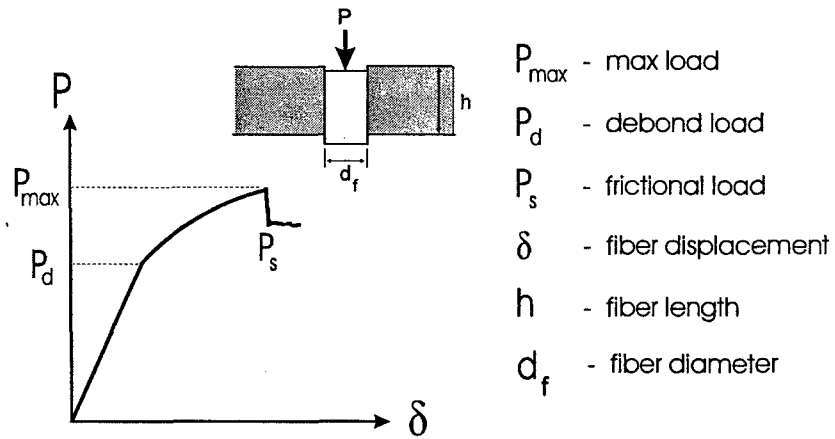
Figure 5-1   Schematic of fiber pushout test

- P_{max} - max load
- P_d - debond load
- P_s - frictional load
- δ - fiber displacement
- h - fiber length
- d_f - fiber diameter

- ε - strain
- σ - applied stress
- σ_{sep} - separation stress
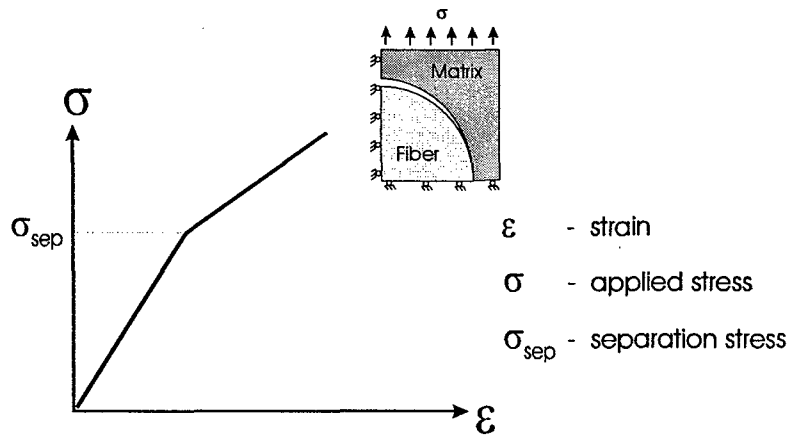
Figure 5-2   Schematic of transverse loading

5.3   The Cohesive Zone (CZ) Concept

The constitutive equation governing decohesion of the fiber/matrix interface expresses

the dependence of the normal or tangential tractions on the interface as a function of the

normal or tangential separation of the cohesive surfaces at the interface. As the interface

separates, the traction increases gradually to a maximum, then decreases to zero, at full

interface separation. This behavior is resembles the dependence of interatomic forces on

134

interatomic separation, although the scale for interface separation is much larger. The behavior incorporates the effect of flaws and voids in the matrix near the interface, as well as areas of poor bonding along the interface.

This separation is based on the relative displacement of the adjacent continuum elements across the interface:

$$\mathbf{u} = \mathbf{u}^+ - \mathbf{u}^-$$

For pure Mode I or Mode II loading, the normal and shear decohesion occur independently. Hence, when separation in either direction exceeds a pre-specified value, $\square_{max}$, the element becomes disconnected and can no longer support a traction across the interface. The value of any traction for relative displacements between $\mathbf{u} = 0$ and $\mathbf{u} = \delta_{max}$ is dependent upon the particular function chosen to represent this relationship.

If separation occurs in both directions simultaneously, decohesion in one direction influences that in the other direction. In this case, the expression for calculation of damage contains terms for both the normal and tangential direction. $\square$ is a dimensionless parameter which expresses the relationship between the amount of interface separation and the normal and shear displacements, where complete separation occurs when $\square = 1$. This parameter can be expressed as:

$$\lambda = \left\{ \left(\frac{\mathbf{u_n}}{\delta_n} \right)^m + \left(\frac{\mathbf{u_t}}{\delta_t} \right)^m \right\}^{1/2}$$

where:

$\mathbf{u_n}$, $\mathbf{u_t}$ is the relative displacement across the interface in the normal and tangential directions, respectively

δ_n, δ_t is the characteristic length corresponding to complete separation (i.e. when $\square$ = 0) in the normal and tangential direction, respectively. Note that this value does

135

not necessarily correspond to any physical distance.[16]

m is the model connection parameter

The model parameter, **m**, gives the connection between the normal and tangential damage, with m=1 being a linear connection and m→ ∞ approaching no influence of one upon the other. For this study, as in most similar work, m = 2, so that the damage is equal to the absolute value of separation.

The shape of the curve representing the traction-displacement relationship is governed by several parameters, including the characteristic length, or maximum relative displacement in the normal and tangential direction, δ_n and δ_t (from the λ term), and some function of the maximum traction on the interface in the normal and tangential directions, $(T_n)_{max}$ and $(T_t)_{max}$. The function used to express this shape, $F(\square)$, is simply a monotonically increasing, then decreasing function of $\square$. Several different forms of this function, $F(\square)$, have been proposed, as shown in Table 5-1. For this study, a polynomial form of the function, as used by Tvergaard [24] has been chosen, which can be expressed as

$$F(\lambda) = \frac{27}{4} T_{max} \left(1 - 2\lambda + \lambda^2\right) = \frac{27}{4} T_{max} \left(1 - \lambda\right)^2$$

The traction across the interface in either direction is given by [24]:

$$T_n = \frac{u_n}{\delta_n} F(\lambda)$$

$$T_t = \alpha \frac{u_t}{\delta_t} F(\lambda)$$

where α represents the ratio of shear to normal stiffness in the interface. In his numerical work, Needleman [16] found that his results were not very sensitive to choices of α, ranging from 1 to 50, so for this study,α is chosen to be 1.

136
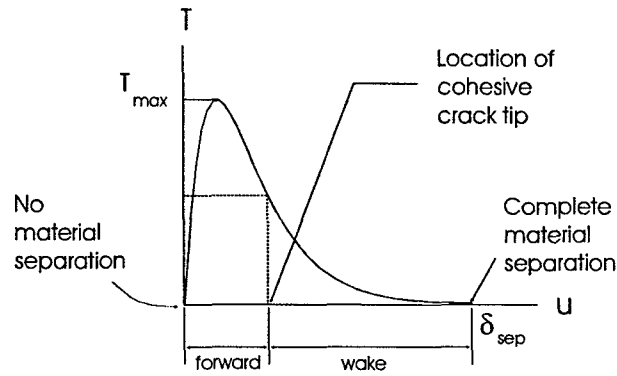
Figure 5-3 Schematic of cohesive zone traction-displacement curve

The general shape of a traction-displacement curve for normal and tangential separation using the concept of a cohesive zone is illustrated in Fig. 5.3. Complete interface decohesion occurs, as shown, Note that normal separation in the negative, or compressive direction is not possible. In the tangential direction, separation can occur due to either the positive or negative displacement, corresponding to sliding of fiber in the matrix in either the postive (up) ore negative (down) direction. For this expression of $F(\lambda)$, the maximum traction occurs at $u = \delta/3$.

The fracture energy, or interface toughness, is related to the traction and displacement, and also $F(\lambda)$ function. It can be expressed as the integral of the traction over the displacement, or the area under the traction- displacement curve between $u = 0$ and $u = \delta$:

$$W_n = \int_0^{\delta_n} T_n\, du_n = E\delta_n \int_0^1 F(\lambda)d\lambda = G_n = G_{Ic}$$

$$W_t = \int_0^{\delta_t} T_t\, du_t = G\delta_t \int_0^1 F(\lambda)d\lambda = G_t = G_{IIc}$$

where:

137

G_{Ic}, G_{IIC} is the Mode I and Mode II interface toughness

T_n, T_t is the traction across the interface in the normal and tangential directions

For the expression of $F(\lambda)$ chosen for this study, a general expression for the work of separation in either direction [16] can be written in terms of the maximum traction across the interface:

$$W = \phi_{sep} = \frac{9}{16} T_{max} \delta$$

In order to appropriately model experimental data, friction must be considered in any cohesive zone model. In this mode friction is introduced only after complete interface decohesion has occurred between any pair of elements. This is an important part of the modeling process, since during progressive debonding, along the length of the interface, elements will be in various stages of decohesion at any time increment. The force necessary to continue the decohesion process along the interface is directly affected by the introduction of friction in each element as $\square$ becomes zero. In fact, it is impossible to accurately model the fiber pushout or transverse loading and match experimental curves without considering friction in the model.

Although in reality, for most loading applications, separation occurs simultaneously in the normal and tangential directions (mixed mode loading), this study will take at an idealistic approach, and consider fiber pushout loading to involve a purely tangential decohesion (mode II). This is a reasonable assumption for the bulk of the composite during fiber pushout testing, although one must acknowledge that at the free surfaces, i.e., the top and bottom of the specimen, a mixed mode condition exists, in part due to bending of the specimen within its supports. Transverse loading, on the other hand, will have to be considered as mixed mode, since during separation, the matrix material elongates around

138

the circular cross-section fibers, and the fiber and matrix surfaces slide over one another, involving a significant amount of friction.

5.4   Tangential Properties

5.4.1   The tangential numerical model

A computational model, consisting of concentric cylinders representing fiber, interphase and matrix, has been built to simulate the debonding of the interphase. This model is very similar to that one described in Chapter 2.3, with the addition of a cohesive zone, which is introduced to represent the deformation and subsequent damage and fracture of the interphase layer. Theis cohesive zone is modeled as a set of non-linear springs, with force-displacement profiles generated from the traction-displacement function discussed above. In this model, the fiber is considered to behave elastically, while the residual stresses in the matrix are generated using a unified viscoplastic theory. An isostrain condition is imposed on one end of the cylinder to represent the generalized plane strain condition in the semi-infinite composite specimen. Initially, the buildup of residual stresses that occur during the cooldown from consolidation temperature to room temperature is established. The isostrain constraint is then removed to simulate the traction free surface generated upon cutting of the composite slice for the pushout testing. The residual stress at various temperatures is modeled by raising the temperature of the "cut" specimen to the required level. To simulate fiber pushout, the fiber portion of the model is displaced until the initiation of a debond crack occurs. Additional displacement is applied to propagate the crack along the length of the composite cylinder. Correlation between the numerically and experimentally generated fiber pushout curves, through an iterative procedure, is used to determine the shape of the T-δ curve which governs decohesion behavior during debonding

139

as a function of temperature.

5.4.2 Results and discussion

Three composite specimens were pushout tested under vacuum conditions at temperatures ranging from 23 to 650 °C. The fiber volume fraction of each of the the composite specimens was approximately 35 % and the specimen thickness is shown in the test grid in Table 5-2. The values used were based on approximate averages and representative curves were chosen from several fibers tested from each specimen.

Table 5-2   Fiber pushout specimen thickness at each of the test temperatures

Test temperature	Specimen thickness
23 °C	0.63 mm
500 °C	1.07 mm
650 °C	1.10 mm

A complete discussion of the experimental results is presented in Chapter 2 and will not be repeated here, except to illustrate the effectiveness of the numerical model to simulate the experiment. Instead, the features of the numerical simulation and its correspondence to the experimental results will be discussed. Note that, based on compliance testing of the fiber pushout apparatus, the load train compliance was mathematically removed from the force-displacement curves to obtain the presented experimental data..

A series of finite element simulations of the fiber pushout at each test temperature was carried out, using the numerical model described in the previous section. The controlling parameters of T_{max} and $\square$ were adjusted iteratively until the numerical output correlated with the experimental curves. The experimental and numerical results for the three temperatures (25, 500°C and 650°C) are shown in Figure 5-4(a-c). Note that the samples

for 500 and 650°C are approximately the same thickness and can be compared directly, while, due to maximum force limitations, the sample for room temperature is thinner. It should be also be noted that for the room temperature (23 °C) tests, an increase in slope was observed approximately 40% of the way up to the maximum. The effect of this increase was amplified by the removal of the load train compliance. This increase can only be attributed to an initial "settling in" of the specimen, perhaps due to slight bowing of the specimen as it was clamped in the specimen holder. Since the displacement is based on relative movement during the fiber pushout test, this change in slope does not affect the experimental data, provided the zero displacement point is aligned with the tr true pushout slope.
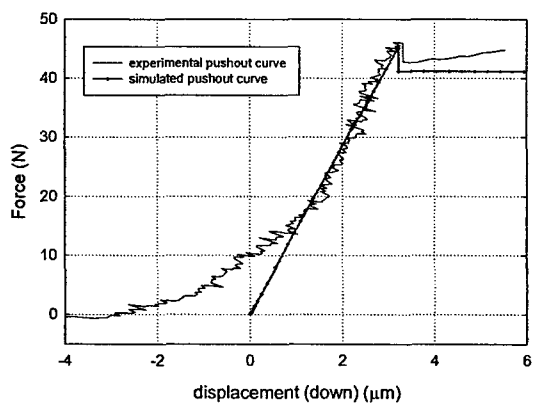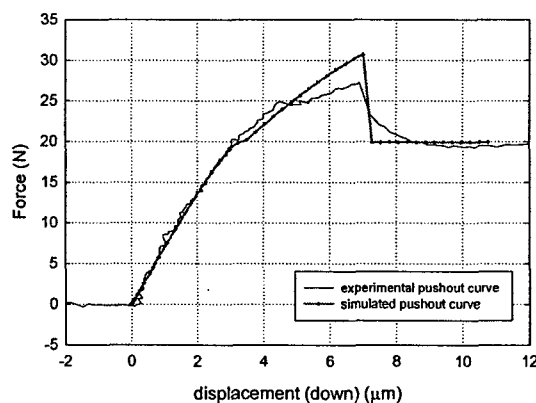

a) 23 oC (h = 0.63 mm)   b) 500 °C (h = 1.07 mm)

Figure 5-4(a-b)   Comparison of experimental results and numerical simulation
                         of fiber pushout tests at various temperatures

141
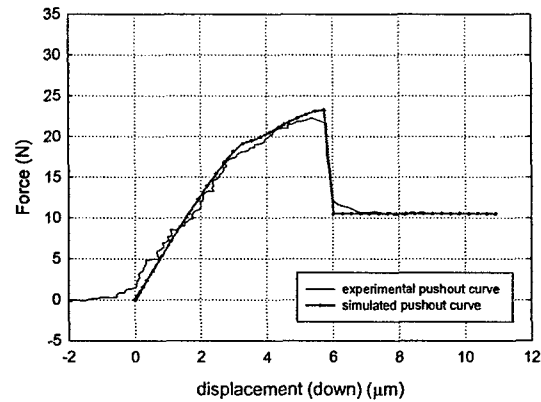
c) 650 °C (h = 1.10 mm)

Figure 5-4(c)   Comparison of experimental results and numerical simulation
             of fiber pushout tests at various temperatures

There are several important features of the experimental curves that have been

successfully captured in the numerical model. The room temperature curve, with the

exception of the "settling in' discussed previously, displays a linear slope, until reaching

the maximum force. At this point, the interface debonds catastrophically, resulting in the

distinct load drop. Due to the high compressive residual stresses in the matrix material

surrounding the fiber (see Figure 3-6), large frictional forces become the controlling

parameter in limiting the magnitude of the drop. Continued fiber sliding behavior is

governed by friction. In the numerical model, friction is considered to be constant. This

works well in capturing the debonding and initial sliding behavior. Clearly, in order to

model continued sliding of the fiber after complete debonding, increasing friction would be

necessary. The increasing force necessary to continue sliding has been addressed in the

discussion of experimental results in Chapter 2. Briefly, it involves an increasing roughness

along the debonded interface due to the accumulation of debris (fracturing carbon layers)

between the two sliding surfaces.

For the elevated temperature curves, the initial change in slope which corresponds to the initiation of the interfacial debond crack, is well matched in the numerical curves. The continually decreasing slope corresponds to the propagation of the interfacial crack as an increasing load is applied. The increasing slope terminates with a substantial drop, corresponding the catastrophic failure of the remaining bonded length. The drop is fairly large in the 500 and 650 °C tests, since the residual stresses are much lower at the elevated temperatures, resulting in a much lower fictional force that at room temperature. The drop is followed by frictional sliding, which is fairly constant, indicating that debris is not accumulating along the interface at the higher temperatures.

Using the iterative process to match the output of the numerical simulation with the experimental data, the cohesive zone model parameters, T_{max} and δ were extracted. Additionally, using the expression discussed previously, the work of separation, $\square_{sep}$, was calculated for each case. These parameters are listed in Table 5-3

Table 5-3   Cohesive zone parameters for tangential decohesion at several temperatures

T (°C)	T_{max} (MPa)	δ (mm)	ϕ_{sep} (J/mm^2)
25	1012.5	2.63e-4	149.8
500	50.48	1.562e-3	44.35
650	38.25	1.686e-3	36.28

5.5   Normal Properties

5.5.1   The normal numerical model and its verification

The finite element method used for analysis in the normal direction is a plane strain quarter fiber/matrix model with fiber and matrix properties similar to those in the

concentric cylinder model described in the previous section. Fig. 5-5 shows the transverse loading model, which consists of two quarter-fibers and the surrounding matrix, representing the smallest repeatable unit cell having perpendicular sides, which simplifies application of boundary conditions. This configuration is necessary to model the hexagonal fiber spacing of this type of composite, as discussed in detail in Chapter 2. The dimensions of the matrix are calculated based on the fiber volume fraction and the size of the fiber.
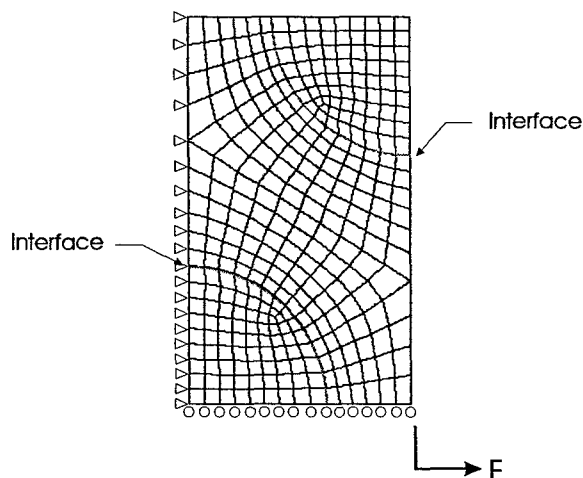
Figure 5-5   Schematic of the numerical model and meshing scheme for the transverse loading simulation with loading direction indicated.

Once residual stresses have been generated by cooling from 815 °C to room temperature, the model is heated to the desired test temperature and loading is simulated in the direction perpendicular to the fiber axis. The loading direction is shown in this Figure 5-5. It is important to note that, due to the fiber/matrix ply layup during consolidation of this composite, the fiber spacing is different in the two directions perpendicular to the fiber axis. Therefore, care must be taken when choosing the direction of load application in the simulation to correspond to the experimental direction.

As a verification of the transverse model, as well as in an attempt to gain insight

into the mechanisms at work during normal debonding, two separate interface conditions were examined. Models with a perfectly bonded and an unbonded interface, representing the two extreme interface conditions, were examined for both an elastic matrix and an elastic-perfectly plastic matrix. ABAQUS output of the model after loading at 650 °C is shown in Fig. 5-6. The separation of the interface is clearly visible in the both models with the unbonded interfaces. When the interface opens, stress are redistributed, resulting in areas of high stress along the interface in the areas where contact remains between the fiber and matrix. The elongation of the hole in the matrix results in compressive radial stresses in these areas. In the models having a fully bonded interace, separation is not allowed. The plasticity of the matrix allows for very concentrated stresses at the points where separation of the interface would occur, if this were permitted.
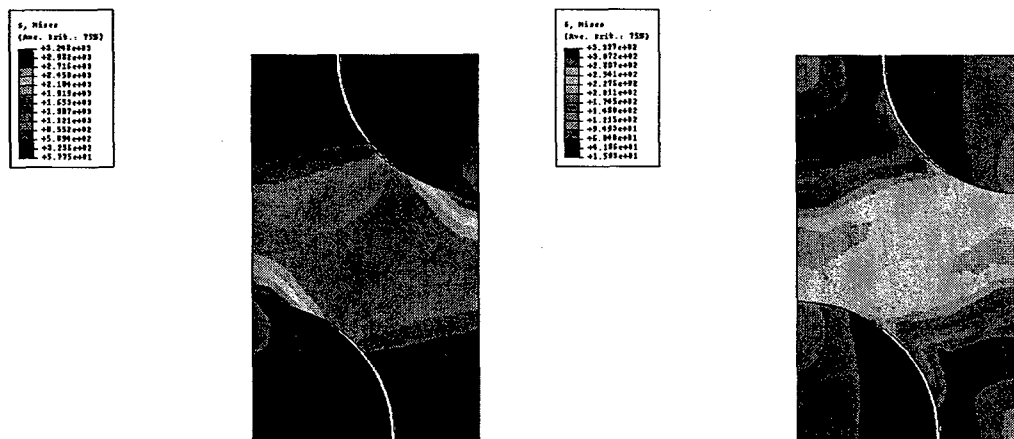
a) unbonded interface, elastic matrix   b) unbonded interface, plastic matrix

Figure 5-6(a-b)   Stress distributions during transverse loading at 650 °C for an unbonded and fully bonded interface, with elastic and elastic-plastic matrix interface (generated by ABAQUS)

c) fully bonded interface, elastic matrix   d) fully bonded interface, plastic matrix

Figure 5-6(c-d)   Stress distributions during transverse loading at 650 °C for an unbonded and fully bonded interface, with elastic and elastic-plastic matrix interface (generated by ABAQUS)

Results of these test simulations, in the form of a global stress vs. strain curve for loading at 23, 500 and 650 °C, respectively, are presented in Fig. 5-7. Superimposed on these figures are the experimental curves for the corresponding temperature. For each temperature, as expected, the numerical curves for the perfectly bonded and unbonded interfaces form the limits for the experimental curve. This acts as a verification of the numerical model. Additionally, when matrix plasticity is included and compared, it becomes clear that the change in slope of the experimental curve is related, not only to the opening of the interface as decohesion occurs, but also to a local plastic deformation of the matrix.

a) 23 °C   b) 500 °C

c) 650 °C

Figure 5-7   Numerical simulation of transverse loading tests with unbonded and fully bonded interface for various temperatures (superimposed is experimental results at corresponding temperature)

5.5.2   Results and Discussion

Transverse loading experiments were performed on specimens at various temperatures from 23 to 650 °C in an ambient environment. Results of these tests are presented and discussed in Chapter 2. Using the numerical model described previously, transverse loading was simulated at 23 and 650 °C. As with the pushout simulations, the controlling

147

parameters of T_{max} and $\square$ were adjusted iteratively until the numerical output correlated with the experimental results at each temperature. The experimental and numerical results are presented in Figure 5-8 as a plot of global applied stress versus strain for these two temperatures.

a) 23 °C   b) 650 °C
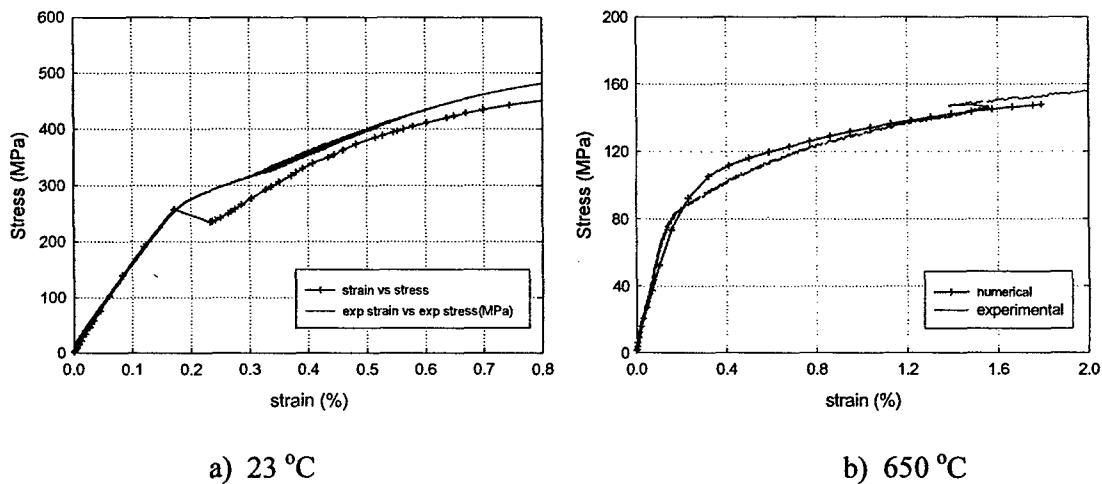
Figure 5-8   Comparison of experimental results and numerical simulation
                    of transverse loading tests at room temperature and 650 °C

Transverse loading at 650 °C will be used to discuss the process of decohesion and how it relates to the features of the stress-strain diagram. These features are typical at all temperatures studied. Figure 5-9 shows the numerical stress – strain diagram for the transverse loading simulation at 650 °C. The labels (a-d) denote points of interest on the curve that will be discussed.
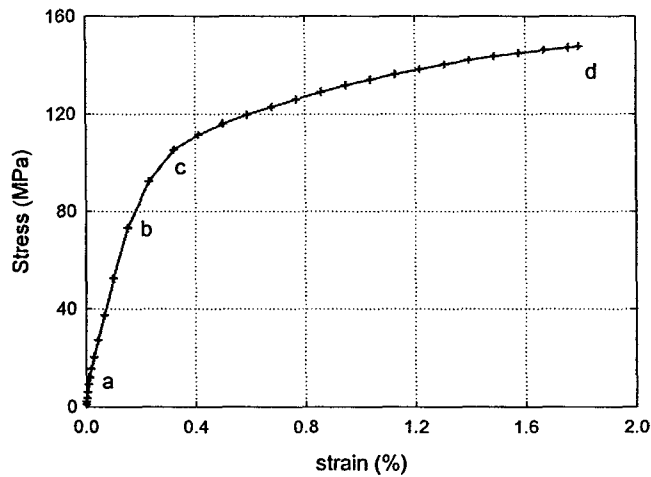
Figure 5-9   Numerical stress-strain diagram for transverse loading at 650 °C
with important features labeled.

Analysis of numerical results show that normal decohesion of the interface begins

early in the test, well below any change in linearity of the curve is observed, which relates

well to what is expected during physical interface debonding. Since the transverse strength

of the interface in this composite is weak, it should be unable to hold any significant

normal load. The decohesion starts around each fiber, in the region where the interface is

perpendicular to the applied load, as indicated in Fig. 5-10(a). At this point, the debonding

has just begun, with complete separation between four elements along the interface. The

white arrow in the figure shows the location of the debond crack tip. (Note that although

attention will focus on the lower fiber, the exact processes are occurring in the upper fiber

simultaneously.) As loading increases, the decohesion progresses around the fiber in the

direction shown in Fig. 5-10(a). The change in slope corresponds to the beginning of

localize matrix yielding, shown in Figure 5-10(b), as the amount of decohesion results in

the load being carried by only a small amount of the matrix. No further debonding is

possible after this point. Continued loading, shown in Fig. 5-10(c), causes the "hole" in the

matrix to elongate. A compressive force is applied by the matrix in the areas where the

149

interface is nearly parallel to the direction of load application, increasing the amount of

contact between the fiber and matrix, seemingly shortening the debond crack length.

Additional matrix yielding leads to a noticeable separation of the matrix from the fiber.

a) decohesion begins

b) localized matrix yielding begins

c) localized yielding progresses

d) opening continues
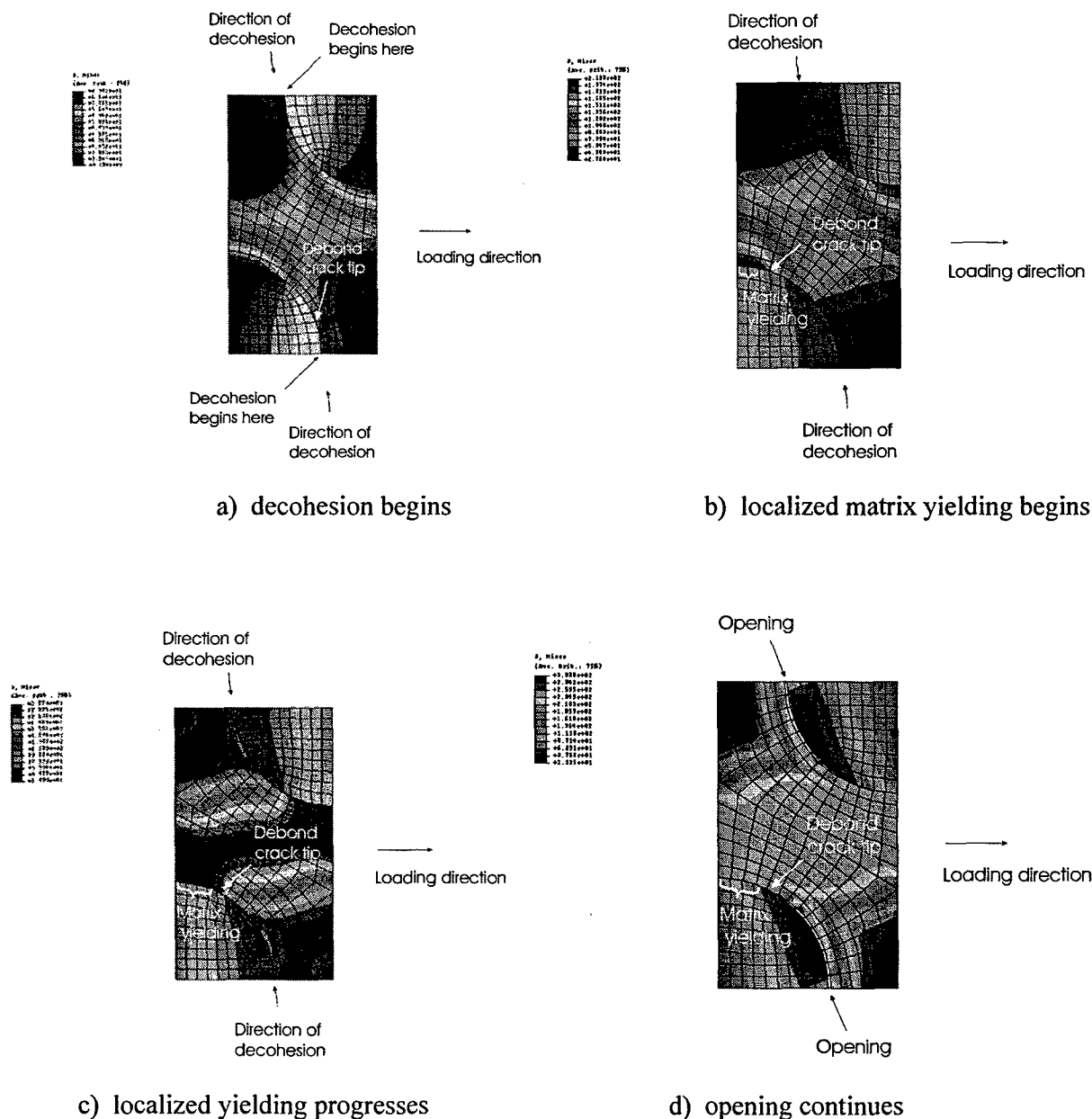
Figure 5-10 Illustration of key events occurring during transverse loading

The iterative process required to match the experimental and numerical stress-strain curves allow the determination of the P-δ curve which controls the transverse decohesion during the debonding process as a function of temperature. These parameters are listed in Table 5-4, as well as the work of separation, $\square_{sep,}$ calculated as discussed previously.

Table 5-3   Cohesive zone parameters for normal decohesion at several temperatures

T (°C)	T_{max} (MPa)	δ (mm)	ϕ_{sep} (J/m^2)
25	118.2	1.5e-4	9.97
650	88.6	7.1e-3	353.9

5.6   Summary and Conclusions

Interface debonding behavior has been established for the MMC composite system SCS-6/Timetal-21S, in terms of the cohesive zone model parameters of maximum traction, maximum separation and cohesive energy, in both the normal and tangential direction, for temperatures from 23 to 650 °C. The major findings of this study can be summarized as follows:

1.   Using a cohesive zone model, experimental results were simulated numerically, with good agreement.

2.   For tangential decohesion, the maximum traction, T_{max}, decreses with increasing temperature, while the $\square$increases substantially from room temperature to elevated temperatures. The work of separation, $\square_{sep}$, also decreases with increasing temperature.

3.   For normal decohesion, T_{max} decreases slightly with increasing temperature, while d also increases as the temperature is increased. This causes the work of separation, $\square_{sep}$, to increase with increasing temperature. Additional testing is necessary to determine the cause of this phenomena.

5.7   References

[1]   Jayaraman, K., K.L. Reifsnider and R.E. Swain, "Elastic and thermal effects in the interphase: Part II. Comments on Modeling Studies." *Journal of Composites Technology and Research,* 15(1), 14-22, 1993

[2]   Kim, J.K. and Mai, Y.W., "High strength high fracture toughness fiber composites with interface control-a review," *Composites Science and Technology,* 41, 333-378, 1991a

[3]   Kim, J.K. and Mai, Y.W., "The effect of interfacial coating and temperature on the fracture behaviors of unidirectional KFRP and CFRP," *Journal of Materials Science,* 26, 4701-4720, 1991b

[4]   Zhou, L.M., Mai, Y.W., Ye, L. and Kim, J.K., "Techniques for evaluating interfacial properties of fiber-matrix composites, " *Key Eng. Mater.* 104-107, pp. 549-600, 1995

[5]   Chandra, N. and Ananth, C. R., (1995c) Analysis of interfacial behavior in MMCs and IMCs using thin-slice push-out tests. *Compos. Sci. Technol* 54, 87-100.

[6]   Liang, C. and Hutchinson, J.W, "Models of the fiber push-out tests," *Mech. Mater.* 14, 207-221, 1993

[7]   Ananth, C.R. and Chandra, N., "Evaluation of interfacial shear properties of metal matrix composites from fiber push-out tests," *Mech. Compos. Mater. Struct* 2, 309-328, 1995

[8]   Mukherjee, S., Ananth, C.R. and Chandra, N, "Effect of residual stresses on the interfacial fracture behavior of metal-matrix composites," *Composites. Sci. Technol.* 57, 501-1512, 1997

[9]   Barenblatt, G.I., "The formation of equilibrium cracks during brittle fracture. General ideas and hypothesis. Axially-symmetric cracks," *PMM,* vol.23, 434-444, 1959

[10]   Barenblatt, G.I., "Mathematical Theory of Equilibrium Cracks," *Advances in Applied Mechanics,* Accademic Press, NewYork 7, 55-125, 1962

[11]   Dugdale, D.S., "Yielding of steel sheets containing slits," *J. Mech. Phys. Solids* 8, 100-104, 1960

[13]   Needleman, A., "An analysis of decohesion along am imperfect interface," *Int. J of Fracture* 42, 21-40, 1990

[14]   Rice, J. R. and Jian-sheng Wang, "Embrittlement of Interfaces by Solute Segregation," *Mater. Sci. Eng. A* 107, 23, 1989

[15]   Wappling, D. Gunnars, J., and Stahle, P., "Crack growth across a strength mismatched bimaterial interface," *Int. J of Fracture* 89, 223-243, 1998

[16]   Needleman, A, "A continuum model for void nucleation by inclusion debonding," *J.Appl. Mech.* 54, 525-531, 1987

[17]   Xu, X. P., and Needleman,A. "Void nucleation by inclusion debonding in a crystal matrix," *Modelling Simul. Mater. Sci. Eng.* 1, 111-132, 1993

[18]   Xu, X. P., and Needleman,A, "Numerical simulation of fast crack growth in brittle solids," *J. Mech. Phys. Solids,* 42, 1397-1434, 1994

[19]   Xu, X. P., and Needleman, A, "Analysis of ductile crack growth by means of a cohesive damage model," *Int. J of Fracture* 81, 99-112, 1995

[20]   Tvergaard, V, Effect of fibre debonding in a whisker-reinforced metal," *Mater. Sci. Eng. A*125, 203, 1990

[21]   Tvergaard, V. and Hutchinson, J.W, "The relation between crack growth resistance and fracture process parameters in elastic-plastic solids," *J. Mech. Phys. Solids* 40, 1377-1397, 1992

[22]   Camacho, G.T. and Ortaz, M, "Computational modeling of impact damage in brittle materials,: *Int. J. Solids Structures* 33, 2899, 1996

[23]   Geubelle, P.H. and Baylor,J, "Impact-induced delamination of laminate composites: a 2D simulation," *Composites* 29B 589, 1998

[24]   Tvergaard, V., "Fibre debonding and breakage in a whisker-reinforced metal," *Materials Science and Engineering A* 190, 215-222, 1995